PASJ: Publ. Astron. Soc. Japan , 1–**??**,

Survey of Period Variations of Superhumps in SU UMa-Type Dwarf Novae. II: The Second Year (2009–2010)

Taichi Kato,[1*] Hiroyuki Maehara,[2] Makoto Uemura,[3] Arne Henden,[4] Enrique de Miguel,[5,6] Ian Miller,[7] Pavol A. Dubovsky,[8] Igor Kudzej,[8] Seiichiro Kiyota,[9] Franz-Josef Hambsch,[10,11,12] Kenji Tanabe,[13] Kazuyoshi Imamura,[13] Nanae Kunitomi,[13] Ryosuke Takagi,[13] Mikiha Nose,[13] Hidehiko Akazawa,[13] Gianluca Masi,[14] Shinichi Nakagawa,[15] Eriko Iino,[15] Ryo Noguchi,[15] Katsura Matsumoto,[15] Daichi Fujii,[15] Hiroshi Kobayashi,[15] Kazuyuki Ogura,[15] Sachi Ohtomo,[15] Kousei Yamashita,[15] Hirofumi Yanagisawa,[15] Hiroshi Itoh,[16] Greg Bolt,[17] Berto Monard,[18] Tomohito Ohshima,[1] Jeremy Shears,[19] Javier Ruiz,[20] Akira Imada,[21] Arto Oksanen,[22] Peter Nelson,[23] Tomas L. Gomez,[24] Bart Staels,[4,25] David Boyd,[26,30] Irina B. Voloshina,[27] Thomas Krajci,[28] Tim Crawford,[29] Chris Stockdale,[31] Michael Richmond,[32] Etienne Morelle,[33] Rudolf Novák,[34] Daisaku Nogami,[2] Ryoko Ishioka,[35] Steve Brady,[36] Mike Simonsen,[37] Elena P. Pavlenko,[38] Frederick A. Ringwald,[39] Tetsuya Kuramoto,[1] Atsushi Miyashita,[40] Roger D. Pickard,[30,41] Tomáš Hynek,[42] Shawn Dvorak,[43] Rod Stubbings,[44] Eddy Muyllaert,[45]

[1] *Department of Astronomy, Kyoto University, Kyoto 606-8502*

**tkato@kusastro.kyoto-u.ac.jp*

[2] *Kwasan and Hida Observatories, Kyoto University, Yamashina, Kyoto 607-8471*

[3] *Astrophysical Science Center, Hiroshima University, Kagamiyama, 1-3-1 Higashi-Hiroshima 739-8526*

[4] *American Association of Variable Star Observers, 49 Bay State Rd., Cambridge, MA 02138, USA*

[5] *Departamento de Física Aplicada, Facultad de Ciencias Experimentales, Universidad de Huelva, 21071 Huelva, Spain*

[6] *Center for Backyard Astrophysics, Observatorio del CIECEM, Parque Dunar, Matalascañas, 21760 Almonte, Huelva, Spain*

[7] *Furzehill House, Ilston, Swansea, SA2 7LE, UK*

[8] *Vihorlat Observatory, Mierova 4, Humenne, Slovakia*

[9] *Variable Star Observers League in Japan (VSOLJ), 405-1003 Matsushiro, Tsukuba, Ibaraki 305-0035*

[10] *Groupe Européen d'Observations Stellaires (GEOS), 23 Parc de Levesville, 28300 Bailleau l'Evêque, France*

[11] *Bundesdeutsche Arbeitsgemeinschaft für Veränderliche Sterne (BAV), Munsterdamm 90, 12169 Berlin, Germany*

[12] *Vereniging Voor Sterrenkunde (VVS), Oude Bleken 12, 2400 Mol, Belgium*

[13] *Department of Biosphere-Geosphere System Science, Faculty of Informatics, Okayama University of Science, 1-1 Ridai-cho, Okayama, Okayama 700-0005*

[14] *The Virtual Telescope Project, Via Madonna del Loco 47, 03023 Ceccano (FR), Italy*

[15] *Osaka Kyoiku University, 4-698-1 Asahigaoka, Osaka 582-8582*

[16] *VSOLJ, 1001-105 Nishiterakata, Hachioji, Tokyo 192-0153*

[17] *Camberwarra Drive, Craigie, Western Australia 6025, Australia*

[18] *Bronberg Observatory, Center for Backyard Astronomy Pretoria, PO Box 11426, Tiegerpoort 0056, South Africa*

[19] *"Pemberton", School Lane, Bunbury, Tarporley, Cheshire, CW6 9NR, UK*

[20] *Observatory of Cantabria, Centro de Investigación del Medio Ambiente (CIMA) Instituto de Física de Cantabria (IFCA), Agrupación Astronómica Cántabra (AAC), Ctra. de Rocamundo s/n, Valderredible, Cantabria, Spain*

[21] *Okayama Astrophysical Observatory, National Astronomical Observatory of Japan, Asakuchi, Okayama 719-0232*

[22] *Nyrola observatory, Jyvaskylan Sirius ry, Vertaalantie 419, FI-40270 Palokka, Finland*

[23] *RMB 2493, Ellinbank 3820, Australia*

[24] *ICMAT (CSIC-UAM-UC3M-UCM), Serrano 113bis, 28006 Madrid, Spain*

[25] *Center for Backyard Astrophysics (Flanders), American Association of Variable Star Observers (AAVSO), Alan Guth Observatory, Koningshofbaan 51, Hofstade, Aalst, Belgium*

[26] *Silver Lane, West Challow, Wantage, OX12 9TX, UK*

[27] *Sternberg Astronomical Institute, Moscow University, Universitetskiy prospekt 13, Moscow 119992, Russia*

[28] *Astrokolkhoz Observatory, Center for Backyard Astrophysics New Mexico, PO Box 1351 Cloudcroft, New Mexico 83117, USA*

[29] *Arch Cape Observatory, 79916 W. Beach Road, Arch Cape, OR 97102*

[30] *The British Astronomical Association, Variable Star Section (BAA VSS), Burlington House, Piccadilly, London, W1J 0DU, UK*

[31] *8 Matta Drive, Churchill, Victoria 3842, Australia*

[32] *Physics Department, Rochester Institute of Technology, Rochester, New York 14623, USA*

[33] *9 rue Vasco de GAMA, 59553 Lauwin Planque, France*

[34] *Institute of Computer Science, Faculty of Civil Engineering, Brno University of Technology, 602 00 Brno, Czech Republic*

[35] *Subaru Telescope, National Astronomical Observatory of Japan, 650 North A'ohoku Place, Hilo, HI 96720, USA*

[36] *5 Melba Drive, Hudson, NH 03051, USA*

[37] AAVSO, C. E. Scovil Observatory, 2615 S. Summers Rd., Imlay City, Michigan 48444, USA
[38] Crimean Astrophysical Observatory, 98409, Nauchny, Crimea, Ukraine
[39] Department of Physics, California State University, Fresno, 2345 East San Ramon Avenue, MS MH37, Fresno, CA 93740-8031, USA
[40] Seikei Meteorological Observatory, Seikei High School
[41] 3 The Birches, Shobdon, Leominster, Herefordshire, HR6 9NG, UK
[42] Project Eridanus, Observatory and Planetarium of Johann Palisa, VSB – Technical University Ostrava, Trida 17. listopadu 15, Ostrava – Poruba 708 33, Czech Republic
[43] Rolling Hills Observatory, 1643 Nightfall Drive, Clermont, FL 34711, USA
[44] Tetoora Observatory, Tetoora Road, Victoria, Australia
[45] Vereniging Voor Sterrenkunde (VVS), Moffelstraat 13 3370 Boutersem, Belgium

(Received 201 0; accepted 201 0)

Abstract

As an extension of the project in Kato et al. (2009a), we collected times of superhump maxima for 61 SU UMa-type dwarf novae mainly observed during the 2009–2010 season. The newly obtained data confirmed the basic findings reported in Kato et al. (2009a): the presence of stages A–C, as well as the predominance of positive period derivatives during stage B in systems with superhump periods shorter than 0.07 d. There was a systematic difference in period derivatives for systems with superhump periods longer than 0.075 d between this study and Kato et al. (2009a). We suggest that this difference is possibly caused by the relative lack of frequently outbursting SU UMa-type dwarf novae in this period regime in the present study. We recorded a strong beat phenomenon during the 2009 superoutburst of IY UMa. The close correlation between the beat period and superhump period suggests that the changing angular velocity of the apsidal motion of the elliptical disk is responsible for the variation of superhump periods. We also described three new WZ Sge-type objects with established early superhumps and one with likely early superhumps. We also suggest that two systems, VX For and EL UMa, are WZ Sge-type dwarf novae with multiple rebrightenings. The $O-C$ variation in OT J213806.6+261957 suggests that the frequent absence of rebrightenings in very short-$P_{\rm orb}$ objects can be a result of sustained superoutburst plateau at the epoch when usual SU UMa-type dwarf novae return to quiescence preceding a rebrightening. We also present a formulation for a variety of Bayesian extension to traditional period analyses.

Key words: accretion, accretion disks — stars: novae, cataclysmic variables — stars: dwarf novae — methods: statistical

1. Introduction

In paper Kato et al. (2009a), we surveyed period variations of superhumps in SU UMa-type dwarf novae (for general information of SU UMa-type dwarf novae and superhumps, see Warner 1995). Kato et al. (2009a) indicated that evolution of superhump period ($P_{\rm SH}$) is generally composed of three distinct stages: early evolutionary stage with a longer superhump period (stage A), middle stage with systematically varying periods (stage B), final stage with a shorter, stable superhump period (C). It was also shown that the period derivatives ($P_{\rm dot} = \dot{P}/P$) during stage B is correlated with $P_{\rm SH}$, or binary mass-ratios ($q = M_2/M_1$). Although this relation commonly applies to classical SU UMa-type dwarf novae, WZ Sge-type dwarf novae, a subtype of SU UMa-type dwarf novae with very infrequent superoutbursts, tend to deviate from this picture: they rarely show a distinct stage B–C transition, and some objects show relatively small period derivatives, and they frequently exhibit unusual multiple post-superoutburst rebrightenings. The origin of these relations is not yet well understood. We have extended the survey in order to test whether this picture is applicable to new SU UMa-type systems and to the degree of diversity between systems in a larger sample. We include in this paper newly recorded objects and superoutbursts since the publication of Kato et al. (2009a). Some of new observations have led to revisions of analysis in Kato et al. (2009a). We also include a few past superoutburst not analyzed in the previous studies.

The structure of the paper follows the scheme in Kato et al. (2009a), in which we mostly restricted to superhump timing analysis. We also include some more details if the paper provides the first solid presentation of individual objects.

2. Observation and Analysis

The data were obtained under campaigns led by the VSNET Collaboration (Kato et al. 2004b). In some objects, we used archival data for published papers, and the public data from the AAVSO International Database[1]. The majority of the data were acquired by time-resolved CCD photometry by using 30 cm-class telescopes, whose observational details on individual objects will be presented in future papers dealing with analysis and discus-

[1] <http://www.aavso.org/data/download/>.

sion on individual objects. The list of outbursts and observers is summarized in table 1. The data analysis was performed just in the same way described in Kato et al. (2009a). In this paper, we introduce Bayesian extension to traditional method (Appendix), and used them if they give significantly improved results.

The derived $P_{\rm SH}$, $P_{\rm dot}$ and other parameters are listed in table 2 as in the same format in Kato et al. (2009a). The definitions of parameters P_1, P_2, E_1, E_2 and $P_{\rm dot}$ are the same as in Kato et al. (2009a). As in Kato et al. (2009a), we present comparisons of $O-C$ diagrams between different superoutbursts since this has been one of the motivations of these surveys (cf. Uemura et al. 2005).

3. Individual Objects

3.1. KX Aquilae

KX Aql has long been known as a dwarf nova with a low outburst frequency. Mayall (1968) and Mayall (1973) reported two outbursts in 1967 and 1972 from AAVSO observations. Garbusov (1979) examined photographic plate archives and estimated an interval between outbursts to be $\sim$ 1000 d. The object underwent a very bright ($m_{\rm vis} = 11.5$) outburst in 1980 November, which was first recorded by S. Fujino on November 9. The long duration of the outburst inferred from the VSOLJ and AAVSO observations is sufficient to imply the SU UMa-type nature. Additional short outbursts were recorded in 1994 December[2] and 2007 May (baavss-alert 582), which later turned out to be a normal outburst.

Tappert, Mennickent (2001) first presented a spectrum of this object clearly showing a dwarf nova at a low mass-transfer rate. Kato et al. (2001a) listed KX Aql as a candidate for a WZ Sge-type dwarf nova. Thorstensen, Fenton (2003) obtained a $P_{\rm orb}$ of 0.06035(3) d from a radial-velocity study.

The long-waited superoutburst was finally recorded in 2010 March by T. Gomez (cvnet-outburst 3626). Subsequent observations detected superhumps (vsnet-alert 11859, 11862, 11884). The outburst was followed by a rebrightening (vsnet-alert 11895).

The times of superhump maxima are listed in table 3. There was an apparent break in the period evolution around $E = 7$. We identified this break as a stage B–C transition since the observed duration of the outburst after the break was only 7 d (in contrast to $\sim$14 d for typical durations of superoutbursts of short-$P_{\rm orb}$ SU UMa-type dwarf novae) and the superhump period was almost constant after the break. The relatively low recorded maximum brightness ($V = 13.6$) for a superoutburst also suggests that the true maximum was missed. The period for stage B was not determined due to the shortness of the observed segment. We adopted a mean superhump period of 0.06128(2) d with the PDM method (figure 1). The recorded ϵ of 1.5 % is slightly low for this $P_{\rm orb}$ (cf. figure 15 in Kato et al. 2009a), but not as low as those of WZ Sge-type dwarf novae with similar $P_{\rm orb}$. This interpretation is consistent with the presence of a single rebrightening, rather than multiple ones in WZ Sge-type systems with similar $P_{\rm orb}$. The scaled q is 0.08 based on the refined relation in Kato et al. (2009a).

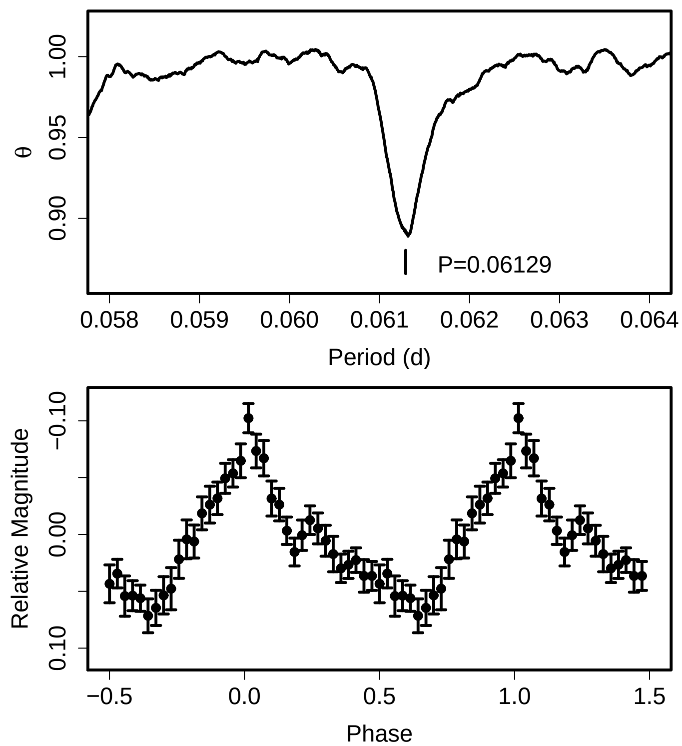

Fig. 1. Superhumps in KX Aql (2010) after BJD 2455266. (Upper): PDM analysis. (Lower): Phase-averaged profile.

3.2. NN Camelopardalis

The superoutburst in 2009 November is the first superoutburst of this object whose entire evolution was first observed in detail [for general information of this object, see Kato et al. (2009a)]. The times of superhump maxima are listed in table 4. The $O-C$ diagram clearly shows all A–C stages. There was a rise in the light curve in accordance with the stage A–B transition (figure 2). The mean $P_{\rm SH}$ and $P_{\rm dot}$ for stage B ($19 \le E \le 87$) were 0.07426(1) d and $+1.1(1.5) \times 10^{-5}$, respectively. There was a distinct stage B–C transition around $E = 87$. The mean period for stage A was calculated for $E \le 15$ although there was significant period shortening even during stage A. Shears et al. (2010b) also recently reported on two superoutbursts of this object in 2007 and 2009. Shears et al. (2010b) did not distinguish stages A–C during the 2009 superoutburst treated in this paper probably due to fragmentary observational coverage.

3.3. V591 Centauri

V591 Cen was discovered by Huruhata (1940) (see also Walker, Olmsted 1958). Although the discovery observation was already suggestive of a superoutburst, this object

[2] <http://www.kusastro.kyoto-u.ac.jp/vsnet/Mail/1994/vsnet-obs/msg00155.html>.

Table 1. List of Superoutbursts.

Subsection	Object	Year	Observers or references*
3.1	KX Aql	2010	Mhh, AAVSO, Kis, GOT, DPV, OKU
3.2	NN Cam	2009	AAVSO, deM, Mhh, JSh, IMi
3.3	V591 Cen	2010	MLF, GBo
3.4	Z Cha	2010	AAVSO, Kis
3.5	PU CMa	2009	OUS, Mhh, Kis
3.6	AQ CMi	2010	GBo
3.7	GZ Cnc	2010	OKU, OAO, Mhh, deM, OUS
3.8	GO Com	2010	deM, Mhh, OKU, DPV
3.9	TV Crv	2009	Kis
3.10	V337 Cyg	2010	IMi, KU, OKU, DPV
3.11	V1113 Cyg	2003	Bakowska et al. (2010)
3.12	V1454 Cyg	2009	HMB, Mhh, IMi, AAVSO
3.13	AQ Eri	2010	Nel, Mhh, Kis, Ioh
3.14	VX For	2009	MLF, Nyr, Nel, AAVSO, Sto, Mhh, Kis
3.15	AW Gem	2010	Hyn
3.16	IR Gem	2010	deM
3.17	V592 Her	2010	AAVSO, OUS, Mhh, OKU, IMi, DPV, RIT, HMB, KU, Boy, OAO, MEV
3.18	V660 Her	2009	AAVSO
3.19	V844 Her	2009	DPV, AAVSO
	V844 Her	2010	Mhh
3.20	CT Hya	2010	Mhh
3.21	V699 Oph	2010	deM, OUS
3.22	V1032 Oph	2010	Mhh, deM, AAVSO, Kis, Rui
3.23	V2051 Oph	2010	Sto, OUS, Kis
3.24	EF Peg	2009	Mhh, IMi, OUS, AAVSO
3.25	V368 Peg	2009	CTX, AAVSO, IMi, Nyr, HMB
3.26	UV Per	2010	DPV, PXR, deM, AAVSO
3.27	EI Psc	2009	GOT, Kis
3.28	EK TrA	2009	Nel
3.29	SU UMa	2010	DPV, SAc
3.30	BC UMa	2009	Nyr, Mhh
3.31	EL UMa	2010	Mhh, Ioh, DPV, HMB
3.32	IY UMa	2009	Kato et al. (2009a), DPV, AAVSO
3.33	KS UMa	2010	OUS
3.34	MR UMa	2010	OUS, OKU
3.35	TY Vul	2010	MEV, AAVSO, IMi, BSt
3.36	1RXS J0423	2010	OUS, Mhh, deM
3.37	1RXS J0532	2009	DPV, Mhh
3.38	ASAS J2243	2009	HMB, Kra, Mhh, JSh, GBo, IMi, deM, Ioh, AAVSO
3.39	Lanning 420	2010	KU, AAVSO, deM, BXS, Mhh, HMB, Rui
3.40	PG 0149	2009	IMi, HMB, Mhh
3.41	RX J1715	2009	Shears et al. (2010d), Mhh
3.42	SDSS J0129	2009	JSh, Mhh, AAVSO, Boy
3.43	SDSS J0310	2009b	IMi
3.44	SDSS J0732	2010	AAVSO, JSh
3.45	SDSS J0838	2010	Mhh, deM
3.46	SDSS J0839	2010	deM, JSh
3.47	SDSS J0903	2010	deM, Vol, AAVSO, Mas, Mhh

*Key to observers: AKh (Astrokolkhoz team), Boy (D. Boyd), BSt‡(B. Staels), BXS‡(S. Brady), CTX‡(T. Crawford), deM (E. de Miguel), DKS‡(S. Dvorak), DPV (P. Dubovsky), GBo (G. Bolt), GOT‡(T. Gomez), HHO (Higashi-Hiroshima Obs.), Hid (Hida Obs.), HMB (F.-J. Hambsch), Hyn (T. Hynek), IMi‡(I. Miller), Ioh (H. Itoh), JSh‡(J. Shears), Kis (S. Kiyota), KU (Kyoto U., campus obs.), Kra (T. Krajci), Mas (G. Masi), MEV‡(E. Morelle), Mhh (H. Maehara), MLF (B. Monard), Nel‡(P. Nelson), Nov (R. Novák), Nyr‡(Nyrola and Hankasalmi Obs.), OAO (Okayama Astrophys. Obs.), OKU (Osaka Kyoiku U.), OUS (Okayama U. of Science), Pav (E. Pavlenko), PXR‡(R. Pickard), Rin (F. Ringwald), RIT (M. Richmond), Rui (J. Ruiz), SAc (Seikei High School), Sto (C. Stockdale), Vol (I. Voloshina), AAVSO (AAVSO database)

†Original identifications or discoverers.

‡Inclusive of observations from the AAVSO database.

Table 1. List of Superoutbursts. (continied)

Subsection	Object	Year	Observers or references*	ID†
3.48	SDSS J1152	2009	Mhh, Kis	
3.49	SDSS J1250	2008	BSt	
	SDSS J1250	2009	IMi, Mhh	
3.50	SDSS J1502	2009	AAVSO, Rin, RIT, Mas, DPV, Mhh, Rui, IMi, Ioh	
3.51	SDSS J1610	2009	GBo, Mhh, HMB, CTX, IMi, Boy	
3.52	SDSS J1625	2010	Nov, deM, RIT, BSt, Mas, HMB, Mhh, IMi	
3.53	SDSS J1637	2004	KU, MLF, GBo, Hid	
3.54	SDSS J1653	2010	OKU, DPV	
3.55	SDSS J2048	2009	IMi	
3.56	OT J0406	2010	Mhh	Itagaki (Yamaoka et al. 2008)
3.57	OT J0506	2009	Mhh, Kryachko et al. (2010), Mas	Kryachko et al. (2010)
3.58	OT J1026	2010	DPV, IMi, Mas	Itagaki (Yamaoka, Itagaki 2009)
3.59	OT J1044	2010	Mhh, OAO, DPV, IMi, Ioh, HMB, Kis, Pav, deM	CSS100217:104411+211307
3.60	OT J1122	2010	MLF, Mhh, AKh, Mas	CSS100603:112253−111037
3.61	OT J1440	2009	Boyd et al. (2010), Kato et al. (2009a)	CSS090530:144011+494734
3.62	OT J1631	2010	Mhh, IMi	CSS080505:163121+103134
3.63	OT J1703	2009	Mas	CSS090622:170344+090835
3.64	OT J1821	2010	OKU, Mhh, deM	Itagaki (vsnet-alert 11952)
3.65	OT J2138	2010	Mhh, deM, OUS, AAVSO, Vol, DPV, HHO, DKS, Kis, GOT, OKU, SXN, Mas, Rui, Ioh	Yi (Yamaoka 2010), Kaneko (Nakano 2010)
3.66	OT J2158	2010	AKh, HMB	CSS100615:215815+094709
3.67	OT J2230	2009	MLF, GBo, Mhh, Mas	CSS090727:223003−145835
3.68	OT J2344	2010	MLF, Mhh, HMB, KU, Mas, deM	MLS100904:234441−001206

Table 3. Superhump maxima of KX Aql (2010).

E	max*	error	$O-C$†	N‡
0	55265.6366	0.0007	−0.0110	145
1	55265.6941	0.0018	−0.0149	52
7	55266.0852	0.0025	0.0077	56
17	55266.6967	0.0028	0.0050	53
26	55267.2439	0.0010	−0.0005	183
27	55267.3082	0.0005	0.0023	148
38	55267.9827	0.0004	0.0012	59
43	55268.2993	0.0007	0.0108	74
50	55268.7192	0.0014	0.0008	43
54	55268.9648	0.0003	0.0008	126
55	55269.0288	0.0007	0.0033	46
59	55269.2728	0.0006	0.0016	238
70	55269.9473	0.0004	0.0006	53
71	55270.0091	0.0008	0.0010	60
75	55270.2611	0.0025	0.0073	127
76	55270.3120	0.0017	−0.0032	113
82	55270.6850	0.0019	0.0013	52
87	55270.9918	0.0026	0.0010	7
99	55271.7243	0.0026	−0.0035	44
103	55271.9691	0.0008	−0.0044	62
119	55272.9490	0.0017	−0.0072	16

*BJD−2400000.
†Against $max = 2455265.6476 + 0.061416E$.
‡Number of points used to determine the maximum.

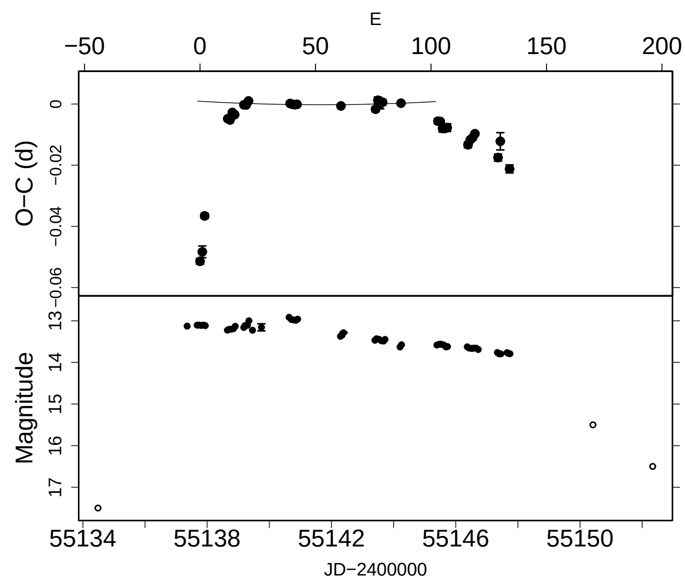

Fig. 2. $O-C$ of superhumps in NN Cam (2009). (Upper): $O-C$ diagram. The $O-C$ values were against the mean period for the stage B ($19 \le E \le 87$, thin curve) (Lower): Light curve. Small open circles are snapshot unfiltered CCD observations. There was a rise in the light curve in accordance with the stage A–B transition.

Table 2. Superhump Periods and Period Derivatives

Object	Year	P_1 (d)	err	E_1*		$P_{\rm dot}$†	err†	P_2 (d)	err	E_2*		$P_{\rm orb}$ (d)	Q‡
KX Aql	2010	–	–	–	–	–	–	0.061322	0.000026	7	119	0.06035	B
NN Cam	2009	0.074264	0.000009	19	87	1.1	1.5	0.073876	0.000045	87	134	0.0717	A
V591 Cen	2010	0.060299	0.000019	0	138	6.5	1.3	–	–	–	–	–	B
Z Cha	2010	–	–	–	–	–	–	0.076977	0.000054	0	80	0.074499	C
PU CMa	2009	0.058090	0.000032	0	90	9.7	2.3	0.057219	0.000129	121	192	0.056694	C
AQ CMi	2010	0.066178	0.000006	15	106	–	–	–	–	–	–	–	C
GZ Cnc	2010	0.092774	0.000021	0	44	–	–	0.089717	0.000124	42	88	0.08825	C
GO Com	2010	0.063072	0.000024	0	103	10.5	0.9	0.062660	0.000027	101	158	–	A
TV Crv	2009	0.065058	0.000027	0	78	9.1	3.0	0.064881	0.000136	77	94	0.0629	C
V337 Cyg	2010	0.070326	0.000042	0	95	2.9	3.2	0.069578	0.000125	95	139	–	C
V1454 Cyg	2009	0.057650	0.000039	0	95	10.3	3.5	–	–	–	–	–	B
AQ Eri	2010	0.062370	0.000068	0	82	20.4	5.2	–	–	–	–	0.06094	C
VX For	2009	0.061327	0.000012	0	101	1.0	1.4	0.061086	0.000056	99	204	–	B
AW Gem	2010	0.079056	0.000025	0	26	–	–	0.078668	0.000027	24	103	0.07621	C
IR Gem	2010	0.070834	0.000005	0	58	–	–	–	–	–	–	0.0684	C
V592 Her	2010	0.056607	0.000016	35	216	7.4	0.6	0.056390	0.000088	216	300	0.0561	BE
V660 Her	2009	–	–	–	–	–	–	0.080692	0.000089	0	61	–	C
V844 Her	2009	0.055923	0.000021	0	111	9.5	1.7	–	–	–	–	0.054643	B
V844 Her	2010	0.055764	0.000004	0	54	–	–	–	–	–	–	0.054643	CG
CT Hya	2010	0.066505	0.000001	14	90	–	–	–	–	–	–	–	C
V699 Oph	2010	0.070319	0.000112	0	42	–	–	0.069880	0.000071	42	99	–	B
V1032 Oph	2010	0.085342	0.000047	0	106	–	–	–	–	–	–	0.081056	CG
V2051 Oph	2010	0.064238	0.000083	0	65	–	–	–	–	–	–	0.062428	C
EF Peg	2009	0.087347	0.000182	10	30	–	–	0.086784	0.000103	68	125	–	C
V368 Peg	2009	0.070358	0.000040	0	99	9.5	1.8	0.069947	0.000022	97	220	–	B
UV Per	2010	0.066708	0.000026	0	32	21.1	6.7	–	–	–	–	0.06489	CG
EI Psc	2009	0.046352	0.000046	0	10	–	–	–	–	–	–	0.044567	C
EK TrA	2009	0.064832	0.000006	29	139	0.8	0.6	–	–	–	–	0.06288	CM
SU UMa	2010	0.079070	0.000034	0	51	–	–	–	–	–	–	0.07635	C
BC UMa	2009	0.064553	0.000029	56	144	9.5	2.7	0.064262	0.000019	141	219	0.06261	B
IY UMa	2009	0.076210	0.000025	46	115	15.1	2.3	0.075729	0.000019	113	182	0.073909	A
MR UMa	2010	–	–	–	–	–	–	0.064820	0.000053	61	125	–	C
TY Vul	2010	0.080465	0.000048	0	39	6.3	10.7	0.080075	0.000027	37	89	–	B
1RXS J0423	2010	0.078456	0.000033	12	40	23.1	7.5	0.077921	0.000075	79	142	0.07632	B
1RXS J0532	2009	0.057136	0.000023	0	145	10.1	1.0	0.056903	0.000030	140	215	0.05620	A
ASAS J2243	2009	0.069809	0.000014	0	101	6.6	1.0	0.069410	0.000047	101	174	–	A
Lanning 420	2010	0.061585	0.000022	0	66	5.2	3.6	0.060941	0.000043	76	175	–	B
PG 0149	2009	0.085096	0.000034	0	60	14.6	2.5	0.084602	0.000029	70	154	0.08242	B
RX J1715	2009	–	–	–	–	–	–	0.070782	0.000083	0	48	0.0683	C
SDSS J0129	2009	0.018050	0.000100	0	30	–	–	–	–	–	–	–	C
SDSS J0310	2009b	0.067863	0.000029	0	31	–	–	–	–	–	–	–	C
SDSS J0732	2010	0.079945	0.000018	0	60	3.9	2.4	0.079300	0.000028	59	129	–	B
SDSS J0839	2010	0.078520	0.000026	0	15	–	–	0.078352	0.000027	13	39	–	C
SDSS J0903	2010	0.060364	0.000050	0	116	13.7	3.2	0.060073	0.000050	116	182	0.059074	B
SDSS J1152	2009	0.068970	0.000042	0	68	–	–	–	–	–	–	0.06770	C
SDSS J1250	2008	0.060330	0.000029	0	83	9.4	2.1	–	–	–	–	0.058736	C
SDSS J1502	2009	0.060463	0.000013	0	101	3.7	1.5	0.060145	0.000019	95	135	0.058909	B
SDSS J1610	2009	0.057820	0.000019	33	150	6.4	1.2	–	–	–	–	0.05695	BE
SDSS J1625	2010	0.096054	0.000047	30	104	14.9	3.7	–	–	–	–	–	B
SDSS J1637	2004	–	–	–	–	–	–	0.069167	0.000033	0	44	0.06739	C

*Interval used for calculating the period (corresponding to E in section 3).

†Unit 10^{-5}.

‡Data quality and comments. A: excellent, B: partial coverage or slightly low quality, C: insufficient coverage or observations with large scatter, G: $P_{\rm dot}$ denotes global $P_{\rm dot}$, M: observational gap in middle stage, 2: late-stage coverage, the listed period may refer to P_2, E: $P_{\rm orb}$ refers to the period of early superhumps. P: $P_{\rm orb}$ refers to a shorter stable periodicity recorded in outburst.

Table 2. Superhump Periods and Period Derivatives (continued)

Object	Year	P_1	err	E_1		$P_{\rm dot}$	err	P_2	err	E_2		$P_{\rm orb}$	Q
SDSS J1653	2010	0.065221	0.000030	0	52	–	–	0.064961	0.000027	50	215	–	C
SDSS J2048	2009	0.061657	0.000024	0	32	–	–	–	–	–	–	0.060597	C
OT J0406	2010	–	–	–	–	–	–	0.079959	0.000027	0	62	–	C
OT J0506	2009	0.069322	0.000053	23	85	18.9	3.5	0.069016	0.000085	81	102	–	B
OT J1026	2010	0.068732	0.000033	0	59	10.1	4.6	0.068564	0.000023	57	118	–	B
OT J1122	2010	0.045440	0.000028	0	96	2.5	4.0	0.045143	0.000131	93	132	–	B
OT J1044	2010	–	–	–	–	–	–	0.060236	0.000040	195	249	0.05909	BEM
OT J1440	2009	0.064615	0.000012	15	54	−5.2	3.2	0.064412	0.000028	53	136	–	B
OT J1631	2010	0.063945	0.000024	14	72	–	–	–	–	–	–	–	C2
OT J1703	2009	0.060853	0.000023	0	51	–	–	–	–	–	–	–	C
OT J1821	2010	–	–	–	–	–	–	0.082094	0.000031	0	86	–	C
OT J2138	2010	0.055019	0.000012	36	164	7.9	0.7	0.054906	0.000006	267	521	0.05450	AE
OT J2158	2010	0.077552	0.000092	0	5	–	–	–	–	–	–	–	C
OT J2344	2010	–	–	–	–	–	–	0.076711	0.000030	0	61	–	C

Table 4. Superhump maxima of NN Cam (2009).

E	max*	error	$O-C$†	N‡
0	55137.7356	0.0010	−0.0396	71
1	55137.8129	0.0019	−0.0366	69
2	55137.8989	0.0009	−0.0249	71
12	55138.6733	0.0006	0.0064	72
13	55138.7472	0.0004	0.0060	70
14	55138.8239	0.0003	0.0084	67
15	55138.8974	0.0003	0.0076	63
19	55139.1977	0.0002	0.0107	109
20	55139.2719	0.0002	0.0106	147
21	55139.3475	0.0003	0.0119	90
39	55140.6834	0.0004	0.0102	46
40	55140.7574	0.0003	0.0099	69
41	55140.8316	0.0003	0.0098	68
42	55140.9059	0.0003	0.0098	63
61	55142.3164	0.0003	0.0085	152
76	55143.4293	0.0008	0.0068	68
77	55143.5065	0.0011	0.0097	33
78	55143.5796	0.0016	0.0084	25
79	55143.6544	0.0009	0.0089	36
87	55144.2482	0.0005	0.0083	140
103	55145.4305	0.0009	0.0017	41
104	55145.5047	0.0007	0.0015	39
105	55145.5767	0.0012	−0.0008	30
106	55145.6509	0.0007	−0.0008	40
107	55145.7255	0.0013	−0.0006	32
116	55146.3882	0.0010	−0.0066	65
117	55146.4641	0.0006	−0.0050	63
118	55146.5391	0.0005	−0.0043	104
119	55146.6146	0.0007	−0.0031	39
129	55147.3495	0.0012	−0.0113	33
130	55147.4291	0.0028	−0.0061	37
134	55147.7171	0.0013	−0.0153	39

*BJD−2400000.
†Against $max = 2455137.7752 + 0.074307E$.
‡Number of points used to determine the maximum.

had long been overlooked due to the apparent small outburst amplitude. The lack of CV-type signature in spectroscopic observation by Schmidtobreick et al. (2005) even led to a non-CV classification. Monitoring for outbursts, however, continued because of its outbursting nature and the likely presence of superoutbursts. In 2006, B. Monard succeeded in obtaining astrometry of the outbursting object, which was 3 arcsec distant from the supposed quiescent counterpart (vsnet-alert 9158). The true V591 Cen was invisible down to 20 mag on DSS images.

The object again underwent a bright outburst in 2010 April (vsnet-alert 11915), and the existence of superhumps was finally confirmed (vsnet-alert 11919; figure 3). Astrometry of the outbursting object also confirmed the identification in 2006 (vsnet-alert 11922).

The times of superhump maxima are listed in table 5. The data clearly shows a positive period derivative $P_{\rm dot} = +6.5(1.3) \times 10^{-5}$, typical for this short $P_{\rm SH}$.

3.4. *Z Chameleontis*

We analyzed AAVSO and our observations of the 2010 January superoutburst of Z Cha. The observation was performed during the late stage of the superoutburst. After removing observations within 0.10 $P_{\rm orb}$ of eclipses for the superoutburst plateau and 0.08 $P_{\rm orb}$ for later observations, we determined times of superhump maxima (table 6). The times for $E \geq 91$ are secondary humps, which are likely traditional late superhumps. The peaks of persistent ordinary superhumps were not determined because they fell on orbital humps and around eclipses. These superhumps ($E < 91$) most likely correspond to stage C superhumps. The period [0.07698(5) d] determined from the superhump maxima is close to the period [0.07681(6) d] of stage C superhumps in 1982 (Kato et al. 2009a).

Although post-superoutburst observation suggests the appearance of traditional late superhumps, this signal was not well traced due to the strong orbital modulation and limited coverage. A better continuous observation is necessary to test whether dominant superhumps in the post-

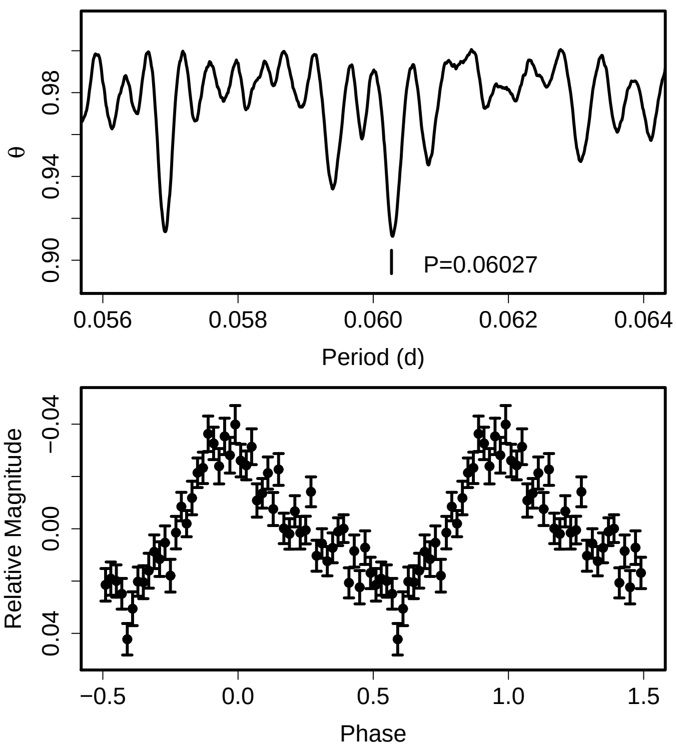

Fig. 3. Superhumps in V591 Cen (2010). (Upper): PDM analysis. The selection of the alias was based on $O-C$ analysis. (Lower): Phase-averaged profile.

Table 5. Superhump maxima of V591 Cen (2010).

E	max*	error	$O-C$†	N‡
0	55296.1418	0.0008	0.0022	111
1	55296.2051	0.0007	0.0052	109
2	55296.2634	0.0011	0.0033	111
17	55297.1647	0.0009	0.0001	110
18	55297.2252	0.0008	0.0003	111
19	55297.2849	0.0011	−0.0003	112
20	55297.3425	0.0014	−0.0030	70
86	55301.3271	0.0032	0.0019	267
87	55301.3806	0.0020	−0.0050	268
88	55301.4362	0.0018	−0.0097	267
89	55301.4977	0.0017	−0.0084	268
102	55302.2868	0.0039	−0.0033	268
133	55304.1630	0.0018	0.0036	61
134	55304.2236	0.0030	0.0040	103
135	55304.2836	0.0015	0.0036	329
136	55304.3447	0.0014	0.0044	281
137	55304.4012	0.0014	0.0006	264
138	55304.4612	0.0027	0.0004	73

*BJD−2400000.
†Against $max = 2455296.1395 + 0.060299E$.
‡Number of points used to determine the maximum.

Table 6. Superhump maxima of Z Cha (2010).

E	max*	error	$O-C$†	N‡
0	55200.0935	0.0008	0.0032	152
13	55201.0794	0.0003	−0.0086	209
14	55201.1575	0.0003	−0.0072	165
15	55201.2328	0.0001	−0.0087	124
27	55202.1711	0.0021	0.0086	24
28	55202.2385	0.0015	−0.0007	22
65	55205.0878	0.0006	0.0088	158
66	55205.1638	0.0005	0.0081	159
67	55205.2385	0.0007	0.0060	94
78	55206.0940	0.0007	0.0173	130
79	55206.1667	0.0011	0.0132	62
80	55206.2399	0.0007	0.0097	159
91	55207.0442	0.0015	−0.0303	168
92	55207.1319	0.0009	−0.0194	169

*BJD−2400000.
†Against $max = 2455200.0902 + 0.076750E$.
‡Number of points used to determine the maximum.

superoutburst stage are stage C superhumps or traditional late superhumps (see also a discussion on the nature of late superhumps in Ohshima et al. 2010).

3.5. PU Canis Majoris

We observed the 2009 superoutburst of this object (table 7). The nightly superhump profiles (figure 4) suggests that the superhump period first increased until BJD 2455164, and then decreased. The stages listed in table 2 reflect this interpretation. A comparison of $O-C$ diagrams between different superoutbursts is shown in figure 5). It would be worth noting that the $O-C$ diagram for the 2008 superoutburst (superoutburst preceded by a precursor) matched others only if E was counted from the start of the main superoutburst, rather than from the precursor. This suggests that superhumps were excited around the ignition of the main superoutburst, rather than during the precursor.

3.6. AQ Canis Minoris

Although the SU UMa-type nature of this object has been well established,[3] there has unfortunately no solid publication on superhumps in this system. The only known superoutburst since the 1997 observation was in 2008 September, which was too badly placed for time-series photometry. The superoutburst in 2010 April brought the first chance to record superhumps since its recognition as an SU UMa-type dwarf nova. The times of superhump maxima are listed in table 8. Although the course of the superhump evolution was not fully recorded, there appears to have been a discontinuous period change around $E = 15$. We attributed this to stage A–B transition because the observation recorded the early stage of the superoutburst. The period derivative was not determined because of a gap in observation. The mean $P_{\rm SH}$

[3] <http://www.kusastro.kyoto-u.ac.jp/vsnet/DNe/aqcmi.html>.

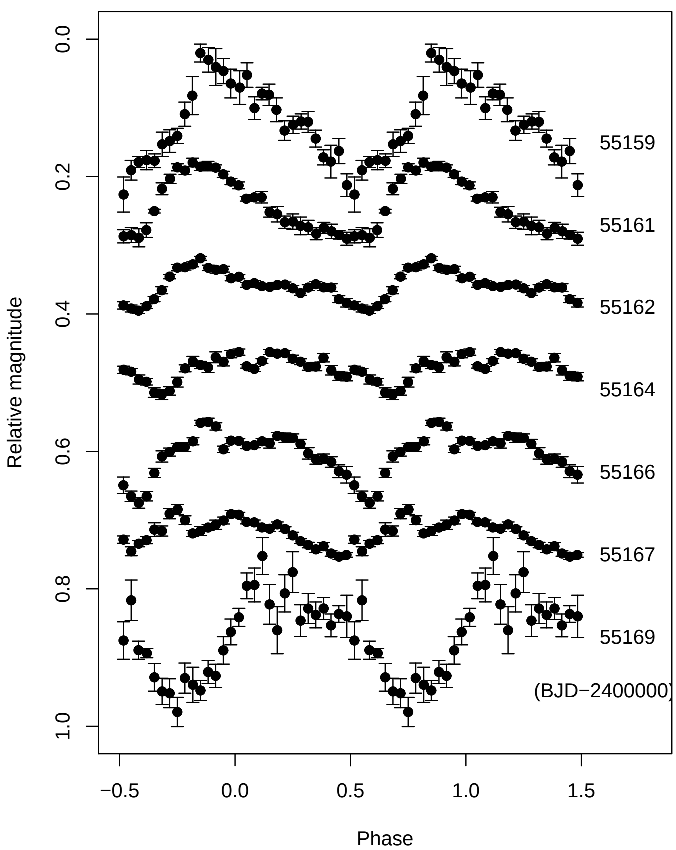

Fig. 4. Superhump profiles of PU CMa (2009). The profiles of superhumps strongly varied between nights. The figure was drawn against a mean period of 0.058020 d.

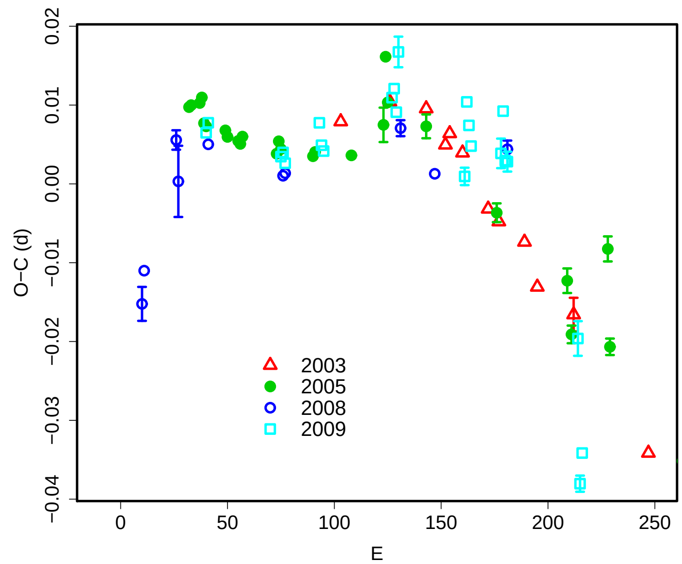

Fig. 5. Comparison of $O-C$ diagrams of PU CMa between different superoutbursts. A period of 0.05801 d was used to draw this figure. Approximate cycle counts (E) after the appearance of the superhumps were used. Since the start of the 2009 superoutburst was not well constrained, we shifted the $O-C$ diagrams to best fit the others. The $O-C$ diagram for the 2008 superoutburst matched others only if E was counted from the start of the main superoutburst, rather than from the precursor.

during the entire observation was 0.06622(1) d (figure 6). This period needs to be treated with caution because it was likely derived from different stages of superhump evolution.

3.7. *GZ Cancri*

GZ Cnc is a variable star discovered by Takamizawa (TmzV34, vsnet-obs 10504), which later turned out to be a dwarf nova (Kato et al. 2001b). Kato et al. (2001b) observed an outburst in 2000 February. Based on the relatively slow rise to an outburst maximum and the lack of periodic modulations, they concluded that the object is likely an SS Cyg-type dwarf nova with a long $P_{\rm orb}$. In 2002, Kato et al. (2002a) noticed an unusually increase in the number of outburst detections, and suggested the similarity to a proposed intermediate polar V426 Oph. Most surprisingly, radial-velocity studies by Tappert, Bianchini (2003) yielded an $P_{\rm orb}$ of 0.08825(28) d, placing the object at the lower edge of the period gap. Although this $P_{\rm orb}$ was seemingly incompatible with behavior of outbursts in this object, later observations have detected abundant short outbursts which are compatible with a short $P_{\rm orb}$-system. The mystery, however, remained why the object did not develop superhumps during its long, 2000 February outburst.

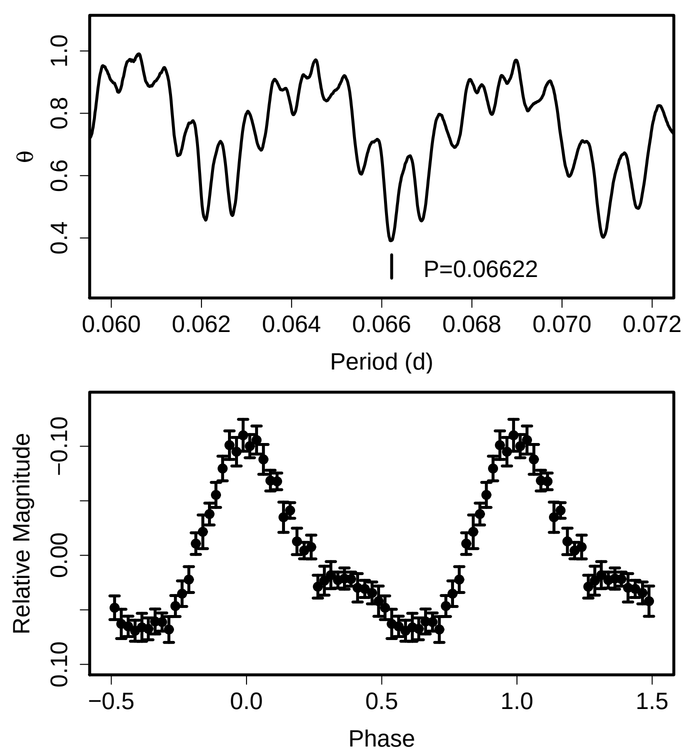

Fig. 6. Superhumps in AQ CMi (2010). (Upper): PDM analysis. The selection of the alias is based on the best period reported from past observations. (Lower): Phase-averaged profile.

Table 7. Superhump maxima of PU CMa (2009).

E	max*	error	$O-C$†	N‡
0	55159.1299	0.0009	−0.0110	66
1	55159.1892	0.0008	−0.0096	65
35	55161.1572	0.0007	−0.0083	53
36	55161.2158	0.0003	−0.0076	84
37	55161.2724	0.0005	−0.0088	82
53	55162.2057	0.0010	−0.0011	193
54	55162.2609	0.0004	−0.0038	186
55	55162.3181	0.0005	−0.0043	179
87	55164.1812	0.0008	0.0076	85
88	55164.2404	0.0008	0.0090	248
89	55164.2954	0.0009	0.0061	249
90	55164.3611	0.0019	0.0139	102
121	55166.1436	0.0011	0.0032	150
122	55166.2110	0.0007	0.0128	334
123	55166.2661	0.0005	0.0100	263
124	55166.3215	0.0006	0.0075	165
137	55167.0993	0.0035	0.0334	128
138	55167.1327	0.0019	0.0089	208
139	55167.1960	0.0006	0.0144	316
140	55167.2478	0.0005	0.0083	273
141	55167.3057	0.0013	0.0083	168
174	55169.1975	0.0022	−0.0087	84
175	55169.2371	0.0010	−0.0270	85
176	55169.2990	0.0007	−0.0229	82
192	55170.2172	0.0017	−0.0304	78

*BJD−2400000.
†Against $max = 2455159.1409 + 0.057847E$.
‡Number of points used to determine the maximum.

Table 8. Superhump maxima of AQ CMi (2010).

E	max*	error	$O-C$†	N‡
0	55295.9806	0.0006	−0.0022	116
1	55296.0489	0.0007	−0.0002	112
15	55296.9775	0.0005	0.0017	104
16	55297.0431	0.0005	0.0011	121
106	55302.9994	0.0009	−0.0004	68

*BJD−2400000.
†Against $max = 2455295.9828 + 0.066198E$.
‡Number of points used to determine the maximum.

Later on, the object again exhibited a long outburst in 2007 December (vsnet-alert 9783), which was unfortunately not observed for searching superhumps. In 2009 January, this object underwent a long, bright outburst (vsnet-alert 10984). Follow-up observations, however, did not detect superhumps (vsnet-alert 11002). GZ Cnc was then considered as a rare object below the period gap without a signature of an SU UMa-type dwarf nova.

In 2010 March, the object again underwent a long, bright outburst (vsnet-alert 11855, 11863). Subsequent observations eventually detected superhumps (vsnet-alert 11881, 11888, 11890, 11894). The object is now confirmed to be a rare object exhibiting three classes of outbursts: normal (narrow) outbursts, long SS Cyg-type (wide) outbursts and SU UMa-type superoutbursts (figure 7). The mystery of the 2000 outburst could be understood if this outburst was a "long" outburst failing to trigger the tidal instability. The only other known object having the same property is TU Men (cf. Bateson 1989; Smak 2000), unusual SU UMa-type dwarf nova above the period gap. If GZ Cnc is indeed a "borderline" SU UMa-type dwarf nova, the object may be analogous to BZ UMa, which also showed an usually slow rise to a full outburst (cf. Kato et al. 2009a).

The times of superhump maxima during the 2010 superoutburst are listed in table 9. The $O-C$ diagram can be reasonably interpreted without a phase jump only if we assume a very large decrease in the period as in AX Cap (figure 8). The mean $P_{\rm SH}$ for $E \le 44$ was 0.09277(2) d (PDM method), which is equivalent to $\epsilon = 5.1$ %. This fractional superhump excess is one of the largest among SU UMa-type dwarf novae below the period gap (cf. figure 15 in Kato et al. 2009a). The mean period 0.08972(12) d after the period decrease corresponds to $\epsilon = 1.7$ %. Since this period was fairly close to $P_{\rm orb}$, this period decrease may have reflected the dominance of orbital humps during the late course of the superoutburst.

3.8. GO Comae Berenices

The 2010 superoutburst was particularly well observed and stages B and C were very clearly defined (table 10). These observations have confirmed the finding in Imada et al. (2005) and Kato et al. (2009a). Figure 11 illustrates a comparison of $O-C$ diagrams between different superoutbursts. The 2010 observation better recorded the stage C superhumps with higher accuracy, while the 2003 observation well recorded the earlier part. A combination of these superoutbursts very well demonstrates the "canonical" period variation in a short-$P_{\rm SH}$ system. It is not clear whether the 2010 superoutburst was preceded by a precursor outburst as in the 2003 one.

3.9. TV Corvi

We observed an superoutburst in 2009 December. The times of superhump maxima are listed in table 11. A combined $O-C$ diagram (figure 12) strengthens the assertion in Kato et al. (2009a) that the $O-C$ behavior is common between different superoutbursts.

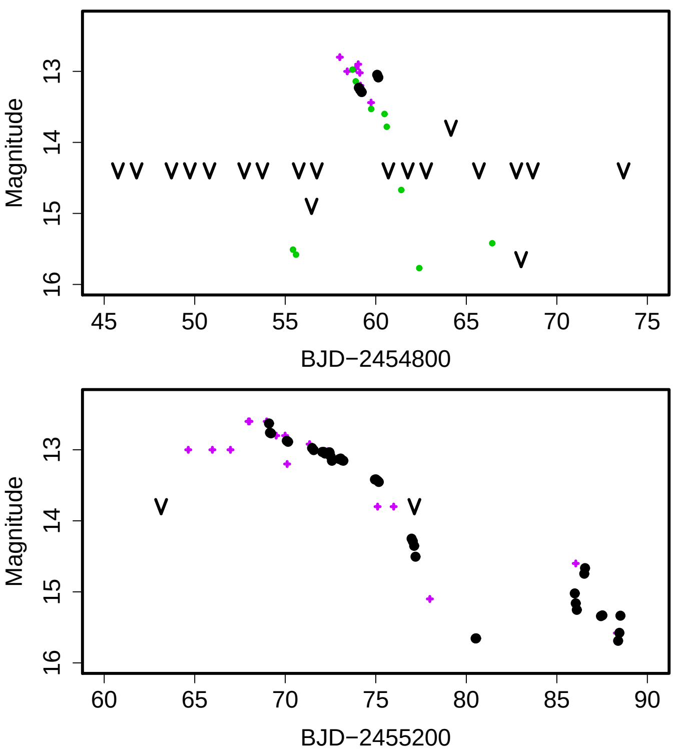

Fig. 7. Comparison of wide outburst (upper, 2009) and superoutburst (lower, 2010) of GZ Cnc. The filled circles, open circles, small crosses and "v"-marks represent CCD observations, ASAS-3 V data and visual observations, and upper limits, respectively. The outburst around BJD 2455287 is a normal outburst.

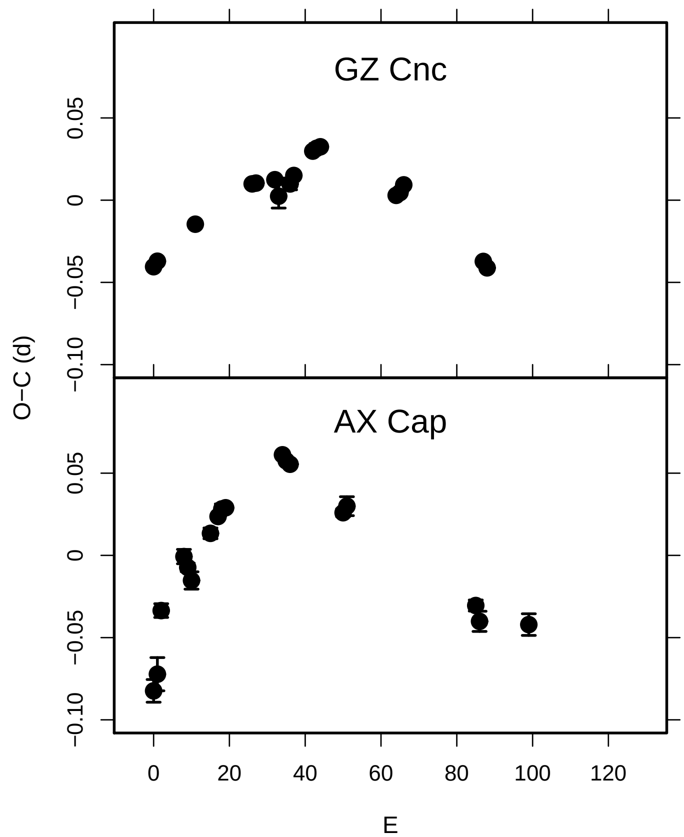

Fig. 8. Comparison of $O-C$ diagrams between GZ Cnc and AX Cap.

Table 9. Superhump maxima of GZ Cnc (2010).

E	max*	error	$O-C$†	N‡
0	55269.0989	0.0007	−0.0405	64
1	55269.1935	0.0007	−0.0371	52
11	55270.1286	0.0008	−0.0146	175
26	55271.5221	0.0007	0.0099	86
27	55271.6139	0.0015	0.0104	55
32	55272.0723	0.0006	0.0124	226
33	55272.1535	0.0072	0.0024	48
36	55272.4347	0.0036	0.0099	57
37	55272.5312	0.0012	0.0150	93
42	55273.0023	0.0016	0.0298	53
43	55273.0952	0.0029	0.0315	74
44	55273.1874	0.0016	0.0325	88
64	55274.9832	0.0010	0.0029	97
65	55275.0761	0.0008	0.0046	276
66	55275.1721	0.0016	0.0093	160
87	55277.0421	0.0006	−0.0373	346
88	55277.1295	0.0007	−0.0412	173

*BJD−2400000.
†Against $max = 2455269.1393 + 0.091265E$.
‡Number of points used to determine the maximum.

3.10. V337 Cygni

We observed the 2010 superoutburst of this object. The times of superhump maxima are listed in table 12. Although the period derivative was not well determined, we detected a stage B–C transition. The obtained parameters are listed in table 2.

3.11. V1113 Cygni

Bakowska et al. (2010) recently reported new observations of 2003 and 2005 superoutbursts, and claimed the presence of a large negative period derivative. Upon examination of their observations, it has become evident that they observed the apparently late stage of a superoutburst in 2003. Using the typical duration ($\sim$ 11 d) of superoutbursts in this system, their observation probably started $\sim$ 94 cycles after the start of the superoutburst, and they most likely caught a stage B–C transition. A combined $O-C$ diagram based on this interpretation, supplemented by early observations reported in Kato et al. (2009a), is shown in figure 13. As judged from this figure, the evolution of the superhump period is not particularly unusual in this system.

3.12. V1454 Cygni

This object was only partly observed during the 2006 superoutburst (Kato et al. 2009a). The 2009 superout-

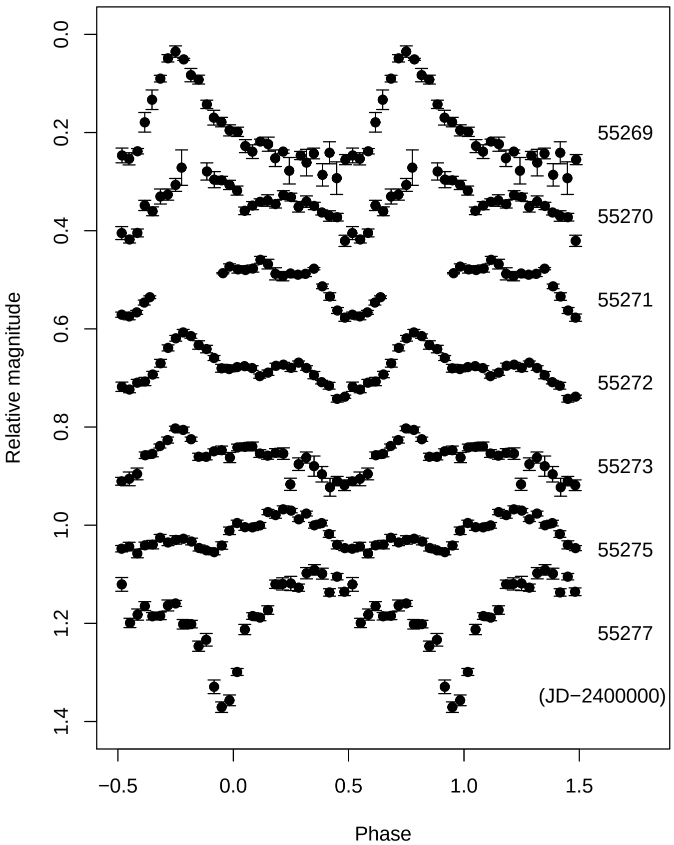

Fig. 9. Superhump profiles of GZ Cnc (2010). The figure was drawn against a mean period of 0.09277 d. JD 2455275 corresponds to the start of the rapid fading from the superoutburst plateau.

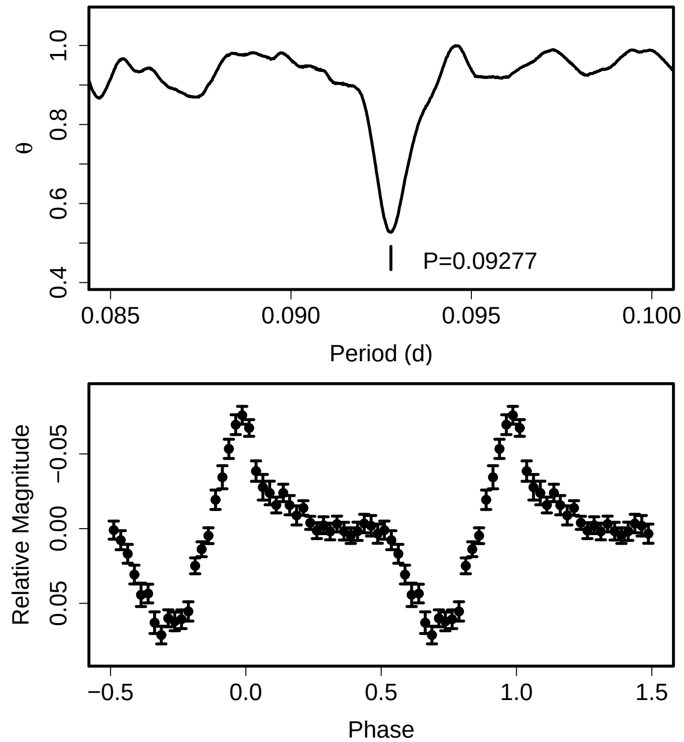

Fig. 10. Superhumps in GZ Cnc before JD 2455274 (2010). (Upper): PDM analysis. (Lower): Phase-averaged profile.

burst was detected during its early stage (I. Miller, baavss-alert 2020, vsnet-alert 11376). A delay of ≥6.5 d in the full growth of ordinary superhumps was recorded (vsnet-alert 11393, 11395). The new observation now clarified the alias selection [0.05769(2) d with the PDM method] and safely excluded the 0.0610 d earlier reported (figure 14). The $P_{\rm dot}$ for stage B was $+10.3(3.5)\times 10^{-5}$, fairly common for this short $P_{\rm SH}$. Although there was likely a stage B–C transition after $E=95$, we could not determine the period of stage C superhumps due to the lack of observations. An analysis of the earlier observation (BJD before 2455058) has yielded a weak signal of 0.05777(2) d. Although the extraction of times of superhump maxima was difficult due to the low amplitudes, this period suggests that this interval involved stage A evolution rather than a manifestation of early superhumps.

3.13. AQ Eridani

We observed another superoutburst in 2010 (table 14). There was a relatively large scatter in the $O-C$ diagram after the rapid fading due to its faintness. We therefore did not attempt to determine the period during stage C. The mean $P_{\rm SH}$ appears to confirm the previous period determination (cf. figure 15).

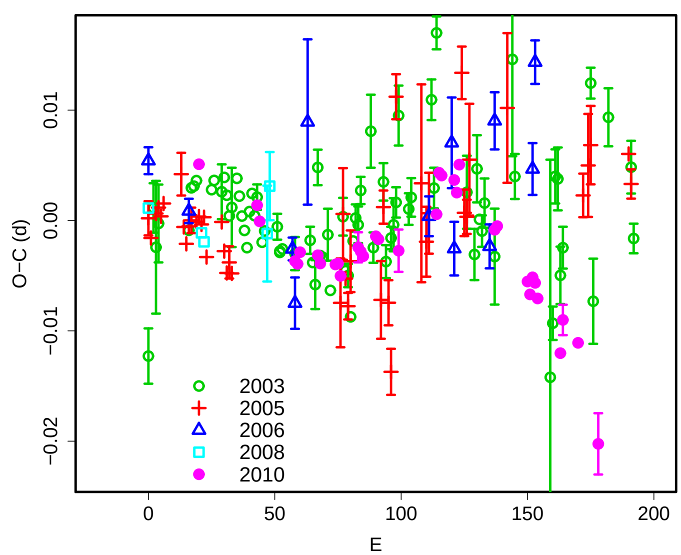

Fig. 11. Comparison of $O-C$ diagrams of GO Com between different superoutbursts. A period of 0.06303 d was used to draw this figure. Approximate cycle counts (E) after the appearance of the superhumps were used.

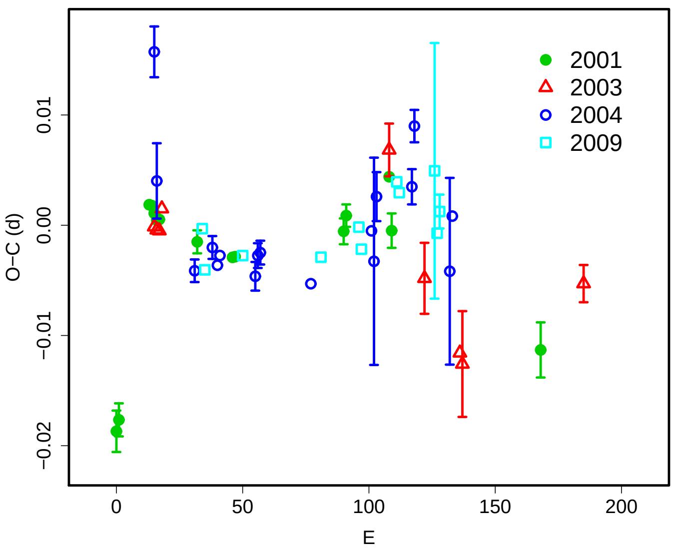

Fig. 12. Comparison of $O-C$ diagrams of TV Crv between different superoutbursts. A period of 0.06500 d was used to draw this figure. Approximate cycle counts (E) after the appearance of the superhumps were used.

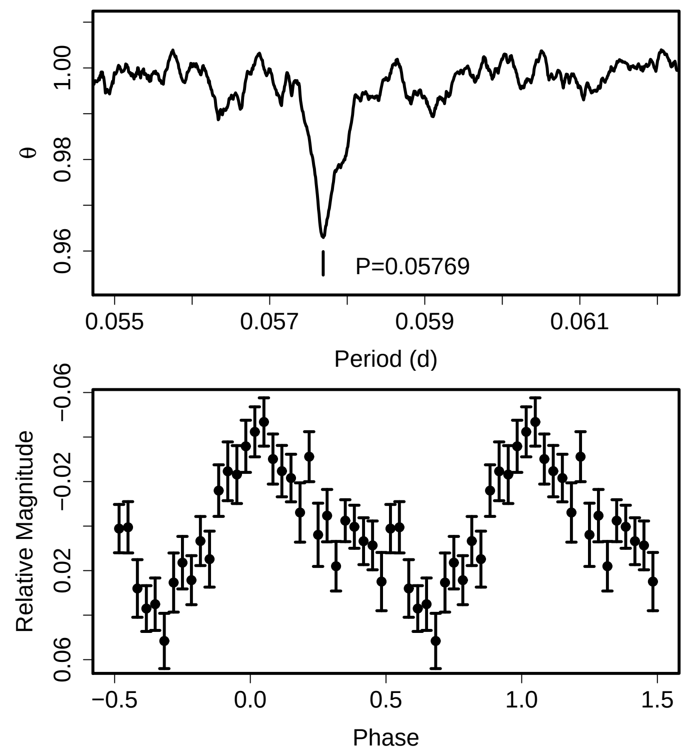

Fig. 14. Superhumps in V1454 Cyg (2009). (Upper): PDM analysis. (Lower): Phase-averaged profile.

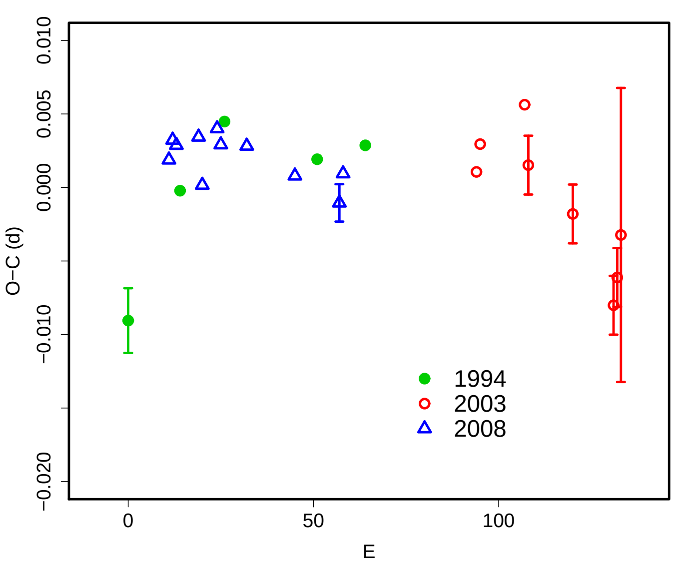

Fig. 13. Comparison of $O-C$ diagrams of V1113 Cyg between different superoutbursts. A period of 0.07911 d was used to draw this figure. Approximate cycle counts (E) after the start of the superoutburst were used.

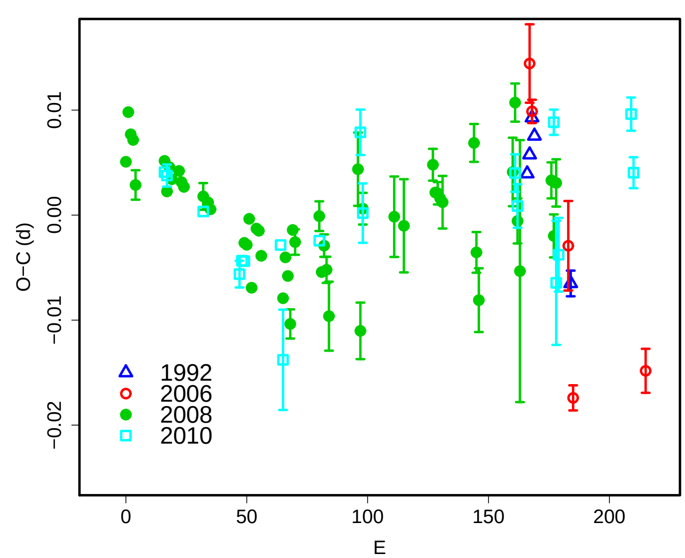

Fig. 15. Comparison of $O-C$ diagrams of AQ Eri between different superoutbursts. A period of 0.06238 d was used to draw this figure. Approximate cycle counts (E) after the appearance of the superhumps were used. Due to the lack of early observations, the $O-C$ diagrams for the 1992 and 2006 were shifted to better match the 2008 one.

Table 10. Superhump maxima of GO Com (2010).

E	max*	error	$O-C$†	N‡
0	55286.1498	0.0006	0.0028	93
23	55287.5958	0.0004	0.0005	61
24	55287.6574	0.0004	−0.0009	37
38	55288.5362	0.0006	−0.0036	41
39	55288.5989	0.0003	−0.0038	61
40	55288.6630	0.0004	−0.0027	55
47	55289.1040	0.0002	−0.0026	127
48	55289.1663	0.0004	−0.0032	127
54	55289.5443	0.0004	−0.0030	50
55	55289.6075	0.0003	−0.0028	66
56	55289.6694	0.0005	−0.0039	66
63	55290.1132	0.0014	−0.0008	40
64	55290.1758	0.0004	−0.0012	40
65	55290.2384	0.0009	−0.0015	40
70	55290.5554	0.0005	0.0006	64
71	55290.6181	0.0004	0.0004	61
79	55291.1213	0.0019	−0.0002	36
94	55292.0701	0.0008	0.0041	135
95	55292.1369	0.0006	0.0079	159
96	55292.1997	0.0006	0.0077	96
101	55292.5144	0.0005	0.0076	60
102	55292.5763	0.0004	0.0065	64
103	55292.6419	0.0005	0.0091	66
117	55293.5184	0.0004	0.0041	60
118	55293.5817	0.0003	0.0045	39
130	55294.3331	0.0006	0.0002	66
131	55294.3949	0.0008	−0.0009	62
132	55294.4595	0.0004	0.0007	77
133	55294.5220	0.0005	0.0003	114
134	55294.5837	0.0004	−0.0011	132
143	55295.1460	0.0009	−0.0055	178
144	55295.2120	0.0014	−0.0024	38
150	55295.5881	0.0005	−0.0041	63
158	55296.0832	0.0028	−0.0128	28

*BJD−2400000.
†Against $max = 2455286.1470 + 0.062968E$.
‡Number of points used to determine the maximum.

Table 11. Superhump maxima of TV Crv (2009).

E	max*	error	$O-C$†	N‡
0	55183.2495	0.0004	0.0028	125
1	55183.3107	0.0003	−0.0010	144
16	55184.2870	0.0005	−0.0005	108
47	55186.3019	0.0006	−0.0024	143
62	55187.2796	0.0008	−0.0005	142
63	55187.3426	0.0007	−0.0025	121
77	55188.2587	0.0008	0.0028	143
78	55188.3227	0.0006	0.0018	144
92	55189.2347	0.0116	0.0030	114
93	55189.2941	0.0009	−0.0027	144
94	55189.3610	0.0015	−0.0008	82

*BJD−2400000.
†Against $max = 2455183.2467 + 0.065054E$.
‡Number of points used to determine the maximum.

Table 12. Superhump maxima of V337 Cyg (2010).

E	max*	error	$O-C$†	N‡
0	55421.4715	0.0012	−0.0046	118
1	55421.5390	0.0007	−0.0072	153
29	55423.5087	0.0007	−0.0009	75
42	55424.4236	0.0007	0.0024	73
43	55424.4944	0.0006	0.0032	72
44	55424.5626	0.0007	0.0012	77
45	55424.6340	0.0011	0.0025	54
51	55425.0473	0.0078	−0.0050	36
52	55425.1288	0.0019	0.0064	63
95	55428.1525	0.0013	0.0149	30
126	55430.3163	0.0065	0.0050	119
138	55431.1449	0.0010	−0.0079	128
139	55431.2128	0.0020	−0.0101	147

*BJD−2400000.
†Against $max = 2455421.4761 + 0.070121E$.
‡Number of points used to determine the maximum.

3.14. VX Fornacis

VX For was discovered in 1990 as a probable dwarf nova showing Balmer, HeI and possibly HeII emission lines (Liller et al. 1990). The large outburst amplitude and the outburst lasting for more than 10 d (Liller et al. 1999) were already suggestive of an SU UMa-type superoutburst. The object has been listed as a good candidate for a WZ Sge-type dwarf nova (Kato et al. 2001a).

The 2009 outburst, first-ever since the initial discovery, was detected by R. Stubbings on 2009 Sep. 14 at a visual magnitude of 13.0 (vsnet-alert 11471). Ordinary superhump were soon observed following this outburst detection (vsnet-alert 11474). Although the early appearance of ordinary superhumps was initially considered as unfavorable for the WZ Sge-type interpretation, a later retrospective detection of earlier positive observation in the ASAS-3 data ($V = 12.61$ on September 10) indicated that the early stage of the outburst was missed when early superhumps were expected (vsnet-alert 11492). Using the empirical classification of WZ Sge-type dwarf novae introduced in Kato et al. (2009a), T. Kato suggested that the object is expected to undergo multiple rebrightenings as in EG Cnc based on relatively small $P_{\rm dot}$ obtained from early observations and a relatively long $P_{\rm SH}$ (vsnet-alert 11492). The object indeed underwent five rebrightenings (vsnet-alert 11521, 11526, 11536, 11577, 11602; figure 16), making it the first object predicted for its multiple rebrightening in real-time. The overall behavior is very similar to that of ASAS J153616−0839.1 (Kato et al. 2009a).

The mean $P_{\rm SH}$ during the plateau phase was 0.061355(7) d (PDM method, figure 17). The times of superhump maxima during the plateau phase and fading stage are listed in table 15.

The superhumps persisted during the post-

Table 13. Superhump maxima of V1454 Cyg (2009).

E	max*	error	$O-C$†	N‡
0	55058.1434	0.0004	0.0055	122
1	55058.2036	0.0013	0.0081	65
39	55060.3868	0.0010	0.0001	57
40	55060.4431	0.0024	−0.0013	54
41	55060.4996	0.0010	−0.0025	56
42	55060.5540	0.0035	−0.0057	54
50	55061.0219	0.0009	0.0009	109
51	55061.0756	0.0019	−0.0031	107
52	55061.1361	0.0024	−0.0003	121
53	55061.1919	0.0020	−0.0021	121
54	55061.2405	0.0033	−0.0112	115
56	55061.3703	0.0016	0.0033	54
57	55061.4258	0.0009	0.0012	52
58	55061.4806	0.0009	−0.0017	56
59	55061.5380	0.0011	−0.0020	57
60	55061.5956	0.0042	−0.0021	52
75	55062.4672	0.0019	0.0046	57
76	55062.5230	0.0027	0.0027	57
86	55063.0867	0.0032	−0.0101	114
87	55063.1513	0.0064	−0.0032	121
88	55063.2097	0.0155	−0.0024	86
92	55063.4463	0.0024	0.0035	56
93	55063.5010	0.0033	0.0005	57
94	55063.5635	0.0023	0.0054	57
95	55063.6254	0.0029	0.0095	30
160	55067.3705	0.0019	0.0066	57
161	55067.4330	0.0020	0.0115	54
163	55067.5267	0.0037	−0.0102	57
164	55067.5890	0.0019	−0.0055	54

*BJD−2400000.
†Against $max = 2455058.1379 + 0.057662E$.
‡Number of points used to determine the maximum.

superoutburst and rebrightening phase. We obtained $P_{\rm SH}$ = 0.06129(2) d, slightly short than that of the superoutburst plateau phase (figure 18). There was some indication of a signal around $P = 0.06156$ d (small excess signal in figure 18) and transient appearance of this period (cf. vsnet-alert 11513). Although this signal needs to be confirmed with better data, this might be analogous to long-period late-stage superhumps in WZ Sge-type dwarf novae (Kato et al. 2008; Kato et al. 2009a).

3.15. *AW Geminorum*

The times of superhump maxima during the 2010 superoutburst is listed in table 16. A stage B–C transition was well recorded. Although only parts of superoutbursts were observed in individual years, the combined $O-C$ diagram (figure 19) clearly demonstrates the universal pattern of period evolution.

3.16. *IR Geminorum*

The times of superhump maxima during the 2010 superoutburst is listed in table 17. Although the object was ob-

Table 14. Superhump maxima of AQ Eri (2010).

E	max*	error	$O-C$†	N‡
0	55201.0094	0.0004	0.0067	54
1	55201.0715	0.0011	0.0064	37
16	55202.0038	0.0003	0.0025	102
31	55202.9335	0.0013	−0.0039	65
32	55202.9972	0.0003	−0.0027	223
33	55203.0595	0.0004	−0.0027	73
48	55203.9967	0.0006	−0.0016	90
49	55204.0482	0.0048	−0.0126	51
64	55204.9952	0.0008	−0.0017	100
81	55206.0660	0.0022	0.0081	45
82	55206.1207	0.0028	0.0004	37
145	55210.0545	0.0018	0.0023	142
146	55210.1137	0.0021	−0.0008	146
161	55211.0574	0.0012	0.0067	68
162	55211.1045	0.0059	−0.0086	65
163	55211.1695	0.0035	−0.0060	101
193	55213.0543	0.0016	0.0065	61
194	55213.1111	0.0015	0.0009	91

*BJD−2400000.
†Against $max = 2455201.0027 + 0.062410E$.
‡Number of points used to determine the maximum.

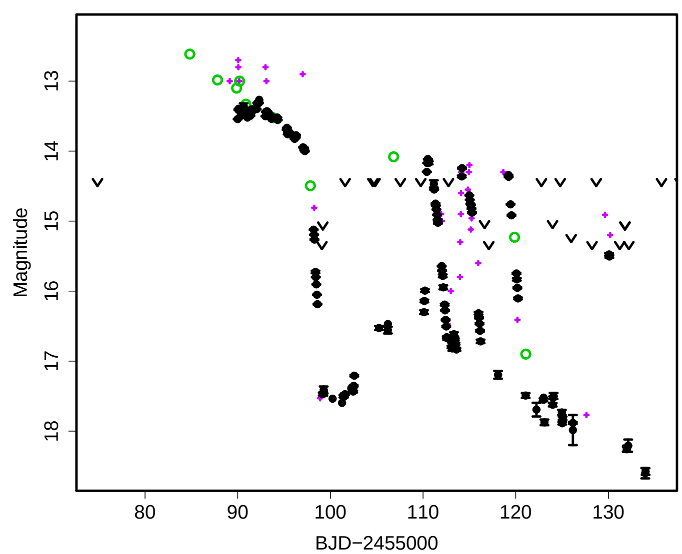

Fig. 16. Light curve of VX For (2009). The filled circles, open circles and small crosses represent CCD observations used here, ASAS-3 V data and visual observations, respectively.

Table 15. Superhump maxima of VX For (2009).

E	max*	error	$O-C$†	N‡
0	55090.0917	0.0002	−0.0100	991
6	55090.4665	0.0004	−0.0026	258
7	55090.5274	0.0004	−0.0029	258
8	55090.5873	0.0003	−0.0042	230
19	55091.2630	0.0007	−0.0019	104
20	55091.3216	0.0006	−0.0046	104
21	55091.3893	0.0004	0.0019	252
22	55091.4483	0.0003	−0.0003	229
23	55091.5073	0.0015	−0.0025	51
24	55091.5683	0.0015	−0.0028	116
32	55092.0586	0.0010	−0.0022	42
33	55092.1223	0.0005	0.0003	68
34	55092.1822	0.0009	−0.0011	66
35	55092.2450	0.0008	0.0005	84
36	55092.3078	0.0007	0.0021	30
48	55093.0420	0.0003	0.0016	349
49	55093.0999	0.0003	−0.0018	127
50	55093.1617	0.0003	−0.0012	159
51	55093.2244	0.0006	0.0003	95
55	55093.4687	0.0003	−0.0003	223
56	55093.5293	0.0003	−0.0009	261
57	55093.5909	0.0003	−0.0006	261
66	55094.1453	0.0015	0.0028	51
67	55094.2044	0.0011	0.0007	41
68	55094.2659	0.0008	0.0010	162
69	55094.3264	0.0018	0.0002	68
85	55095.3094	0.0012	0.0037	126
87	55095.4308	0.0008	0.0026	258
88	55095.4932	0.0006	0.0038	214
89	55095.5545	0.0005	0.0039	213
99	55096.1696	0.0013	0.0068	52
100	55096.2289	0.0011	0.0049	46
101	55096.2960	0.0020	0.0108	33
115	55097.1400	0.0049	−0.0024	24
132	55098.1979	0.0017	0.0147	22
133	55098.2561	0.0012	0.0117	32
137	55098.4994	0.0014	0.0100	258
149	55099.2215	0.0059	−0.0025	23
185	55101.4220	0.0094	−0.0061	134
186	55101.4843	0.0031	−0.0050	134
187	55101.5307	0.0027	−0.0198	134
201	55102.3908	0.0103	−0.0169	125
202	55102.4749	0.0167	0.0061	135
203	55102.5323	0.0018	0.0022	135
204	55102.5907	0.0018	−0.0006	133

*BJD−2400000.
†Against $max = 2455090.1017 + 0.061224E$.
‡Number of points used to determine the maximum.

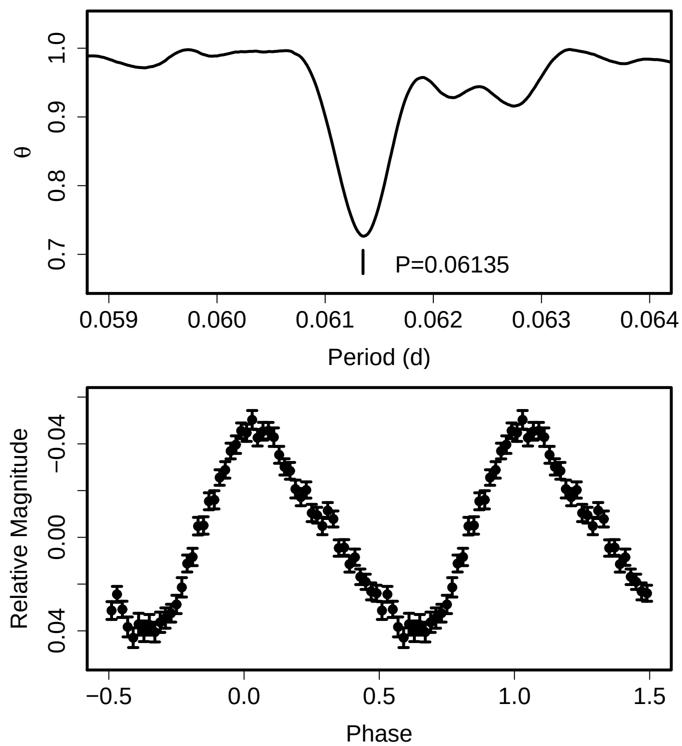

Fig. 17. Superhumps in VX For during the superoutburst plateau (2009). (Upper): PDM analysis. (Lower): Phase-averaged profile.

Table 16. Superhump maxima of AW Gem (2010).

E	max*	error	$O-C$†	N‡
0	55257.3860	0.0002	−0.0033	72
1	55257.4640	0.0003	−0.0040	40
2	55257.5425	0.0004	−0.0042	69
24	55259.2830	0.0004	0.0040	81
25	55259.3619	0.0004	0.0041	80
26	55259.4398	0.0005	0.0033	80
51	55261.4091	0.0004	0.0041	69
52	55261.4873	0.0005	0.0035	61
53	55261.5602	0.0012	−0.0024	37
101	55265.3439	0.0029	0.0018	43
102	55265.4189	0.0008	−0.0020	78
103	55265.4946	0.0006	−0.0050	79

*BJD−2400000.
†Against $max = 2455257.3892 + 0.078742E$.
‡Number of points used to determine the maximum.

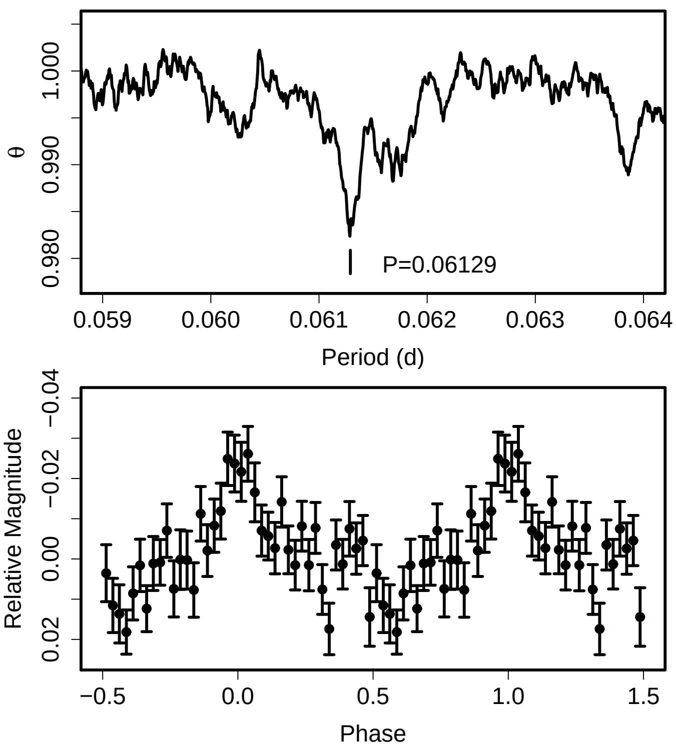

Fig. 18. Superhumps in VX For during the post-superoutburst and rebrightening phase (2009). (Upper): PDM analysis. (Lower): Phase-averaged profile.

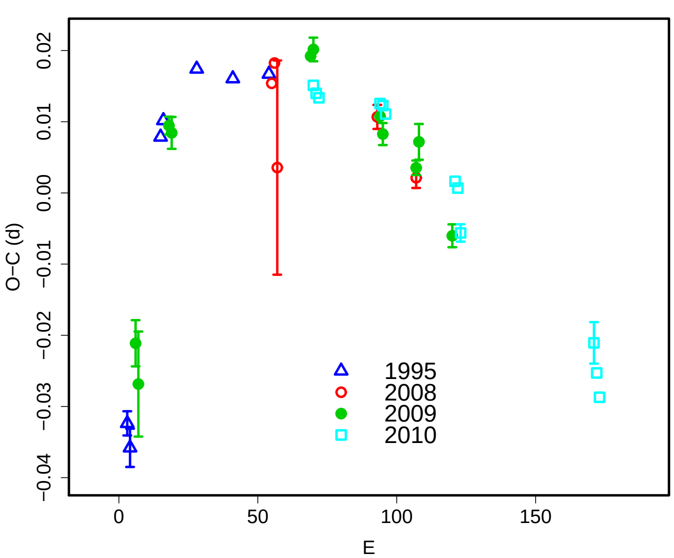

Fig. 19. Comparison of $O-C$ diagrams of AW Gem between different superoutbursts. A period of 0.07915 d was used to draw this figure. Approximate cycle counts (E) after the start of the superoutburst were used. Since the start of 2008 and 2010 superoutburst were poorly constrained, we shifted the $O-C$ diagrams to best match other other superoutbursts.

Table 17. Superhump maxima of IR Gem (2010).

E	max*	error	$O-C$†	N‡
0	55265.4201	0.0004	0.0003	65
1	55265.4903	0.0004	−0.0003	67
56	55269.3867	0.0003	0.0002	71
57	55269.4573	0.0004	−0.0000	73
58	55269.5280	0.0007	−0.0002	50

*BJD−2400000.
†Against $max = 2455265.4198 + 0.070834E$.
‡Number of points used to determine the maximum.

served on only two nights, the period is in good agreement with earlier observations. The observations was likely performed during stage B.

3.17. V592 Herculis

V592 Her was discovered as a possible fast nova in 1968 on Sonneberg plates (Richter 1968). Richter (1991) further discovered a second outburst in 1986 on historical plates. In 1998, another outburst was recorded which led to the identification of this object as being a WZ Sge-type dwarf nova (Duerbeck, Mennickent 1998; Kato et al. 2002b). Kato et al. (2002b) first identified the true superhump period of 0.05648(2) d, although their observation was not very sufficient to determine its period variation.

The 2010 outburst of this object was detected by M. Reszelski at a relatively faint magnitude of 14.16 (unfiltered CCD magnitude, vsnet-obs 67929). Subsequent observations detected growing superhumps (vsnet-alert 12092, 12094, 12095). This new outburst has confirmed the selection of the superhump period in (Kato et al. 2002b; figure 20).

The times of superhump maxima are listed in table 18. All A–C stages for superhump evolution were clearly detected (figure 21). We obtained a clearly positive $P_{\rm dot}$ of $+7.4(0.6) \times 10^{-5}$ during stage B, which is likely a more reliable value than the 1998 estimate thanks to the greatly improved statistics. As judged from this relatively large period derivative and the presence of stage C evolution, this object is less likely an extreme WZ Sge-type dwarf nova with a very small period variation what was supposed from the 1998 data Kato et al. (2002b). The relatively short ($\sim$ 12 yr) recurrence time would qualify the system as a WZ Sge-type dwarf nova similar to HV Vir (Ishioka et al. 2003). The lack of repetitive rebrightenings would also support this classification.

There was a weaker signal slightly shorter than the superhump period (figure 20), which might be attributed to the orbital period. Although the detection was not statistically significant, a similar periodicity may have been present before the appearance of ordinary superhumps (figure 22). Since this period agrees with the candidate period from radial-velocity study (Mennickent et al. 2002; see Kato et al. 2002b for the alias selection), we adopted it as a candidate for the orbital period, which corresponds to a fractional superhump excess of 0.9 %.

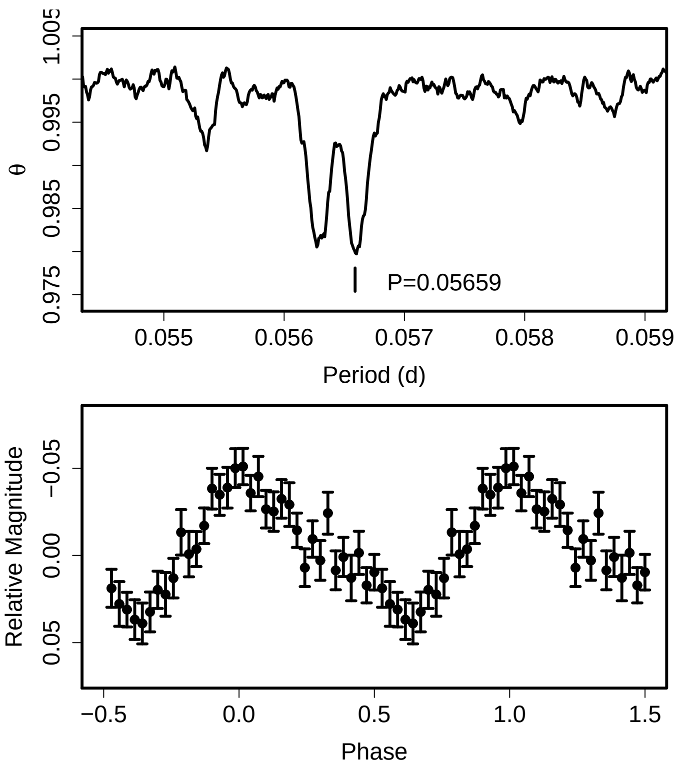

Fig. 20. Superhumps in V592 Her (2010). (Upper): PDM analysis. (Lower): Phase-averaged profile.

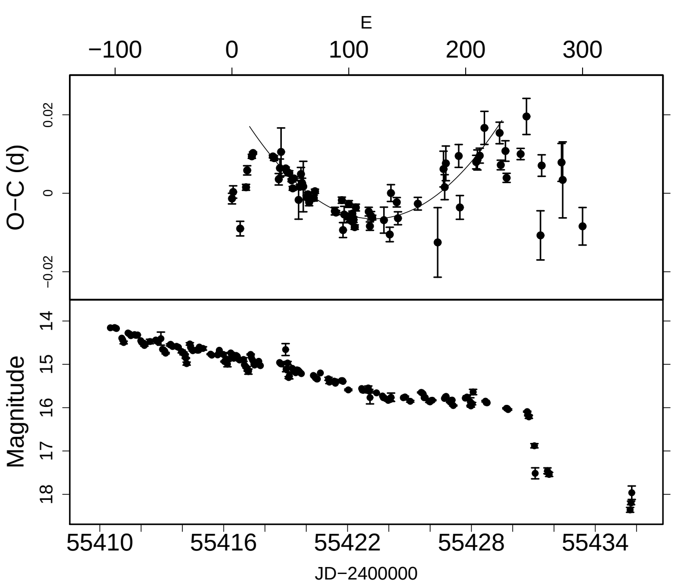

Fig. 21. $O-C$ of superhumps in V592 Her (2010). (Upper): $O-C$ diagram. The $O-C$ values were against the mean period for the stage B ($35 \leq E \leq 216$, thin curve) (Lower): Light curve. The outburst entered the rapid decline phase soon after the stage B–C transition.

Table 18. Superhump maxima of V592 Her (2010).

E	max*	error	$O-C$†	N‡
0	55413.7374	0.0014	−0.0009	53
1	55413.7957	0.0016	0.0008	53
7	55414.1260	0.0019	−0.0086	82
12	55414.4196	0.0008	0.0018	53
13	55414.4805	0.0012	0.0061	54
17	55414.7105	0.0005	0.0096	48
18	55414.7679	0.0003	0.0105	53
35	55415.7294	0.0004	0.0094	52
36	55415.7856	0.0006	0.0089	38
40	55416.0066	0.0015	0.0035	58
41	55416.0661	0.0023	0.0063	79
42	55416.1268	0.0061	0.0104	127
46	55416.3490	0.0003	0.0062	33
47	55416.4049	0.0002	0.0054	104
48	55416.4612	0.0003	0.0051	71
49	55416.5176	0.0006	0.0049	42
51	55416.6290	0.0003	0.0031	62
52	55416.6836	0.0005	0.0010	69
53	55416.7427	0.0004	0.0035	52
57	55416.9637	0.0049	−0.0020	71
58	55417.0236	0.0006	0.0013	175
59	55417.0835	0.0017	0.0046	89
60	55417.1378	0.0013	0.0022	82
61	55417.1935	0.0064	0.0013	50
64	55417.3606	0.0005	−0.0015	89
65	55417.4180	0.0005	−0.0007	143
66	55417.4725	0.0009	−0.0027	55
70	55417.7001	0.0008	−0.0017	35
71	55417.7584	0.0005	0.0000	51
88	55418.7157	0.0010	−0.0053	52
89	55418.7719	0.0005	−0.0057	51
94	55419.0581	0.0008	−0.0026	27
95	55419.1071	0.0019	−0.0102	68
96	55419.1677	0.0021	−0.0062	66
99	55419.3370	0.0008	−0.0068	61
100	55419.3968	0.0009	−0.0036	71
101	55419.4498	0.0009	−0.0072	75
102	55419.5057	0.0004	−0.0080	62
103	55419.5641	0.0006	−0.0061	38
104	55419.6192	0.0007	−0.0077	62
105	55419.6739	0.0006	−0.0096	72
106	55419.7355	0.0009	−0.0046	53
117	55420.3571	0.0011	−0.0058	62
118	55420.4101	0.0011	−0.0095	69
119	55420.4693	0.0011	−0.0069	20
120	55420.5254	0.0006	−0.0074	52
130	55421.0909	0.0033	−0.0081	62
135	55421.3703	0.0018	−0.0119	60
136	55421.4374	0.0021	−0.0013	68
141	55421.7181	0.0012	−0.0037	52
142	55421.7706	0.0016	−0.0078	41
159	55422.7367	0.0016	−0.0043	52
176	55423.6891	0.0089	−0.0144	42
181	55423.9909	0.0046	0.0042	149
182	55424.0429	0.0032	−0.0004	113
183	55424.1055	0.0044	0.0056	60
194	55424.7301	0.0029	0.0073	52

*BJD−2400000.

†Against $max = 2455413.7383 + 0.056621E$.

‡Number of points used to determine the maximum.

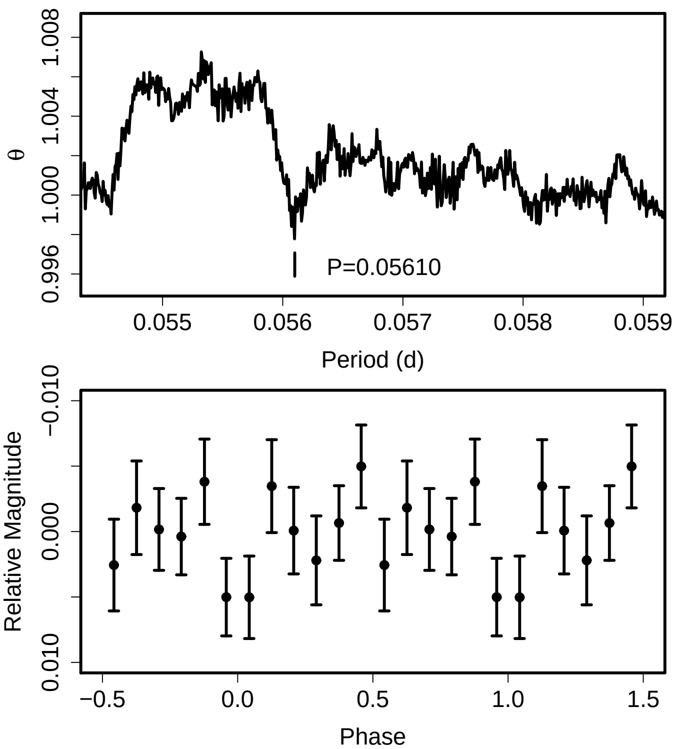

Fig. 22. Candidate early superhumps in V592 Her (2010). (Upper): PDM analysis. (Lower): Phase-averaged profile.

Table 18. Superhump maxima of V592 Her (2010). (continued)

E	max*	error	$O-C$†	N‡
195	55424.7736	0.0030	−0.0058	42
209	55425.5776	0.0017	0.0056	47
210	55425.6348	0.0026	0.0061	59
212	55425.7491	0.0019	0.0072	53
216	55425.9826	0.0042	0.0142	162
229	55426.7172	0.0027	0.0127	53
230	55426.7657	0.0012	0.0046	45
234	55426.9957	0.0026	0.0081	82
235	55427.0454	0.0012	0.0012	113
247	55427.7308	0.0014	0.0071	53
252	55428.0234	0.0046	0.0166	62
264	55428.6724	0.0063	−0.0138	36
265	55428.7468	0.0027	0.0039	52
282	55429.7099	0.0048	0.0045	52
283	55429.7621	0.0097	0.0000	52
300	55430.7126	0.0048	−0.0120	50

*BJD−2400000.
†Against $max = 2455413.7389 + 0.056620E$.
‡Number of points used to determine the maximum.

Table 19. Superhump maxima of V660 Her (2009).

E	max*	error	$O-C$†	N‡
0	55056.4789	0.0008	−0.0032	30
12	55057.4501	0.0007	−0.0004	36
25	55058.5061	0.0019	0.0067	9
49	55060.4337	0.0049	−0.0023	17
61	55061.4035	0.0098	−0.0008	23

*BJD−2400000.
†Against $max = 2455056.4821 + 0.080692E$.
‡Number of points used to determine the maximum.

3.18. V660 Herculis

The times of superhump maxima during the 2009 superoutburst are listed in table 19. Since the late stage of the superoutburst was only observed, the recorded superhumps are likely stage C superhumps.

3.19. V844 Herculis

Two further superoutbursts in 2009 February–March (table 20) and in 2010 April–May (table 21; see also vsnet-alert 11959 for the outburst detection) were observed. Both superoutbursts were relatively faint and short ones. During the former superoutburst We obtained a clearly positive $P_{\rm dot}$ of $+9.5(1.7) \times 10^{-5}$ (likely for stage B).

The object underwent yet another superoutburst between them: 2009 October–November (vsnet-alert 11622). There was also a normal outburst in 2009 June (vsnet-alert 11289, 11290). The object was thus unusually active for this star (cf. Kato, Uemura 2000; Oizumi et al. 2007). As suggested in Kato et al. (2008) and Kato et al. (2009a), these superoutburst would provide an excellent opportunity to study the dependence of period derivatives on the extent of the superoutburst. As already seen, the $P_{\rm dot}$ of the 2009 superoutburst is not significantly different from those of longer superoutbursts. Although the superhumps had already developed at the epoch of initial observation ($\sim$ 1.5 d after the initial outburst detection), we couldn't severely constrain the delay time in evolution of superhumps since there was a three-day gap of observation before this detection. The 2010 observation started $\sim$ 1 d after the rising phase of the outburst, and superhumps were already present. Although these superhumps were possibly stage A superhumps (see figure 23), this observations seems to support the hypothesis in Kato et al. (2009a) that the delay time in development of superhumps is shorter in smaller superoutbursts.

3.20. CT Hydrae

The times of superhump maxima during the 2010 superoutburst is listed in table 22. This observation first time recorded a stage A–B transition and growth of superhumps.

3.21. V699 Ophiuchi

Our new observation of the 2010 superoutburst (table 23) clearly caught a stage B–C transition. A comparison

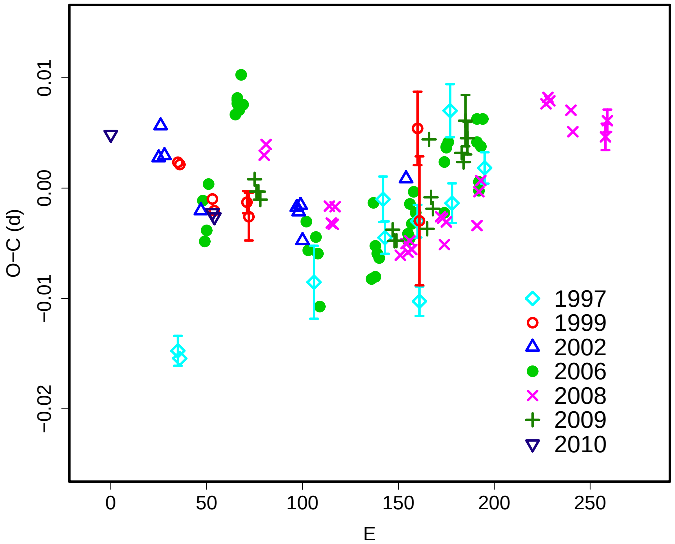

Fig. 23. Comparison of $O-C$ diagrams of V844 Her between different superoutbursts. A period of 0.05590 d was used to draw this figure. Approximate cycle counts (E) after the start of the superoutburst were used. Since the start of the 2009 superoutburst was not well constrained, we shifted the $O-C$ diagram to best match the others. The initial superhump maximum of the 2010 superoutburst may have a one-cycle ambiguity in the cycle count, and the large $O-C$ may have been a result of the rapidly evolving stage A superhumps.

Table 20. Superhump maxima of V844 Her (2009).

E	max*	error	$O-C$†	N‡
0	54887.4721	0.0003	0.0024	87
1	54887.5268	0.0002	0.0012	104
2	54887.5827	0.0002	0.0012	109
3	54887.6379	0.0002	0.0005	125
72	54891.4923	0.0003	−0.0038	101
73	54891.5472	0.0003	−0.0049	108
74	54891.6031	0.0004	−0.0049	108
90	54892.4986	0.0008	−0.0042	105
91	54892.5626	0.0008	0.0039	108
92	54892.6132	0.0006	−0.0014	107
93	54892.6681	0.0009	−0.0024	93
108	54893.5116	0.0006	0.0023	106
109	54893.5667	0.0005	0.0014	103
110	54893.6264	0.0023	0.0052	60
111	54893.6807	0.0015	0.0035	51

*BJD−2400000.
†Against $max = 2454887.4697 + 0.055923E$.
‡Number of points used to determine the maximum.

Table 21. Superhump maxima of V844 Her (2010).

E	max*	error	$O-C$†	N‡
0	55316.1758	0.0002	−0.0000	101
53	55319.1315	0.0002	0.0001	134
54	55319.1870	0.0002	−0.0001	177

*BJD−2400000.
†Against $max = 2455316.1758 + 0.055764E$.
‡Number of points used to determine the maximum.

Table 22. Superhump maxima of CT Hya (2010).

E	max*	error	$O-C$†	N‡
0	55269.0068	0.0049	−0.0021	91
1	55269.0698	0.0024	−0.0057	143
14	55269.9458	0.0013	0.0047	86
15	55270.0122	0.0005	0.0045	129
90	55275.0002	0.0009	−0.0014	142

*BJD−2400000.
†Against $max = 2455269.0089 + 0.066585E$.
‡Number of points used to determine the maximum.

of $O-C$ diagrams is shown in figure 24.

3.22. *V1032 Ophiuchi*

V1032 Oph was originally discovered as a candidate RR Lyr-type variable star (Kinman et al. 1965). Based on its bright UV emission, Wils, Henden (2009) conducted a systematic observation which led to a conclusion that the object is a likely SU UMa-type dwarf nova.

The 2010 outburst was detected by E. Muyllaert (vsnet-alert 11898). E. de Miguel and H. Maehara confirmed that this object is an eclipsing SU UMa-type dwarf nova (vsnet-alert 11904, 11905). The times of recorded eclipses, determined with the Kwee and van Woerden (KW) method (Kwee, van Woerden 1956), are summarized in table 24. We obtained an ephemeris of

$$\mathrm{Min(BJD)} = 2455286.68267(17) + 0.0810564(13)E. \quad (1)$$

In the following analysis, we removed observations within 0.07 P_{orb} of eclipses. The times of superhump maxima are listed in table 25. Due to the faintness of the object and overlapping eclipsing feature, the scatter is relatively large. The last maximum ($E = 117$) may have been a traditional late superhump with an ~0.5 phase offset, when the observation was performed after a brightness drop from the superoutburst. A linear fit to the observed epochs for $E < 117$ yielded a mean period of 0.08529(12) d. This period is in agreement with 0.08534(5) d determined with the PDM method (figure 25). We adopted the latter because of a smaller error. Although the period derivative could not be unambiguously determined, restricting to well-defined maxima ($E = 30, 47, 85, 86, 117$) and allowing a large period variation (as in MN Dra), we can derive a global P_{dot} of $-36(3) \times 10^{-5}$. This value needs to be confirmed by future observations. The fractional superhump excess amounts to 5.3 %, which is one

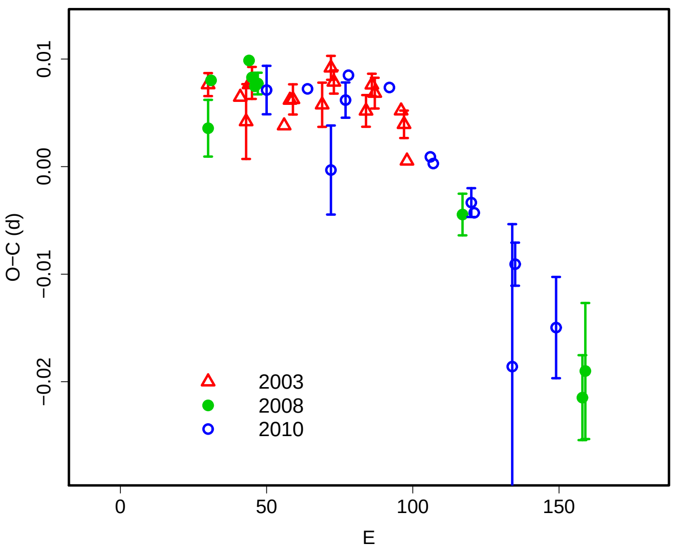

Fig. 24. Comparison of $O-C$ diagrams of V699 Oph between different superoutbursts. A period of 0.07031 d was used to draw this figure. Since the start of the superoutbursts or appearance of superhumps were not well constrained, we shifted the $O-C$ diagrams to best fit each other.

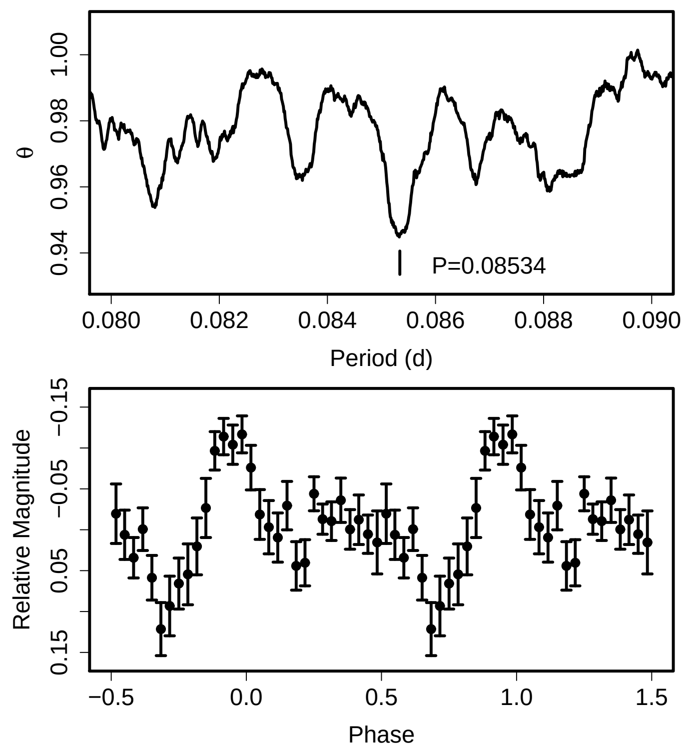

Fig. 25. Superhumps in V1032 Oph (2010). (Upper): PDM analysis. (Lower): Phase-averaged profile.

Table 23. Superhump maxima of V699 Oph (2010).

E	max*	error	$O-C$†	N‡
0	55362.5280	0.0023	−0.0044	12
14	55363.5125	0.0007	−0.0008	77
22	55364.0674	0.0041	−0.0064	47
27	55364.4254	0.0016	0.0014	41
28	55364.4981	0.0007	0.0039	68
42	55365.4813	0.0007	0.0063	65
56	55366.4592	0.0008	0.0033	69
57	55366.5288	0.0008	0.0029	60
70	55367.4392	0.0013	0.0025	62
71	55367.5086	0.0008	0.0018	62
84	55368.4083	0.0132	−0.0092	39
85	55368.4882	0.0020	0.0005	67
99	55369.4666	0.0047	−0.0019	65

*BJD−2400000.
†Against $max = 2455362.5324 + 0.070061E$.
‡Number of points used to determine the maximum.

of the largest among SU UMa-type dwarf novae below the period gap (cf. subsection 3.7).

3.23. V2051 Ophiuchi

The times of superhump maxima during the 2010 superoutburst are listed in table 26. Although the outburst was detected during its relatively early stage (vsnet-alert 12049), the subsequent observational coverage was rather insufficient. The observed superhumps were likely stage B superhumps. We could not meaningfully determine Kato et al. (2009a).

3.24. EF Pegasi

EF Peg is one of representatives of long-$P_{\rm SH}$ SU UMa-type dwarf novae with infrequent outbursts. Kato et al. (2009a) reported mildly negative $P_{\rm dot}$ for the 1991 and 1997 superoutbursts. The object underwent an outburst in 2009 December (vsnet-alert 11738, baavss-alert 2177, vsnet-alert 11740), first time since its 2001 superoutburst. The outburst was caught during its early stage and the development of superhumps was recorded.

The times of superhump maxima are listed in table 27. Due to the short visibility in the evening sky, the number of maxima was relatively small. The $O-C$ diagram, however, clearly shows the presence of stage A during the evolutionary stage of superhumps ($E \leq 11$), and subsequent phase of a slow period decrease. We attributed the latter phase to a transition from stage B to C and identified the periods in table 2.

Table 24. Eclipse Minima of V1032 Oph.

E	Minimum*	error	$O-C$†
0	55286.6829	0.0008	0.0002
32	55289.2765	0.0006	0.0001
49	55290.6544	0.0007	-0.0000
69	55292.2763	0.0010	0.0008
74	55292.6809	0.0006	0.0001
89	55293.8967	0.0005	0.0000
90	55293.9775	0.0004	-0.0002
99	55294.7075	0.0006	0.0002
102	55294.9505	0.0004	0.0001
103	55295.0310	0.0006	-0.0004
111	55295.6801	0.0006	0.0001
114	55295.9231	0.0004	0.0000
115	55296.0041	0.0005	-0.0001
122	55296.5710	0.0005	-0.0005
123	55296.6517	0.0004	-0.0009
212	55303.8664	0.0011	-0.0002
213	55303.9478	0.0009	0.0001
238	55305.9747	0.0006	0.0006
296	55310.6754	0.0005	0.0001

*BJD−2400000.
†Against equation 1.

Table 25. Superhump maxima of V1032 Oph (2010).

E	max*	error	$O-C$†	N‡
0	55286.6842	0.0023	0.0062	74
24	55288.7046	0.0018	−0.0174	24
30	55289.2294	0.0011	−0.0036	167
41	55290.1909	0.0040	0.0210	126
43	55290.3086	0.0017	−0.0316	73
47	55290.6862	0.0006	0.0053	73
65	55292.2223	0.0023	0.0083	147
66	55292.3013	0.0072	0.0022	141
85	55293.9201	0.0012	0.0028	34
86	55294.0063	0.0015	0.0039	32
94	55294.6949	0.0015	0.0110	65
97	55294.9549	0.0018	0.0156	37
98	55295.0222	0.0083	−0.0023	26
100	55295.2186	0.0035	0.0238	37
106	55295.6961	0.0060	−0.0097	60
117	55296.6072	0.0006	−0.0355	69

*BJD−2400000.
†Against $max = 2455286.6780 + 0.085169E$.
‡Number of points used to determine the maximum.

Table 26. Superhump maxima of V2051 Oph (2010).

E	max*	error	$O-C$†	N‡
0	55382.9240	0.0003	0.0014	107
1	55382.9876	0.0003	0.0008	104
2	55383.0492	0.0002	−0.0019	78
3	55383.1165	0.0003	0.0012	94
14	55383.8220	0.0014	0.0000	34
17	55384.0142	0.0006	−0.0004	92
18	55384.0865	0.0005	0.0076	89
34	55385.1019	0.0009	−0.0048	71
35	55385.1613	0.0027	−0.0096	40
65	55387.1037	0.0013	0.0057	37

*BJD−2400000.
†Against $max = 2455382.9226 + 0.064238E$.
‡Number of points used to determine the maximum.

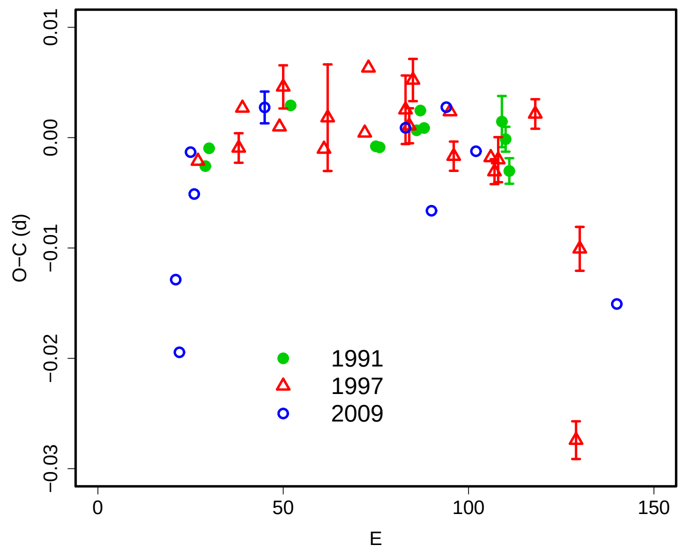

Fig. 26. Comparison of $O-C$ diagrams of EF Peg between different superoutbursts. A period of 0.08705 d was used to draw this figure. Approximate cycle counts (E) after the start of the superoutburst were used.

A comparison of $O-C$ variations between different superoutbursts is presented in figure 26. Among long-P_{SH} systems, the $O-C$ variation looks similar to those of AX Cap and SDSS J1627 (cf. Kato et al. 2009a) with a discontinuous period variation between stages B and C. It would be noteworthy that all systems are known to show only rare superoutbursts.

3.25. V368 Pegasi

We also observed the 2009 superoutburst. This outburst was one of the brightest in recent years (cf. vsnet-alert 11507). The times of superhump maxima are listed in table 28, which clearly shows a stage B–C transition. The superhumps were not very apparent on the first night (BJD 2455102), and it was likely that the development of superhumps took more than 1 d. The relatively large

Table 27. Superhump maxima of EF Peg (2009).

E	max*	error	$O-C$†	N‡
0	55187.3273	0.0007	−0.0296	229
6	55187.8804	0.0008	0.0006	353
7	55187.9609	0.0007	−0.0061	521
10	55188.2402	0.0005	0.0117	287
11	55188.3234	0.0004	0.0078	277
30	55189.9852	0.0014	0.0135	296
68	55193.2913	0.0005	0.0073	268
75	55193.8931	0.0008	−0.0010	464
79	55194.2507	0.0005	0.0080	80
87	55194.9431	0.0008	0.0031	440
125	55198.2372	0.0006	−0.0151	77

*BJD−2400000.
†Against $max = 2455187.3569 + 0.087163E$.
‡Number of points used to determine the maximum.

Table 28. Superhump maxima of V368 Peg (2009).

E	max*	error	$O-C$†	N‡
0	55102.8556	0.0009	−0.0046	109
35	55105.3047	0.0030	−0.0110	31
36	55105.3797	0.0003	−0.0062	73
37	55105.4512	0.0004	−0.0048	69
38	55105.5209	0.0005	−0.0053	43
40	55105.6602	0.0008	−0.0063	24
55	55106.7133	0.0003	−0.0056	110
97	55109.6732	0.0006	0.0078	153
98	55109.7456	0.0005	0.0100	156
99	55109.8159	0.0004	0.0102	148
113	55110.7965	0.0006	0.0087	36
114	55110.8657	0.0006	0.0076	33
115	55110.9358	0.0008	0.0076	26
125	55111.6361	0.0004	0.0064	74
126	55111.7060	0.0004	0.0061	102
127	55111.7756	0.0006	0.0056	56
128	55111.8544	0.0065	0.0142	13
137	55112.4750	0.0006	0.0033	57
138	55112.5466	0.0007	0.0049	73
177	55115.2731	0.0007	−0.0048	49
178	55115.3412	0.0009	−0.0068	46
179	55115.4090	0.0016	−0.0092	50
180	55115.4822	0.0018	−0.0061	50
181	55115.5469	0.0018	−0.0115	49
220	55118.2843	0.0009	−0.0103	30

*BJD−2400000.
†Against $max = 2455102.8602 + 0.070156E$.
‡Number of points used to determine the maximum.

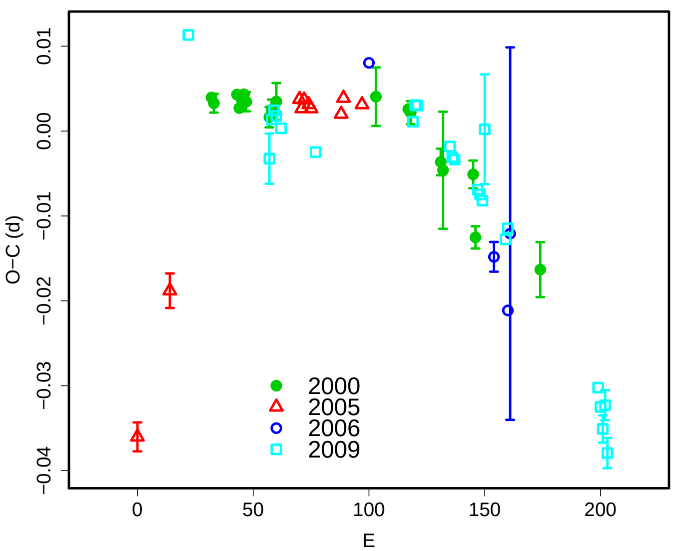

Fig. 27. Comparison of $O-C$ diagrams of V368 Peg between different superoutbursts. A period of 0.07039 d was used to draw this figure. Approximate cycle counts (E) after the start of the superoutburst were used.

$P_{\rm dot}$ for stage B strongly depends on $E = 0$, and may not be real. A comparison of $O-C$ diagrams between different superoutbursts is shown in figure 27. Despite its brightness, the behavior of the 2009 superoutburst was not strikingly different from that of other superoutbursts.

3.26. UV Persei

We observed the 2010 superoutburst during this middle and final stages (table 29). Although a stage B–C transition was recorded, the long gap in observation hindered precise determination of periods. We only list representative values for stage B. Late-stage superhumps superimposed on the rapid fading from the superoutburst plateau were clearly recorded as in the 1992 superoutburst. A comparison of $O-C$ diagrams between different superoutbursts is shown in figure 28. This figure is an improvement of the corresponding one presented in Kato et al. (2009a).

3.27. EI Piscium

We observed the 2009 superoutburst first detected by ASAS-3 on June 8 at $V = 12.46$. Due to the poor seasonal condition, we could only determine the mean superhump period of 0.04635(5) d (with the PDM method), in agreement with previous measurements. The times of superhump maxima are listed in table 30. The overall light curve of the outburst suggests that the main superoutburst plateau lasted less than 10 d and experienced a rebrightening on June 18. The course of the outburst could have been similar to the 2005 one (Uemura et al. 2002; Skillman et al. 2002). The shortness of the superoutburst plateau in such short-$P_{\rm orb}$ systems with evolved secondaries would require a special explanation.

3.28. EK Trianguli Australis

We observed the 2009 superoutburst. A clear stae A–B transition was recorded (table 31). Although the period variation was alost absent during the supposed stage B ($E \geq 29$), this may have been a result of fragmentary observations of stages B and C.

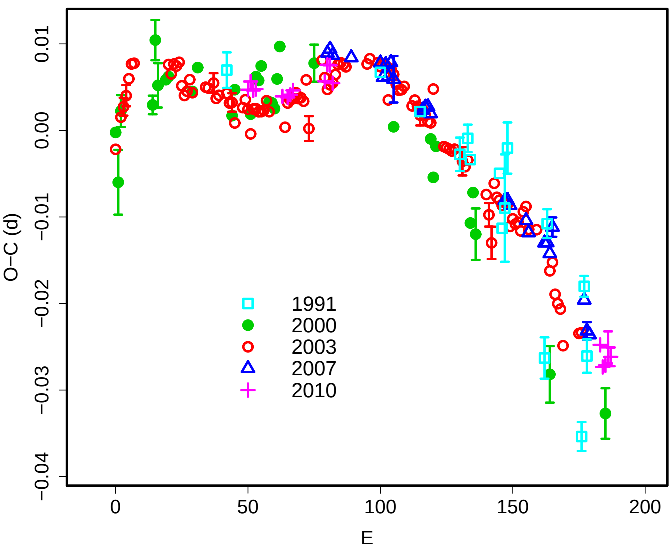

Fig. 28. Comparison of $O-C$ diagrams of UV Per between different superoutbursts. A period of 0.06665 d was used to draw this figure. Approximate cycle counts (E) after the appearance of the superhumps were used.

Table 29. Superhump maxima of UV Per (2010).

E	max*	error	$O-C$†	N‡
0	55203.4188	0.0003	−0.0041	74
1	55203.4864	0.0004	−0.0029	74
2	55203.5521	0.0003	−0.0037	73
3	55203.6189	0.0004	−0.0033	62
13	55204.2845	0.0004	−0.0016	71
15	55204.4177	0.0005	−0.0012	40
16	55204.4847	0.0004	−0.0006	46
17	55204.5518	0.0006	0.0001	34
29	55205.3527	0.0005	0.0042	41
30	55205.4212	0.0005	0.0063	35
31	55205.4878	0.0006	0.0065	37
32	55205.5524	0.0009	0.0047	28
133	55212.2538	0.0004	−0.0001	63
134	55212.3179	0.0008	−0.0024	67
135	55212.3847	0.0009	−0.0019	62
136	55212.4535	0.0018	0.0004	48
137	55212.5190	0.0011	−0.0004	62

*BJD−2400000.
†Against $max = 2455203.4229 + 0.066398E$.
‡Number of points used to determine the maximum.

Table 30. Superhump maxima of EI Psc (2009).

E	max*	error	$O-C$†	N‡
0	54994.1841	0.0011	0.0006	44
1	54994.2292	0.0005	−0.0006	67
10	54994.6467	0.0004	0.0001	29

*BJD−2400000.
†Against $max = 2454994.1836 + 0.046311E$.
‡Number of points used to determine the maximum.

Table 31. Superhump maxima of EK TrA (2009).

E	max*	error	$O-C$†	N‡
0	55027.0310	0.0029	−0.0009	74
1	55027.0787	0.0026	−0.0181	118
29	55028.9255	0.0002	0.0101	159
30	55028.9901	0.0003	0.0098	100
76	55031.9722	0.0003	0.0043	180
77	55032.0358	0.0003	0.0030	184
137	55035.9273	0.0011	−0.0023	108
138	55035.9924	0.0006	−0.0022	137
139	55036.0559	0.0005	−0.0036	139

*BJD−2400000.
†Against $max = 2455027.0319 + 0.064947E$.
‡Number of points used to determine the maximum.

3.29. SU Ursae Majoris

The 2010 January superoutburst was observed for its early and late stages (table 32). Although we could only measure the mean period of stage B, the value is in agreement with those obtained during previous superoutbursts. The humps observed for $E \geq 163$ may not be genuine superhumps.

3.30. BC Ursae Majoris

BC UMa underwent a superoutburst in 2009 September–October after a period of 6.7 yr (cf. vsnet-alert 11514). The start of the outburst was not well constrained dur to the poor visibility in the morning sky. Superhumps were observed despite unfavorable seasonal conditions (cf. vsnet-alert 11540, 11550, 11559). The times of superhump maxima are listed in table 33. There was a clear stage B–C transition and the P_{dot} for stage B ($56 \leq E \leq 144$) was $+9.5(2.7) \times 10^{-5}$. We attributed the interval $E \leq 2$ to likely stage A superhumps based on comparison with other superoutbursts (figure 29). If this identification is correct, the superhumps during this superoutburst appears to have taken a longer time to fully develop.

3.31. EL Ursae Majoris

Although EL UMa was discovered as an eruptive object relatively early in the history (Pesch, Sanduleak 1987), only little had been known until recent years. Kato et al. (2001a) listed this object among candidate WZ Sge-type dwarf novae. Based on the similarity of its quiescent SDSS

Table 32. Superhump maxima of SU UMa (2010).

E	max*	error	$O-C$†	N‡
0	55219.5098	0.0002	−0.0003	132
1	55219.5883	0.0002	−0.0009	149
2	55219.6689	0.0002	0.0005	150
7	55220.0702	0.0014	0.0061	89
11	55220.3809	0.0002	0.0002	145
12	55220.4613	0.0002	0.0014	156
13	55220.5392	0.0002	0.0002	153
14	55220.6182	0.0004	−0.0001	157
15	55220.6987	0.0003	0.0013	122
25	55221.4871	0.0004	−0.0018	155
26	55221.5668	0.0004	−0.0012	151
27	55221.6454	0.0004	−0.0018	154
50	55223.4634	0.0004	−0.0044	96
51	55223.5457	0.0004	−0.0012	118
163	55232.4126	0.0012	0.0006	75
164	55232.4926	0.0012	0.0014	83

*BJD−2400000.
†Against $max = 2455219.5101 + 0.079153E$.
‡Number of points used to determine the maximum.

Table 33. Superhump maxima of BC UMa (2009).

E	max*	error	$O-C$†	N‡
0	55105.2681	0.0022	−0.0189	70
2	55105.3853	0.0013	−0.0310	43
56	55108.9240	0.0016	0.0181	182
92	55111.2424	0.0004	0.0101	49
125	55113.3725	0.0007	0.0076	45
126	55113.4388	0.0004	0.0093	84
138	55114.2105	0.0021	0.0056	40
139	55114.2800	0.0004	0.0104	86
140	55114.3451	0.0005	0.0109	72
141	55114.4106	0.0005	0.0117	85
142	55114.4740	0.0005	0.0105	86
143	55114.5395	0.0005	0.0114	87
144	55114.6037	0.0004	0.0109	87
170	55116.2768	0.0005	0.0039	113
203	55118.3985	0.0013	−0.0070	67
204	55118.4593	0.0007	−0.0108	72
205	55118.5248	0.0006	−0.0099	73
206	55118.5888	0.0005	−0.0105	73
207	55118.6512	0.0014	−0.0128	45
219	55119.4198	0.0007	−0.0196	46

*BJD−2400000.
†Against $max = 2455105.2870 + 0.064623E$.
‡Number of points used to determine the maximum.

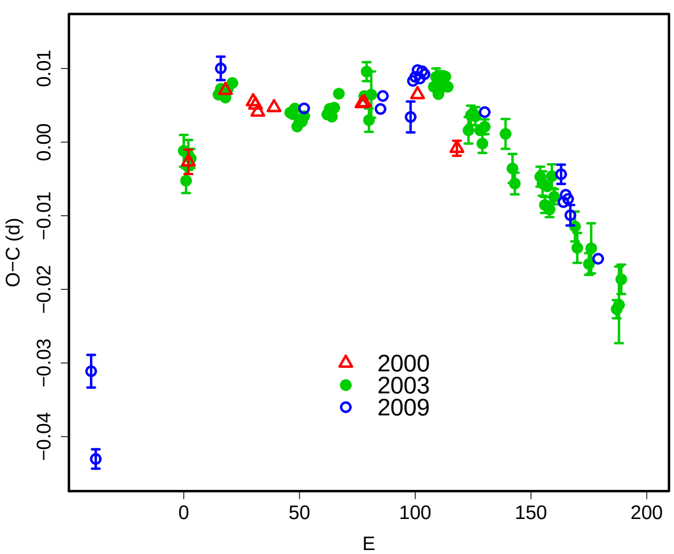

Fig. 29. Comparison of $O-C$ diagrams of BC UMa between different superoutbursts. A period of 0.06455 d was used to draw this figure. Approximate cycle counts (E) after the appearance of the superhumps were used.

color to those of known WZ Sge-type dwarf novae, we started monitoring since 2008. Another outburst at r = 13.7 in 2003 April was found on an archival image (Wils et al. 2010).

On 2009 January 13, H. Maehara finally detected this object in outburst at an unfiltered CCD magnitude of 17.4 (vsnet-alert 11771) The object further brightened to a magnitude of 14.9 on January 16 (vsnet-alert 11772). The object has been confirmed to be a hydrogen-rich dwarf niva in outburst by spectroscopy (Takahashi and Kinugasa, private communication). Although the nature of this brightening was unclear at the time, the detection of additional sequence of outbursts (vsnet-alert 11789, 11808), led to an interpretation that they are post-superoutburst rebrightenings of a WZ Sge-type superoutburst, whose main superoutburst was missed (vsnet-alert 11795). The detection of modulations attributable to superhumps seems to strengthen this interpretation (vsnet-alert 11799). We include this object based on this interpretation.

A period analysis of the rebrightening phase, after subtracting the trends of outbursts (cf. Kato et al. 2009b), has yielded a period of 0.06045(6) d (figure 30). Although this period needs to be confirmed by future observations, its relatively long $P_{\rm SH}$ appears to be similar to that of VX For (subsection 3.14) that underwent multiple rebrightenings (figure 31). There is a common tendency that the quiescent interval preceding the last rebrightening is longer than the other intervals between rebrightenings.

This object is a good candidate for a CV passed the

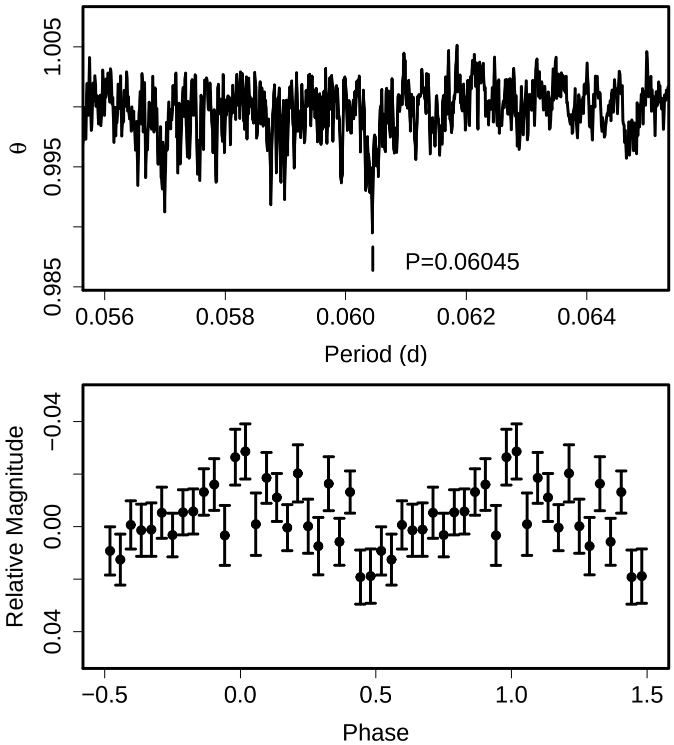

Fig. 30. Superhumps of EL UMa during the rebrightening phase (2010). (Upper): PDM analysis. (Lower): Phase-averaged profile.

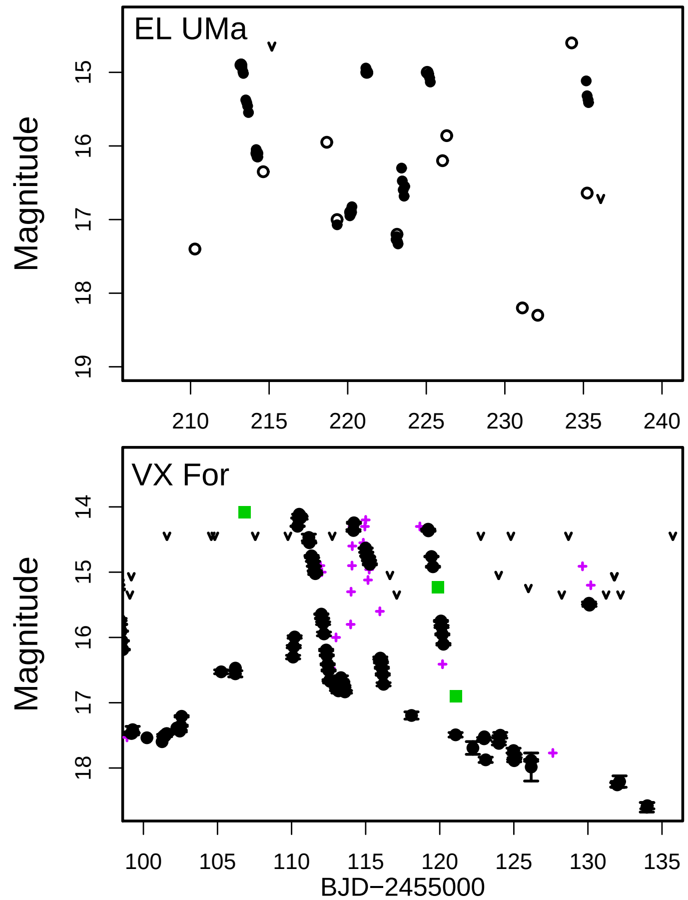

Fig. 31. Light curve of EL UMa during the rebrightening phase (2010). (Upper): EL UMa. Open circles and "v" signs are snapshot CCD observations and upper limits, respectively. (Lower): VX For (2009, cf. figure 16). The overall feature is remarkably similar between these objects.

period minimum in evolution (see a discussion in Kato et al. 2009a). Further radial-velocity study in quiescence in encouraged in order to determine the orbital period and the nature of the period during the rebrightening phase.

3.32. *IY Ursae Majoris*

Although the 2009 superoutburst of this object was reported in Kato et al. (2009a), we provide greatly improved results by combining newly available observations. The times of superhump maxima (table 34) now clearly illustrate the presence of all A–C stages, and a definitely positive $P_{\rm dot} = +15.1(2.3) \times 10^{-5}$ for stage B superhumps, confirming the suggestion in Kato et al. (2009a) based on the combined $O-C$ diagram (cf. figure 32). Although there was a signature of distinct stages during stage A, we listed a mean period in table 2. There was a very clear signature of a stage B–C transition thanks to the high quality of data. Although the phases of superhump at late epochs ($E \geq 189$) deviate from extrapolations of stage C superhumps, they can still be interpreted as a continuation of stage C superhump, rather than traditional late superhumps.

This object showed a strong "textbook" beat phenomenon between superhumps and orbital modulations (figure 33). The period of the beat phenomenon was shorter ($\sim$ 2.5 d) during stage B, while it became longer ($\sim$ 3.0 d) during stage C. These periods are in very good agreement with the expected beat periods for stage B and C superhumps, 2.45 d and 3.08 d, respectively. This can be understood if the variation of the beat period reflects the variation of the angular velocity of the apsidal motion of the elliptical accretion disk. The close correlation between the beat period and the superhump period suggests that the change in the angular velocity of the global apsidal motion is more responsible for the stage B–C transition rather than the appearance of a more localized new component.

3.33. *KS Ursae Majoris*

The times of superhump maxima during the 2010 superoutburst are listed in table 35. Since there was a large gap in observations, we did not attempt to determine $P_{\rm dot}$ from these data. The observation was probably recorded during stages B and C.

3.34. *MR Ursae Majoris*

The times of superhump maxima during the 2010 superoutburst are listed in table 36. Since there were relatively large gaps in observations, we did not attempt to determine $P_{\rm dot}$ from these data. The period of the presum-

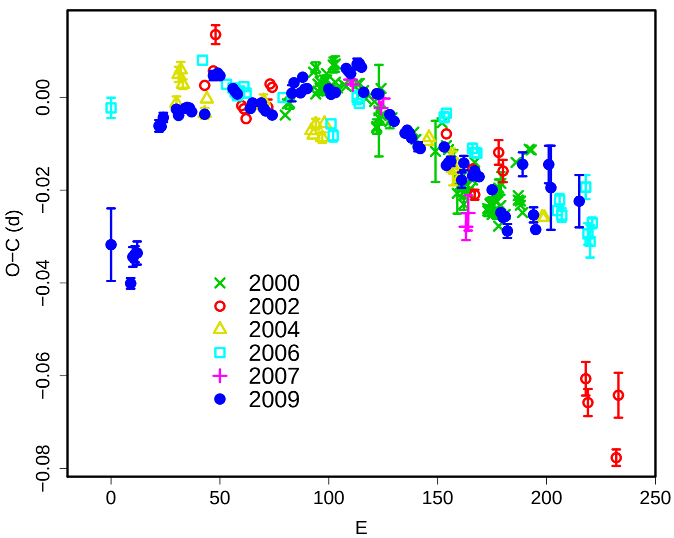

Fig. 32. Comparison of $O-C$ diagrams of IY UMa between different superoutbursts. A period of 0.07616 d was used to draw this figure. Approximate cycle counts (E) after the start of the superoutburst were used. The figure is an improvement of the corresponding figure in Kato et al. (2009a). The base period and symbols were modified for better visibility.

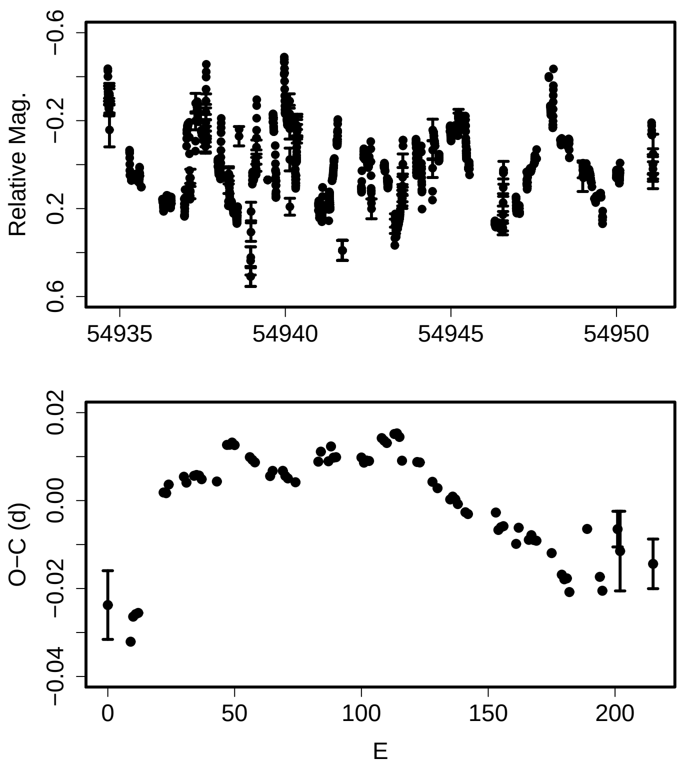

Fig. 33. Beat phenomenon in IY UMa (2009). (Upper): Residuals from the global trend (fitted by a third-order polynomial) of the outburst outside the eclipses. Each point represents an average of one superhump period. (Lower): $O-C$ of superhumps.

Table 34. Superhump maxima of IY UMa (2009).

E	max*	error	$O-C$†	N‡
0	54934.6865	0.0078	−0.0294	52
9	54935.3637	0.0011	−0.0372	77
10	54935.4455	0.0021	−0.0315	74
11	54935.5222	0.0017	−0.0309	64
12	54935.5987	0.0025	−0.0305	33
22	54936.3877	0.0013	−0.0026	105
23	54936.4637	0.0010	−0.0027	121
24	54936.5418	0.0010	−0.0007	82
30	54937.0005	0.0003	0.0014	144
31	54937.0753	0.0002	0.0001	201
34	54937.3054	0.0002	0.0019	59
35	54937.3817	0.0003	0.0021	68
36	54937.4578	0.0003	0.0020	63
37	54937.5331	0.0003	0.0012	66
43	54937.9895	0.0007	0.0010	119
47	54938.3025	0.0010	0.0096	66
48	54938.3787	0.0009	0.0097	68
49	54938.4553	0.0008	0.0102	67
50	54938.5309	0.0007	0.0097	58
56	54938.9851	0.0003	0.0073	123
57	54939.0607	0.0002	0.0067	125
58	54939.1363	0.0003	0.0062	82
64	54939.5901	0.0007	0.0034	86
65	54939.6675	0.0002	0.0047	122
69	54939.9721	0.0003	0.0049	83
70	54940.0471	0.0004	0.0038	123
71	54940.1227	0.0007	0.0033	108
74	54940.3503	0.0009	0.0026	61
83	54941.0404	0.0017	0.0077	104
84	54941.1189	0.0009	0.0101	97
87	54941.3452	0.0003	0.0080	136
88	54941.4247	0.0004	0.0115	133
89	54941.4983	0.0004	0.0090	105
90	54941.5746	0.0002	0.0091	130
100	54942.3361	0.0002	0.0096	151
101	54942.4111	0.0002	0.0085	254
102	54942.4877	0.0003	0.0090	203
103	54942.5638	0.0004	0.0090	134
108	54942.9498	0.0008	0.0144	53
109	54943.0254	0.0006	0.0139	88
110	54943.1010	0.0004	0.0134	62
113	54943.3315	0.0012	0.0156	68
114	54943.4078	0.0008	0.0158	67
115	54943.4832	0.0007	0.0151	62
116	54943.5539	0.0008	0.0097	27
122	54944.0106	0.0005	0.0098	86
123	54944.0867	0.0005	0.0097	88
128	54944.4631	0.0004	0.0056	51
130	54944.6139	0.0008	0.0042	65
135	54944.9922	0.0004	0.0020	177
136	54945.0690	0.0004	0.0027	213

*BJD−2400000.
†Against $max = 2454934.7159 + 0.076106E$.
‡Number of points used to determine the maximum.

Table 34. Superhump maxima of IY UMa (2009) (continued).

E	max*	error	$O-C$†	N‡
137	54945.1445	0.0006	0.0021	79
138	54945.2196	0.0008	0.0011	79
141	54945.4462	0.0010	−0.0006	37
142	54945.5220	0.0010	−0.0010	55
153	54946.3601	0.0009	−0.0000	67
154	54946.4323	0.0008	−0.0040	66
155	54946.5090	0.0006	−0.0033	65
156	54946.5854	0.0010	−0.0030	30
161	54946.9622	0.0016	−0.0067	44
162	54947.0420	0.0016	−0.0030	61
166	54947.3439	0.0007	−0.0055	72
167	54947.4212	0.0007	−0.0044	156
168	54947.4962	0.0005	−0.0055	134
169	54947.5722	0.0006	−0.0056	103
175	54948.0264	0.0008	−0.0081	139
179	54948.3261	0.0006	−0.0128	67
180	54948.4012	0.0005	−0.0138	67
181	54948.4776	0.0008	−0.0135	64
182	54948.5506	0.0015	−0.0166	64
189	54949.0981	0.0026	−0.0018	191
194	54949.4680	0.0016	−0.0124	66
195	54949.5410	0.0007	−0.0156	67
201	54950.0120	0.0041	−0.0012	169
202	54950.0831	0.0091	−0.0062	149
215	54951.0703	0.0056	−0.0084	108

*BJD−2400000.
†Against $max = 2454934.7159 + 0.076106E$.
‡Number of points used to determine the maximum.

Table 35. Superhump maxima of KS UMa (2010).

E	max*	error	$O-C$†	N‡
0	55304.0436	0.0004	−0.0009	92
1	55304.1148	0.0003	0.0002	100
2	55304.1837	0.0003	−0.0011	99
3	55304.2563	0.0006	0.0013	99
99	55310.9915	0.0013	0.0034	99
100	55311.0610	0.0011	0.0028	100
101	55311.1262	0.0011	−0.0021	96
102	55311.1953	0.0011	−0.0031	100
103	55311.2691	0.0012	0.0005	93
113	55311.9785	0.0015	0.0086	87
114	55312.0382	0.0023	−0.0019	95
115	55312.1023	0.0018	−0.0079	75

*BJD−2400000.
†Against $max = 2455304.0445 + 0.070136E$.
‡Number of points used to determine the maximum.

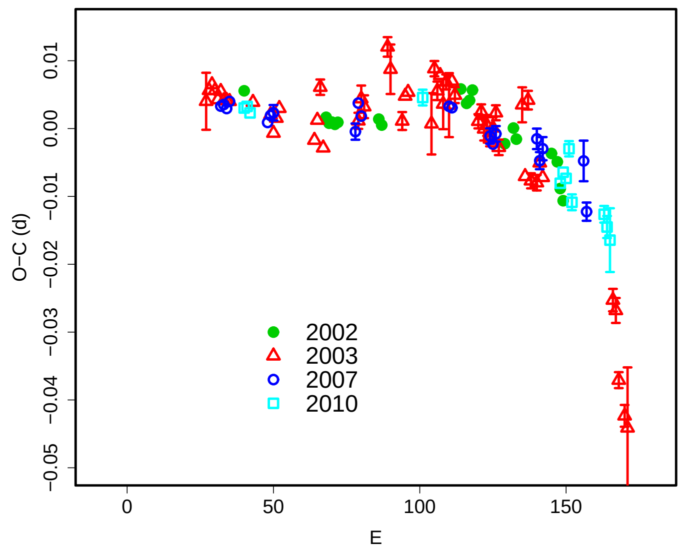

Fig. 34. Comparison of $O-C$ diagrams of MR UMa between different superoutbursts. A period of 0.06512 d was used to draw this figure. Approximate cycle counts (E) after the start of the 2007 superoutburst were used. Since the starts of the other superoutbursts were not well constrained, we shifted the $O-C$ diagrams to best fit the 2007 one.

Table 36. Superhump maxima of MR UMa (2010).

E	max*	error	$O-C$†	N‡
0	55303.9991	0.0002	0.0004	155
1	55304.0645	0.0005	0.0007	107
2	55304.1286	0.0005	−0.0001	97
61	55307.9730	0.0012	0.0074	42
108	55311.0210	0.0009	−0.0011	150
109	55311.0877	0.0009	0.0007	157
110	55311.1519	0.0006	−0.0002	158
111	55311.2214	0.0011	0.0043	113
112	55311.2787	0.0012	−0.0035	89
123	55311.9932	0.0012	−0.0043	138
124	55312.0565	0.0016	−0.0061	155
125	55312.1196	0.0047	−0.0079	71
184	55315.9675	0.0006	0.0031	37
185	55316.0361	0.0019	0.0067	44

*BJD−2400000.
†Against $max = 2455303.9987 + 0.065031E$.
‡Number of points used to determine the maximum.

able stage C superhumps is listed in table 2. An updated comparison of $O-C$ diagrams between different superoutbursts is given in figure 34.

3.35. TY Vulpeculae

The 2010 superoutburst of this SU UMa-type dwarf nova was relatively well-observed during its later stage. The times of superhump maxima are listed in table 37. The period evolution now clearly demonstrates the presence of stage B–C transition, whose existence was sug-

Table 37. Superhump maxima of TY Vul (2010).

E	max*	error	$O-C$†	N‡
0	55368.7467	0.0008	−0.0048	41
1	55368.8262	0.0004	−0.0055	39
9	55369.4721	0.0007	−0.0017	202
10	55369.5530	0.0003	−0.0010	188
13	55369.7944	0.0009	−0.0003	40
14	55369.8748	0.0008	−0.0002	39
21	55370.4365	0.0007	−0.0003	135
22	55370.5183	0.0008	0.0012	160
23	55370.5991	0.0008	0.0018	89
25	55370.7518	0.0030	−0.0060	20
26	55370.8390	0.0007	0.0009	40
27	55370.9180	0.0008	−0.0004	32
33	55371.3982	0.0090	−0.0017	64
34	55371.4837	0.0011	0.0036	158
35	55371.5635	0.0008	0.0031	154
37	55371.7267	0.0017	0.0059	37
38	55371.8037	0.0033	0.0026	39
39	55371.8884	0.0033	0.0070	22
46	55372.4457	0.0004	0.0026	105
47	55372.5236	0.0004	0.0002	163
48	55372.6074	0.0005	0.0037	74
58	55373.4079	0.0011	0.0017	51
59	55373.4872	0.0005	0.0007	156
60	55373.5673	0.0006	0.0005	146
75	55374.7689	0.0014	−0.0016	27
76	55374.8473	0.0019	−0.0035	27
88	55375.8077	0.0021	−0.0061	58
89	55375.8919	0.0033	−0.0022	109

*BJD−2400000.
†Against $max = 2455368.7515 + 0.080254E$.
‡Number of points used to determine the maximum.

gested from the 2003 observation (Kato et al. 2009a). The sudden change in the superhump period at this transition favors the suggestion in Kato et al. (2009a) that this object is analogous to AX Cap and SDSS J1627.

3.36. 1RXS J042332+745300

In Kato et al. (2009a), we reported observations of the 2008 superoutburst of this object (=HS 0417+7445, hereafter 1RXS J0423). The 2010 superoutburst was again fortunately detected during its rising stage and early stage evolution of superhumps was recorded.

The times of superhump maxima are listed in table 38. A stage A–B and transition was clearly recorded. The shorter superhump period after $E = 79$ probably corresponds to stage C superhumps. Although the later half of the stage B and the stage B–C transition itself were not observed, there was a possible indication of a positive $P_{\rm dot}$ during the stage B. The parameters are listed in table 2.

Figure 35 illustrates the comparison of $O-C$ diagrams between the 2008 and 2010 superoutbursts. Although the later parts of the $O-C$ diagrams were similar, there was a distinction during the early stage. This may have been

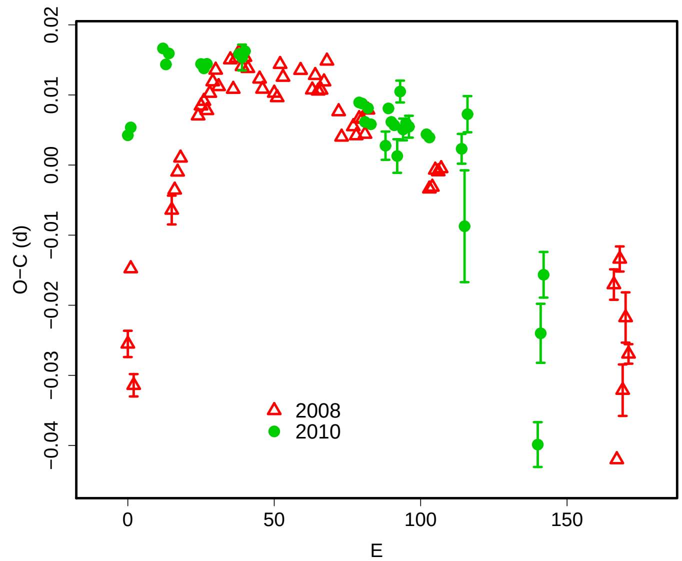

Fig. 35. Comparison of $O-C$ diagrams of 1RXS J0423 between different superoutbursts. A period of 0.07845 d was used to draw this figure. Approximate cycle counts (E) after the start of the superoutburst were used.

a result of the presence of a precursor outburst and early appearance of superhumps during the 2008 superoutburst (cf. Kato et al. 2009a). The $O-C$ evolution in the 2010 superoutburst resembled those of ordinary SU UMa-type dwarf novae than in the 2008 superoutburst.

3.37. 1RXS J053234.9+624755

The period evolution of this SU UMa-type dwarf nova during the 2005 and 2008 superoutbursts has been described in Imada et al. (2009) and Kato et al. (2009a).

We also observed the 2009 superoutburst which was accompanied by a precursor outburst, as in the 2005 one (figure 36). The times of superhump maxima are listed in table 39. Superhumps were already present during the fading stage of the rebrightening, and the period was smoothly decreasing as in the 2005 one Imada et al. (2009). This indicates that the stage B, rather than stage A, already started during the precursor outburst. This behavior very well reproduced the features observed during the 2005 superoutburst. The observed $P_{\rm dot}$ for stage B ($E \leq 145$) was $+10.1(1.0) \times 10^{-5}$, similar to the one observed in 2008, but is larger than in 2005. The 2009 outburst was also well-observed during the post-superoutburst stage. Although times of individual superhumps were not sufficiently measured due to strong flickering, the period analysis has yielded a periodicity of 0.05690(2) d (BJD 2455081.2–2455090.6, figure 37), which is in agreement with the period of stage C superhumps. The signal from the orbital period, if present, was still much smaller than the superhump signal. This analysis suggests the long endurance of superhumps even after the termination of the superoutburst.

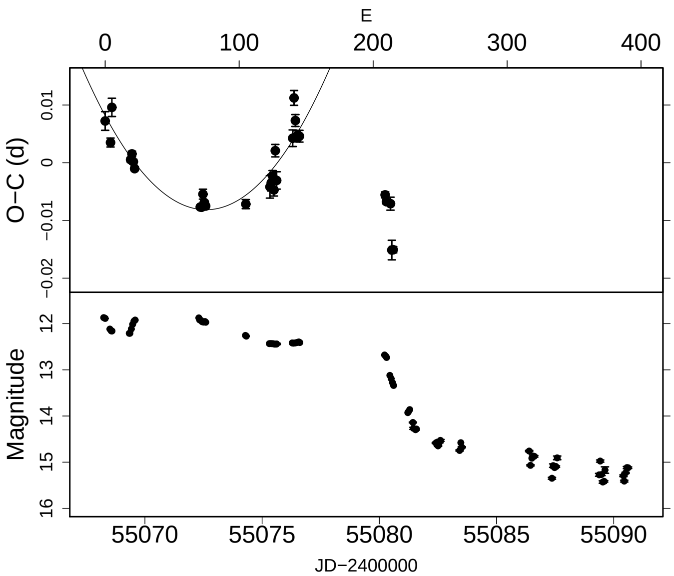

Fig. 36. $O-C$ of superhumps 1RXS J0532 (2009). (Upper): $O-C$ diagram. The $O-C$ values were against the mean period for the stage B ($E \le 145$, thin curve) (Lower): Light curve.

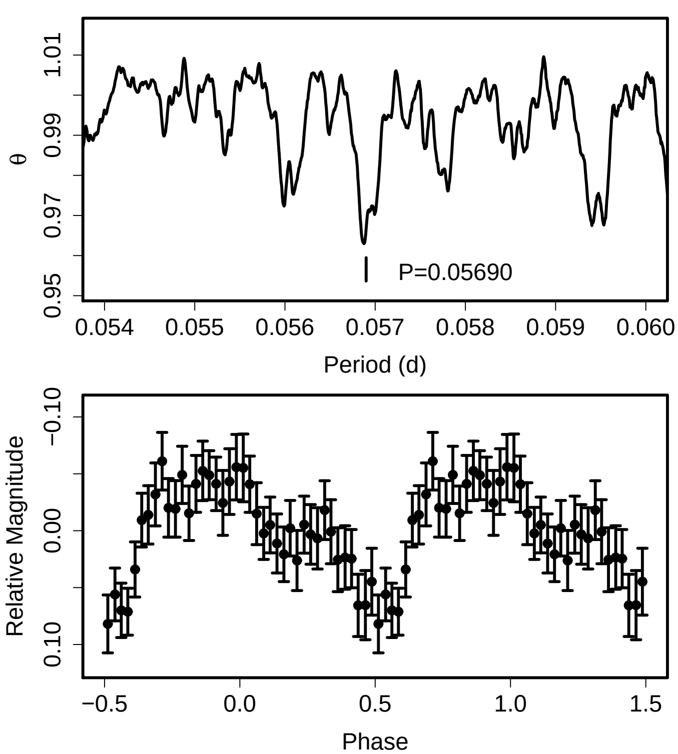

Fig. 37. Superhumps during the post-superoutburst stage in 1RXS J0532 (2009). (Upper): PDM analysis. (Lower): Phase-averaged profile.

Table 38. Superhump maxima of 1RXS J0423 (2010).

E	max*	error	$O-C$†	N‡
0	55442.1696	0.0006	−0.0155	124
1	55442.2491	0.0005	−0.0141	94
12	55443.1233	0.0003	−0.0007	114
13	55443.1995	0.0004	−0.0028	309
14	55443.2795	0.0008	−0.0010	108
25	55444.1410	0.0004	−0.0003	268
26	55444.2188	0.0002	−0.0007	470
27	55444.2979	0.0003	0.0001	406
38	55445.1623	0.0007	0.0037	67
39	55445.2402	0.0018	0.0034	42
40	55445.3196	0.0007	0.0045	73
79	55448.3718	0.0009	0.0049	47
80	55448.4501	0.0004	0.0050	79
81	55448.5259	0.0004	0.0025	76
82	55448.6063	0.0005	0.0047	79
83	55448.6825	0.0010	0.0026	62
88	55449.0717	0.0020	0.0005	157
89	55449.1554	0.0008	0.0061	240
90	55449.2320	0.0009	0.0043	475
91	55449.3099	0.0005	0.0041	205
92	55449.3840	0.0024	−0.0001	49
93	55449.4716	0.0016	0.0093	80
94	55449.5447	0.0015	0.0041	78
95	55449.6240	0.0009	0.0052	79
96	55449.7020	0.0016	0.0048	42
102	55450.1716	0.0009	0.0050	218
103	55450.2496	0.0007	0.0047	197
114	55451.1109	0.0021	0.0053	90
115	55451.1783	0.0080	−0.0056	114
116	55451.2728	0.0026	0.0106	108
140	55453.1084	0.0032	−0.0318	77
141	55453.2028	0.0042	−0.0157	87
142	55453.2896	0.0033	−0.0071	85

*BJD−2400000.
†Against $max = 2455442.1850 + 0.078251E$.
‡Number of points used to determine the maximum.

3.38. *ASAS J224349+0809.5*

ASAS J224349+0809.5 (hereafter ASAS J2243) was selected as a dwarf nova by P. Wils (cvnet-discussion 1320; Shears et al. (2010e)). The 2009 outburst and the superhumps were detected by I. Miller (cvnet-outburst 3358). The object showed well-developed superhumps and their time-evolution was intensively studied. The times of superhump maxima are listed in table 40. As also reported in Shears et al. (2010e), a textbook stage B–C transition was observed. The $P_{\rm dot}$ during stage B was $+6.6(1.0) \times 10^{-5}$ ($E \le 101$).[4] The object also showed a post-superoutburst rebrightening (figure 38).

[4] Shears et al. (2010e) reported dP/dt of $+1.24(5) \times 10^{-3}$. Our analysis of their timing data yielded $P_{\rm dot}$ of $+9.4(0.7) \times 10^{-5}$ ($E \le 97$) by our definition.

Table 39. Superhump maxima of 1RXS J0532 (2009).

E	max*	error	$O-C$†	N‡
0	55068.3087	0.0016	0.0047	106
4	55068.5335	0.0008	0.0011	114
5	55068.5967	0.0016	0.0072	72
19	55069.3875	0.0004	−0.0013	106
20	55069.4457	0.0005	−0.0003	114
21	55069.5014	0.0004	−0.0016	111
22	55069.5574	0.0003	−0.0027	113
71	55072.3504	0.0003	−0.0075	112
72	55072.4075	0.0004	−0.0075	114
73	55072.4669	0.0009	−0.0052	36
74	55072.5226	0.0004	−0.0066	72
75	55072.5791	0.0003	−0.0071	107
105	55074.2935	0.0008	−0.0056	108
123	55075.3249	0.0019	−0.0019	115
124	55075.3828	0.0014	−0.0012	102
125	55075.4411	0.0009	0.0000	97
126	55075.4958	0.0011	−0.0023	108
127	55075.5598	0.0011	0.0045	114
128	55075.6117	0.0015	−0.0006	77
140	55076.3047	0.0014	0.0072	112
141	55076.3688	0.0013	0.0142	114
142	55076.4220	0.0010	0.0103	113
143	55076.4764	0.0009	0.0076	112
144	55076.5335	0.0006	0.0076	107
145	55076.5907	0.0010	0.0077	110
209	55080.2372	0.0005	0.0001	145
210	55080.2932	0.0004	−0.0011	172
213	55080.4643	0.0011	−0.0013	63
214	55080.5134	0.0017	−0.0093	54
215	55080.5705	0.0006	−0.0092	44

*BJD−2400000.
†Against $max = 2455068.3040 + 0.057097E$.
‡Number of points used to determine the maximum.

3.39. Lanning 420

Lanning 420 was selected as a UV-bright transient object (Lanning, Meakes 2000), which was considered to be a possible nova because of the absence on the Digitized Sky Survey image. Brady et al. (2008) listed Lanning CVs and further investigated these objects. S. Brady indeed detected an outburst in 2007 and another one in 2010, which turned out to be a superoutburst (BAAVSS alert 2374). Follow-up observation confirmed the presence of superhumps (vsnet-alert 12131, 12132, 12138; figure 39).

The times of superhump maxima are listed in table 41. There was a distinct shortening of the superhump period around $E = 70$, which we interpreted as a stage B–C transition. The last two epochs were measured during the early post-superoutburst stage. We included these epochs because short-P_{SH} tend to show persistent superhumps during this stage and the times of maxima were in good agreement with extrapolated stage C superhumps. The measured period derivative during the stage B had a relatively large error because only the late stage of the stage B

Table 40. Superhump maxima of ASAS J2243 (2009).

E	max*	error	$O-C$†	N‡
0	55113.0454	0.0002	0.0005	132
1	55113.1144	0.0003	−0.0003	131
2	55113.1842	0.0003	−0.0001	132
5	55113.3918	0.0003	−0.0017	64
6	55113.4596	0.0003	−0.0036	75
7	55113.5328	0.0003	−0.0001	67
10	55113.7392	0.0002	−0.0028	182
11	55113.8079	0.0002	−0.0039	182
15	55114.0866	0.0003	−0.0040	134
23	55114.6442	0.0002	−0.0041	184
24	55114.7131	0.0003	−0.0049	180
25	55114.7841	0.0003	−0.0036	179
26	55114.8539	0.0005	−0.0035	104
29	55115.0633	0.0004	−0.0033	109
30	55115.1365	0.0007	0.0003	64
36	55115.5479	0.0010	−0.0067	16
38	55115.6896	0.0004	−0.0044	55
47	55116.3174	0.0004	−0.0039	57
48	55116.3881	0.0003	−0.0030	83
49	55116.4581	0.0005	−0.0027	69
50	55116.5269	0.0007	−0.0036	31
51	55116.6073	0.0017	0.0071	39
52	55116.6714	0.0013	0.0014	49
53	55116.7374	0.0005	−0.0023	104
54	55116.8085	0.0022	−0.0009	69
56	55116.9463	0.0019	−0.0025	30
62	55117.3650	0.0009	−0.0020	80
63	55117.4344	0.0005	−0.0023	87
64	55117.5049	0.0005	−0.0015	76
65	55117.5769	0.0018	0.0008	22
71	55117.9965	0.0006	0.0020	196
72	55118.0654	0.0005	0.0012	176
75	55118.2775	0.0011	0.0042	26
76	55118.3461	0.0009	0.0030	35
77	55118.4148	0.0010	0.0021	58
78	55118.4790	0.0013	−0.0034	56
79	55118.5559	0.0013	0.0038	57
89	55119.2535	0.0025	0.0043	24
91	55119.3946	0.0012	0.0059	56
92	55119.4650	0.0007	0.0066	65
93	55119.5342	0.0009	0.0060	32
94	55119.6046	0.0007	0.0068	90
95	55119.6740	0.0005	0.0065	81
96	55119.7461	0.0005	0.0088	83
97	55119.8138	0.0005	0.0068	79
100	55120.0233	0.0004	0.0072	143
101	55120.0937	0.0004	0.0079	149
106	55120.4399	0.0005	0.0055	63
108	55120.5797	0.0007	0.0060	73
109	55120.6490	0.0004	0.0055	91
110	55120.7186	0.0004	0.0054	88
111	55120.7870	0.0006	0.0041	88
118	55121.2762	0.0015	0.0053	113
119	55121.3420	0.0004	0.0014	156
120	55121.4116	0.0007	0.0013	182
121	55121.4811	0.0008	0.0011	149
122	55121.5515	0.0009	0.0017	92
123	55121.6190	0.0003	−0.0005	182

*BJD−2400000.
†Against $max = 2455113.0449 + 0.069712E$.
‡Number of points used to determine the maximum.

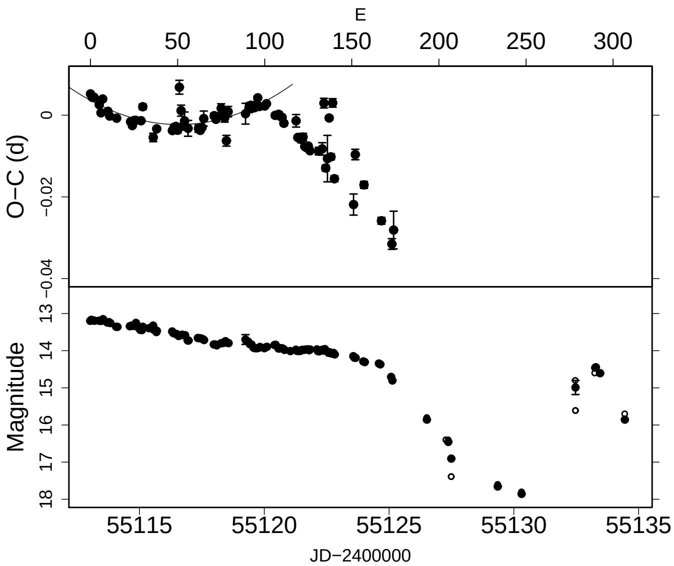

Fig. 38. $O-C$ of superhumps ASAS J2243 (2009). (Upper): $O-C$ diagram. The $O-C$ values were against the mean period for the stage B ($E \leq 101$, thin curve) (Lower): Light curve. Open circles are snapshot unfiltered CCD observations.

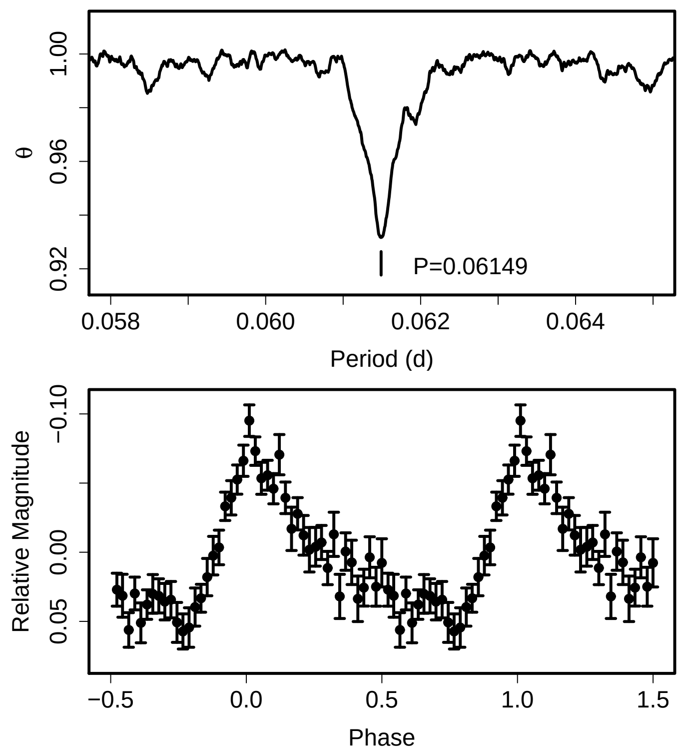

Fig. 39. Superhumps in Lanning 420 (2010). (Upper): PDM analysis. (Lower): Phase-averaged profile.

Table 40. Superhump maxima of ASAS J2243 (2009) (continued).

E	max*	error	$O-C$†	N‡
124	55121.6885	0.0003	−0.0006	182
125	55121.7587	0.0005	−0.0002	184
126	55121.8274	0.0004	−0.0012	130
131	55122.1763	0.0009	−0.0008	131
133	55122.3165	0.0015	−0.0001	24
134	55122.3975	0.0012	0.0112	140
135	55122.4514	0.0007	−0.0046	220
136	55122.5235	0.0057	−0.0022	85
137	55122.6033	0.0005	0.0079	178
138	55122.6636	0.0007	−0.0016	181
139	55122.7466	0.0010	0.0117	178
140	55122.7979	0.0007	−0.0067	180
151	55123.5594	0.0026	−0.0120	94
152	55123.6415	0.0013	0.0004	178
157	55123.9831	0.0009	−0.0066	147
167	55124.6724	0.0008	−0.0144	92
173	55125.0856	0.0013	−0.0195	149
174	55125.1588	0.0046	−0.0160	73

*BJD−2400000.
†Against $max = 2455113.0449 + 0.069712E$.
‡Number of points used to determine the maximum.

was observed. Observations of the earlier stage are crucial to better characterize the period variation in this system.

3.40. PG 0149+138

This object (hereafter PG 0149) was originally discovered as an eruptive object with strong UV excess, and was suspected to be a supernova (Green et al. 1986). Szkody et al. (2002b) selected this object during the course of the SDSS survey and classified it as a CV (dwarf nova). The object as been monitored as a dwarf nova since then. Dillon et al. (2008) photometrically identified a $P_{\rm orb}$ of 0.08242(3) d.

The 2009 September outburst of this object was detected by the the Catalina Real-time Transient Survey (CRTS, Drake et al. 2009)[5] (= CSS090911:015152+140047). Superhumps were detected immediately following the announcement (vsnet-alert 11465). The mean $P_{\rm SH}$ with the PDM method was 0.08495(2) d (figure 40). The times of superhump maxima are summarized in table 42. There was a clear stage B–C transition with a positive $P_{\rm dot} = +14.6(2.5) \times 10^{-5}$ ($E \leq 60$). Such a positive $P_{\rm dot}$ is rare for SU UMa-type dwarf novae with this $P_{\rm SH}$. The behavior in the superhump period resemble that of long-$P_{\rm SH}$ systems like QW Ser (cf. Nogami et al. 2004; Kato et al. 2009a).

[5] <http://nesssi.cacr.caltech.edu/catalina/>. For the information of the individual Catalina CVs, see <http://nesssi.cacr.caltech.edu/catalina/AllCV.html>.

Table 41. Superhump maxima of Lanning 420 (2010).

E	max*	error	$O-C$†	N‡
0	55438.5841	0.0005	−0.0084	20
1	55438.6469	0.0005	−0.0070	26
2	55438.7074	0.0005	−0.0078	24
3	55438.7691	0.0005	−0.0075	25
4	55438.8277	0.0018	−0.0102	24
14	55439.4478	0.0011	−0.0033	51
15	55439.5051	0.0018	−0.0074	46
16	55439.5672	0.0011	−0.0066	89
17	55439.6314	0.0012	−0.0037	86
18	55439.6895	0.0010	−0.0069	88
19	55439.7535	0.0008	−0.0042	76
20	55439.8132	0.0012	−0.0059	46
21	55439.8767	0.0009	−0.0037	60
22	55439.9369	0.0008	−0.0048	56
23	55439.9982	0.0012	−0.0049	45
24	55440.0589	0.0015	−0.0055	125
25	55440.1225	0.0030	−0.0032	115
31	55440.4990	0.0049	0.0054	20
32	55440.5511	0.0022	−0.0039	21
33	55440.6082	0.0073	−0.0081	19
34	55440.6785	0.0020	0.0008	49
35	55440.7379	0.0006	−0.0010	56
36	55440.7997	0.0009	−0.0006	31
37	55440.8611	0.0006	−0.0005	45
38	55440.9243	0.0007	0.0014	56
39	55440.9852	0.0023	0.0009	163
40	55441.0392	0.0054	−0.0064	128
41	55441.1128	0.0018	0.0059	253
42	55441.1713	0.0019	0.0031	115
46	55441.4149	0.0030	0.0014	15
47	55441.4792	0.0028	0.0044	21
48	55441.5345	0.0020	−0.0017	25
49	55441.5992	0.0038	0.0017	39
50	55441.6608	0.0016	0.0019	48
51	55441.7225	0.0008	0.0023	73
52	55441.7874	0.0017	0.0059	60
53	55441.8443	0.0020	0.0015	53
54	55441.9112	0.0015	0.0071	56
55	55441.9710	0.0019	0.0056	56
62	55442.4036	0.0011	0.0088	21
63	55442.4636	0.0010	0.0075	71
64	55442.5285	0.0026	0.0111	21
65	55442.5846	0.0016	0.0059	21
66	55442.6469	0.0029	0.0068	21
76	55443.2586	0.0018	0.0053	110
78	55443.3918	0.0051	0.0159	35
79	55443.4458	0.0014	0.0085	48
80	55443.5039	0.0015	0.0053	46
81	55443.5651	0.0017	0.0051	48
82	55443.6274	0.0015	0.0061	45
83	55443.6835	0.0083	0.0009	17
92	55444.2430	0.0024	0.0085	122
93	55444.3012	0.0021	0.0053	63
94	55444.3635	0.0024	0.0064	15
95	55444.4301	0.0130	0.0116	21
96	55444.4863	0.0023	0.0065	20

*BJD−2400000.
†Against $max = 2455438.5926 + 0.061325E$.
‡Number of points used to determine the maximum.

Table 41. Superhump maxima of Lanning 420 (2010) (continued).

E	max*	error	$O-C$†	N‡
97	55444.5442	0.0020	0.0031	15
98	55444.6082	0.0026	0.0058	19
99	55444.6637	0.0014	−0.0001	19
109	55445.2851	0.0155	0.0081	65
116	55445.7083	0.0024	0.0020	17
117	55445.7670	0.0032	−0.0006	16
118	55445.8309	0.0017	0.0019	16
124	55446.1980	0.0028	0.0011	111
125	55446.2583	0.0046	0.0001	80
126	55446.3132	0.0059	−0.0063	60
174	55449.2331	0.0071	−0.0301	117
175	55449.2880	0.0028	−0.0365	109

*BJD−2400000.
†Against $max = 2455438.5926 + 0.061325E$.
‡Number of points used to determine the maximum.

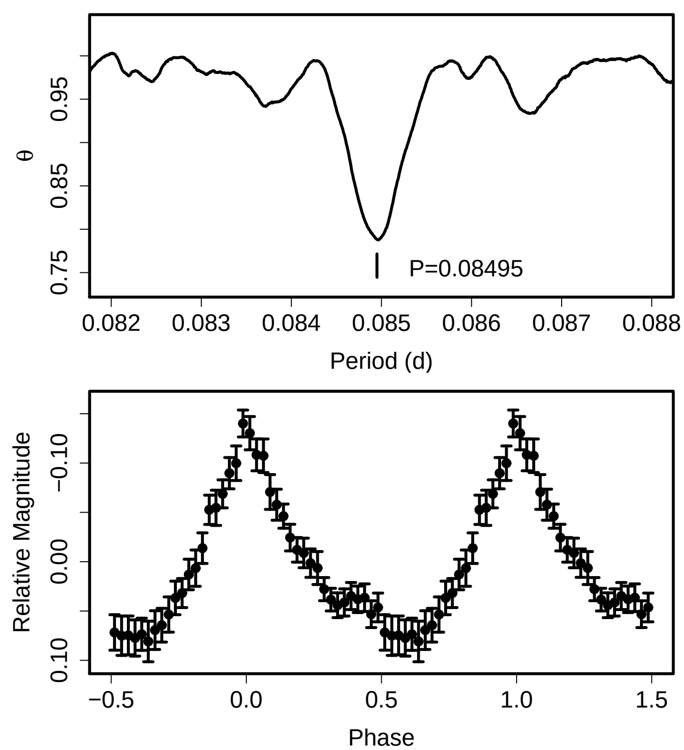

Fig. 40. Superhumps in PG 0149 (2009). (Upper): PDM analysis. (Lower): Phase-averaged profile.

Table 42. Superhump maxima of PG 0149 (2009).

E	max*	error	$O-C$†	N‡
0	55086.5129	0.0008	−0.0038	44
1	55086.5987	0.0003	−0.0028	89
11	55087.4448	0.0007	−0.0055	57
12	55087.5312	0.0005	−0.0040	114
13	55087.6173	0.0005	−0.0029	89
23	55088.4654	0.0006	−0.0036	40
24	55088.5484	0.0006	−0.0054	83
55	55091.1917	0.0006	0.0065	180
59	55091.5320	0.0007	0.0073	77
60	55091.6176	0.0008	0.0080	89
70	55092.4661	0.0006	0.0076	91
71	55092.5517	0.0007	0.0083	130
72	55092.6371	0.0006	0.0089	111
93	55094.4113	0.0014	0.0005	40
94	55094.4977	0.0009	0.0020	45
95	55094.5776	0.0009	−0.0029	44
103	55095.2556	0.0008	−0.0039	146
154	55099.5741	0.0013	−0.0145	78

*BJD−2400000.
†Against $max = 2455086.5166 + 0.084883E$.
‡Number of points used to determine the maximum.

3.41. RX J1715.6+6856

This object (hereafter RX J1715) is a CV identified from the ROSAT North Ecliptic Pole survey (Pretorius et al. 2007). Pretorius et al. (2007) reported the detection of a 1.64(2) hr period from radial-velocity study. Shears et al. (2010d) identified the dwarf-nova type behavior and detected superhumps during a superoutburst in 2009 August. We analyzed the combined data from Shears et al. (2010d) (from the AAVSO database) and our own observations. As reported in Shears et al. (2010d), these observations covered the final stage of the superoutburst.

The times of maxima are listed in table 43. Since the $O-C$'s for maxima for $E \geq 63$ largely deviate from the earlier trend, these humps are less likely a continuation of superhumps observed during the plateau phase ($E \leq 48$). Restricting to $E \leq 48$, we obtained a mean $P_{\rm SH}$ of 0.07074(4) d with the PDM method (figure 41). and is in agreement with the corresponding period of 0.07086(78) d by Shears et al. (2010d) within respective errors. The ϵ against $P_{\rm orb}$ was 3.5 %. Since the observation covered the final part of the superoutburst, these superhumps are likely stage C superhumps.

Although Shears et al. (2010d) interpreted observed humps for $E \geq 63$ (rapid fading stage and post-superoutburst stage) as orbital humps, the reported period [0.06944(90) d] is somewhat different from the one reported from radial-velocity study. Our analysis also confirmed a significant phase offset during the rapid fading stage (figure 42). We could not, however, determine whether the newly arising signals were from orbital humps or were from traditional late superhumps because the amplitude on JD 2455069 was very small and it was difficult to derive a meaningful period based on the last two nights of observations. Future observations are needed to confirm the nature of these large-amplitude humps. Since stage C superhumps frequently endure during the post-superoutburst stage in many well-observed systems (cf. Kato et al. 2009a), the early disappearance of superhumps in RX J1715 appears to be rather unique. The case may be similar to DT Oct (cf. Kato et al. (2009a)), which showed an early switch to traditional late superhumps. Although both relatively low outburst amplitudes and the relatively strong X-ray emission are common to these objects, the frequency of outbursts in RX J1715 appears to be smaller (Shears et al. 2010d). A further detailed comparison between these objects might be fruitful.

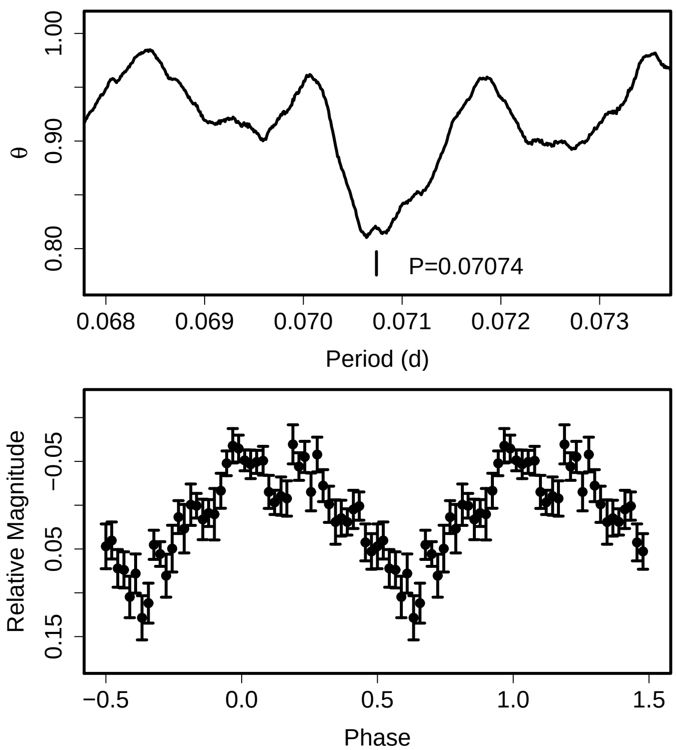

Fig. 41. Superhumps in RX J1715 (2009). (Upper): PDM analysis. (Lower): Phase-averaged profile.

3.42. SDSS J012940.05+384210.4

This object (hereafter SDSS J0129) is an AM CVn-type CV selected during the course of the SDSS (Anderson et al. 2005), who reported broad HeI emission lines. The orbital period has not been reported yet.

The object was reported in outburst on 2009 November 29 at a unfiltered CCD magnitude of 14.5 (cvnet-outburst 3479, vsnet-alert 11702). Two days after this detection, the object started to fade rapidly. Immediately following this transient fading, the object experienced rebrightenings on December 4 and 18 (vsnet-alert 11707, 11737). The overall behavior of the outburst (figure 43) was extremely similar to the 2003 August superoutburst of V803

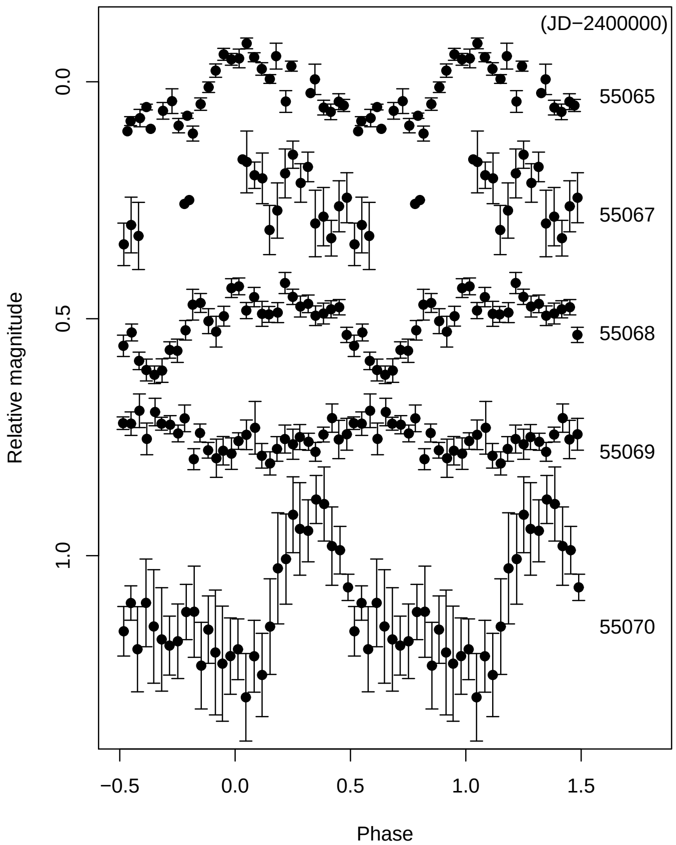

Fig. 42. Nightly variation of profiles of superhumps in RX J1715 (2009). The profiles were drawn against a period of 0.07074 d, determined from the superoutburst plateau. Although this period well expresses the variations on the first three nights, there was a significant phase offset at later stages.

Table 43. Superhump maxima of RX J1715 (2009).

E	max*	error	$O-C$†	N‡
0	55065.3776	0.0007	0.0037	61
1	55065.4528	0.0010	0.0078	87
2	55065.5181	0.0008	0.0021	30
23	55067.0079	0.0080	−0.0000	86
39	55068.1405	0.0021	−0.0041	134
42	55068.3635	0.0014	0.0058	62
43	55068.4183	0.0014	−0.0105	90
44	55068.4953	0.0015	−0.0045	101
47	55068.7020	0.0021	−0.0110	37
48	55068.7722	0.0024	−0.0118	27
63	55069.8143	0.0045	−0.0353	37
63	55069.8756	0.0019	0.0259	38
64	55069.9378	0.0010	0.0171	32
75	55070.7114	0.0019	0.0092	27
76	55070.7752	0.0016	0.0020	25
77	55070.8431	0.0024	−0.0012	26
78	55070.9205	0.0012	0.0051	24

*BJD−2400000.
†Against $max = 2455065.3739 + 0.071044E$.
‡Number of points used to determine the maximum.

Cen (Kato et al. 2004a; vsnet-alert 11709).

The object developed hump signals during its terminal stage of the plateau phase (figures 44, 45). Although these humps may reflect orbital modulations, we identified them as superhumps based on extreme analogy with V803 Cen (Kato et al. 2004a). The mean period determined with the PDM method was 0.01805(10) d. The period is also very similar to that of V803 Cen (P = 0.018686(4) d = 1614.5(4) s, Kato et al. 2004a).

The times of maxima during the fading branch from the superoutburst are listed in table 44.

Table 44. Superhump maxima of SDSS J0129 (2009).

E	max*	error	$O-C$†	N‡
0	55166.3297	0.0030	−0.0020	40
1	55166.3491	0.0037	−0.0007	40
2	55166.3686	0.0012	0.0007	41
4	55166.4080	0.0013	0.0039	41
5	55166.4231	0.0006	0.0009	52
6	55166.4433	0.0013	0.0031	62
7	55166.4567	0.0012	−0.0016	61
8	55166.4739	0.0015	−0.0026	22
18	55166.6542	0.0011	−0.0032	17
19	55166.6730	0.0011	−0.0024	17
20	55166.6947	0.0017	0.0012	17
22	55166.7329	0.0019	0.0031	17
23	55166.7458	0.0017	−0.0020	17
25	55166.7840	0.0010	0.0000	17
26	55166.8034	0.0012	0.0013	17
28	55166.8384	0.0010	0.0001	17
29	55166.8547	0.0017	−0.0016	16
30	55166.8764	0.0008	0.0020	16

*BJD−2400000.
†Against $max = 2455166.3317 + 0.018090E$.
‡Number of points used to determine the maximum.

3.43. SDSS J031051.66−075500.3

In addition to the 2004 superoutburst of this object (hereafter SDSS J0310), two superoutbursts were recorded in 2009. Table 45 gives the times of superhump maxima during its second superoutburst in 2009 (2009 November, designated as 2009b in table in order to avoid confusion with the 2009 superoutburst described in Kato et al. 2009a). The mean $P_{\rm SH}$ during this superoutburst was 0.06786(3) d (PDM method, alias selected based on the 2004 observation), which is shorter than the period obtained during the 2004 superoutburst. Although this dif-

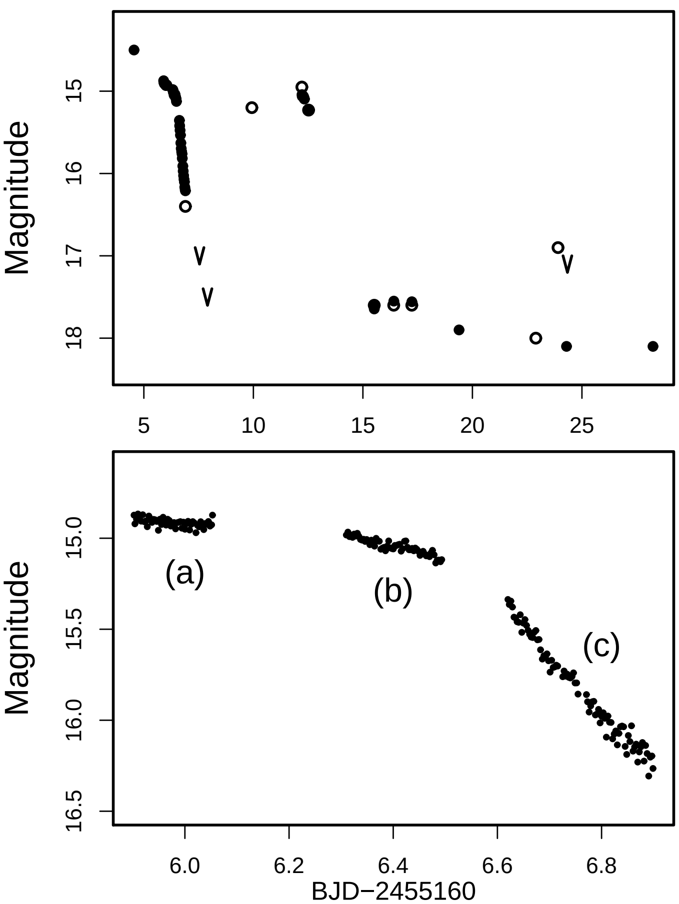

Fig. 43. Outburst of SDSS J0129 in 2009 November–December. (Upper): Overall outburst including the rebrightening phase. (Lower): Enlargement of the main superoutburst. The segments (a)–(c) correspond to the intervals to draw figure 45.

Table 45. Superhump maxima of SDSS J0310 (2009 November).

E	max*	error	$O-C$†	N‡
0	55144.5155	0.0003	0.0028	67
1	55144.5777	0.0003	−0.0029	73
31	55146.6161	0.0009	0.0001	61

*BJD−2400000.
†Against $max = 2455144.5127 + 0.067848E$.
‡Number of points used to determine the maximum.

ference may have resulted from different stages observed in different outbursts, the difference appears to be larger than those associated with typical stage B–C transitions (Kato et al. 2009a). This needs to be clarified by future observations. The shortest interval between superoutbursts was 284 d, which is likely the supercycle of this object.

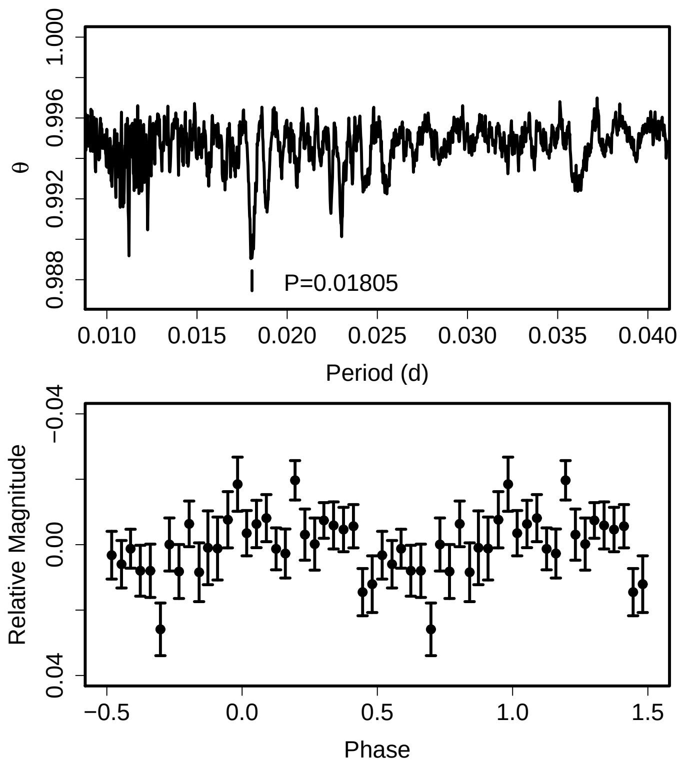

Fig. 44. Superhumps in SDSS J0129 (2009). (Upper): PDM analysis. The signal around $P = 0.036$ is the first harmonic of the fundamental period. (Lower): Phase-averaged profile.

3.44. SDSS J073208.11+413008.7

This object (hereafter SDSS J0732) was selected using SDSS and CRTS data as a candidate dwarf nova by Wils et al. (2010).[6] The object was detected in outburst by J. Shears on 2009 December 31 at an unfiltered CCD magnitude of 16.2 (cvnet-outburst 3528; Shears et al. (2010c)). Subsequent observations confirmed the presence of superhumps (cvnet-outburst 3535, figure 46).

The times of superhump maxima determined from AAVSO observations are listed in table 46.[7] The object showed a clear stage B–C transition around $E = 60$. The $P_{\rm dot}$ for stage B was $+3.9(2.4) \times 10^{-5}$.[8] Relatively few objects with similar $P_{\rm SH}$, including RZ Leo and QY Per, are known to show positive $P_{\rm dot}$ (Kato et al. 2009a). Although the relatively large (5.2 mag) outburst amplitude also might suggest a low mass-transfer rate as in

[6] Although this object was not discovered during the regular course of the SDSS survey, we used SDSS designation for convention.

[7] We designated this outburst as SDSS J0732 (2010) because all time-resolved observation were undertaken in 2010.

[8] Shears et al. (2010c) reported dP/dt of $+2.81(9) \times 10^{-3}$. They used a data set including our present data set. We do not attempt to choose a better $P_{\rm dot}$ between ours and theirs, since $P_{\rm dot}$ is dependent on the segment used, and the observed baseline for the stage B was too short. The $P_{\rm dot}$ determined from the timing data in Shears et al. (2010c) was $+22.5(6.5) \times 10^{-5}$ ($E \leq 41$) while it was $-1.7(3.3) \times 10^{-5}$ for $E \leq 64$ (both values are by our definition of $P_{\rm dot}$).

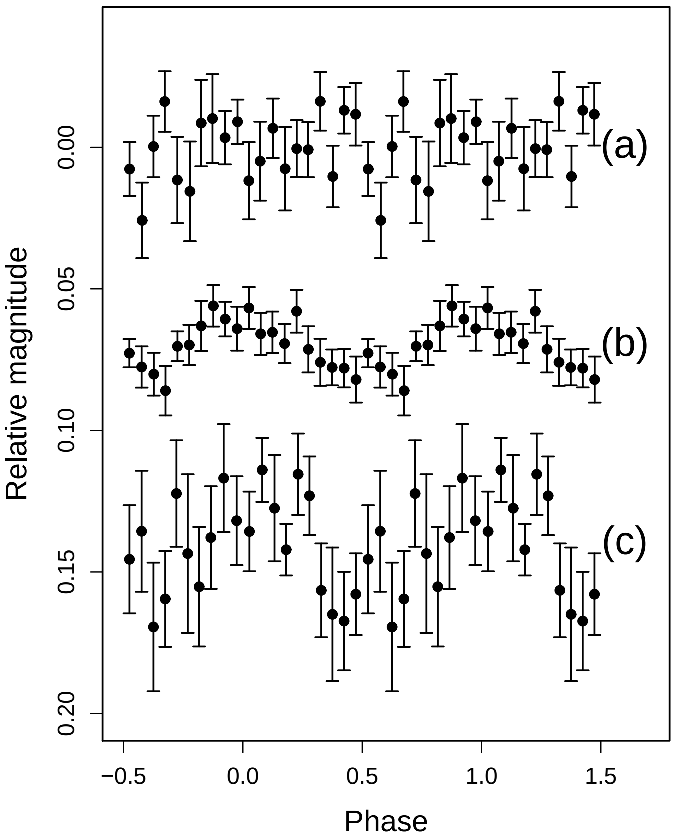

Fig. 45. Variation of superhump profiles during the fading stage of the superoutburst of SDSS J0129 (2009). A mean period of 0.01805 d was used to draw this figure. The segments (a)–(c) are shown in figure 43.

RZ Leo and QY Per, the outburst frequency estimated in Shears et al. (2010c) is much higher than in these objects. An exact determination of $P_{\rm dot}$ during the next superoutburst is desired.

3.45. SDSSp J083845.23+491055.5

This object (hereafter SDSS J0838) underwent another superoutburst in 2010 in addition to the 2007 and 2009 ones discussed in Kato et al. (2009a). The 2010 superoutburst was notable in that it was preceded by a prominent precursor outburst (vsnet-alert 11910). Although only two superhump maxima were measured, we listed them in table 47. The interval between maxima is in agreement with the period of stage C superhumps in 2009. Since the 2010 observation was undertaken during the early stage of the superoutburst, the period is expected to be close to the $P_{\rm SH}$ at the start of stage B. As discussed in Kato et al. (2009a), this period is expected to be close to $P_{\rm SH}$ for stage C superhumps. The present finding is consistent with this interpretation. There was a slight indication of modulation at a period around 0.0709 d and an amplitude of 0.07 mag. Although the presence of this signal is not conclusive, the periodicity might suggest a rare evolution of $P_{\rm SH}$ starting from $P_{\rm orb}$, as recorded in QZ Vir Kato (1997). This needs to be confirmed by future observa-

Table 46. Superhump maxima of SDSS J0732 (2010).

E	max*	error	$O-C$†	N‡
0	55199.6270	0.0020	−0.0080	42
1	55199.7096	0.0007	−0.0050	83
2	55199.7887	0.0006	−0.0054	76
3	55199.8666	0.0006	−0.0071	81
4	55199.9462	0.0008	−0.0071	82
10	55200.4238	0.0018	−0.0071	60
14	55200.7446	0.0006	−0.0047	82
15	55200.8244	0.0007	−0.0044	68
16	55200.9040	0.0006	−0.0044	82
17	55200.9833	0.0011	−0.0047	73
26	55201.7046	0.0006	0.0003	82
27	55201.7859	0.0007	0.0020	82
28	55201.8656	0.0008	0.0020	74
29	55201.9427	0.0010	−0.0004	82
30	55202.0233	0.0012	0.0005	83
38	55202.6663	0.0010	0.0068	71
39	55202.7456	0.0007	0.0065	82
40	55202.8253	0.0006	0.0066	76
41	55202.9044	0.0009	0.0061	82
42	55202.9841	0.0011	0.0062	75
59	55204.3438	0.0017	0.0129	88
60	55204.4230	0.0011	0.0125	90
75	55205.6122	0.0006	0.0077	73
76	55205.6924	0.0007	0.0083	83
77	55205.7727	0.0008	0.0090	82
78	55205.8501	0.0007	0.0069	79
79	55205.9295	0.0007	0.0067	82
90	55206.8014	0.0006	0.0031	76
91	55206.8798	0.0008	0.0019	82
92	55206.9602	0.0010	0.0027	67
114	55208.7037	0.0013	−0.0049	82
115	55208.7840	0.0011	−0.0042	75
116	55208.8664	0.0010	−0.0014	83
117	55208.9413	0.0011	−0.0061	75
118	55209.0165	0.0023	−0.0104	82
126	55209.6628	0.0019	−0.0009	83
127	55209.7402	0.0013	−0.0031	76
128	55209.8098	0.0014	−0.0130	76
129	55209.8958	0.0014	−0.0067	82

*BJD−2400000.

†Against $max = 2455199.6349 + 0.079593E$.

‡Number of points used to determine the maximum.

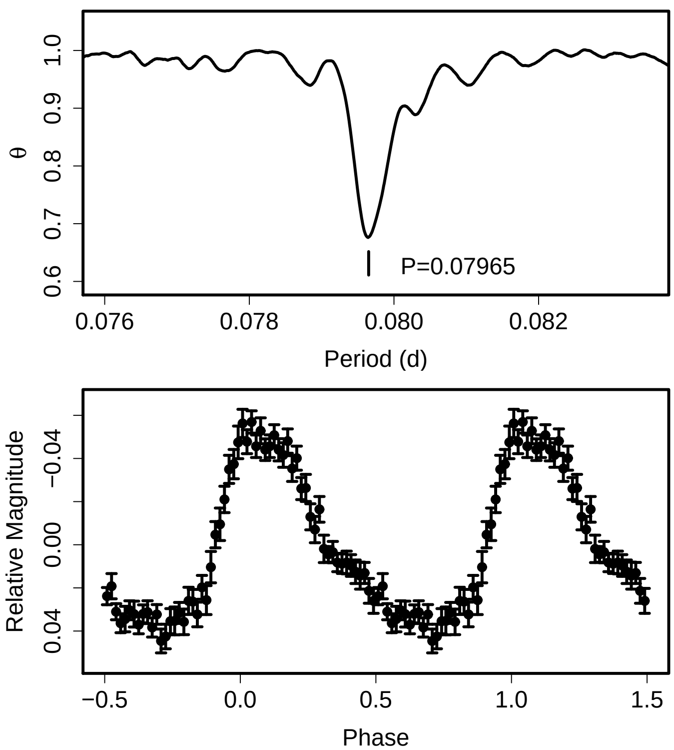

Fig. 46. Superhumps in SDSS J0732 (2010). (Upper): PDM analysis. (Lower): Phase-averaged profile.

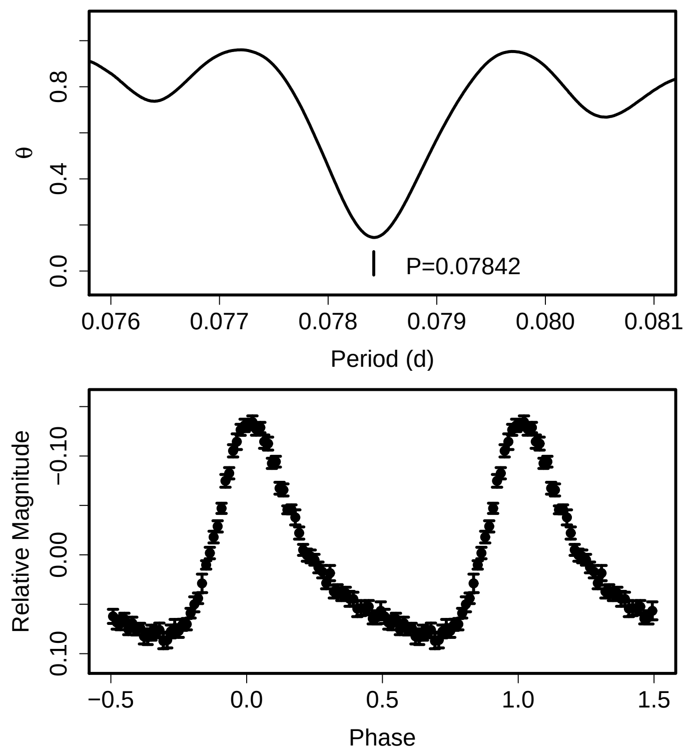

Fig. 47. Superhumps in SDSS J0839 (2010). (Upper): PDM analysis. (Lower): Phase-averaged profile.

Table 47. Superhump maxima of SDSS J0838 (2010).

E	max*	error	$N^\dagger$
0	55294.9551	0.0008	99
1	55295.0289	0.0004	153

*BJD−2400000.
†Number of points used to determine the maximum.

tions.

3.46. SDSS J083931.35+282824.0

This object (hereafter SDSS J0839) was selected as a CV during the course of SDSS Szkody et al. (2005). Although the spectrum was suggestive of that of a dwarf nova, no outburst had been recorded. On 2010 April 8, K. Itagaki detected an outbursting object which can be identified with this CV (vsnet-alert 11911). Subsequent observations have confirmed the presence of superhumps (vsnet-alert 11916, 11921, 11926, 11930).

The times of superhump maxima are listed in table 48. There was an apparent break in the $O-C$ diagram around $E = 15$, which is likely a stage B–C transition. The periods given in table 2 are based on this interpretation. The mean $P_{\rm SH}$ determined with the PDM method is 0.078423(7) d (figure 47).

Table 48. Superhump maxima of SDSS J0839 (2010).

E	max*	error	$O-C^\dagger$	$N^\ddagger$
0	55295.3531	0.0002	−0.0003	190
1	55295.4309	0.0002	−0.0009	220
2	55295.5099	0.0004	−0.0003	83
13	55296.3732	0.0004	0.0006	79
14	55296.4518	0.0003	0.0007	78
15	55296.5311	0.0007	0.0016	41
26	55297.3919	0.0008	−0.0000	78
27	55297.4694	0.0005	−0.0009	78
38	55298.3319	0.0006	−0.0008	128
39	55298.4115	0.0003	0.0003	246

*BJD−2400000.
†Against $max = 2455295.3534 + 0.078403E$.
‡Number of points used to determine the maximum.

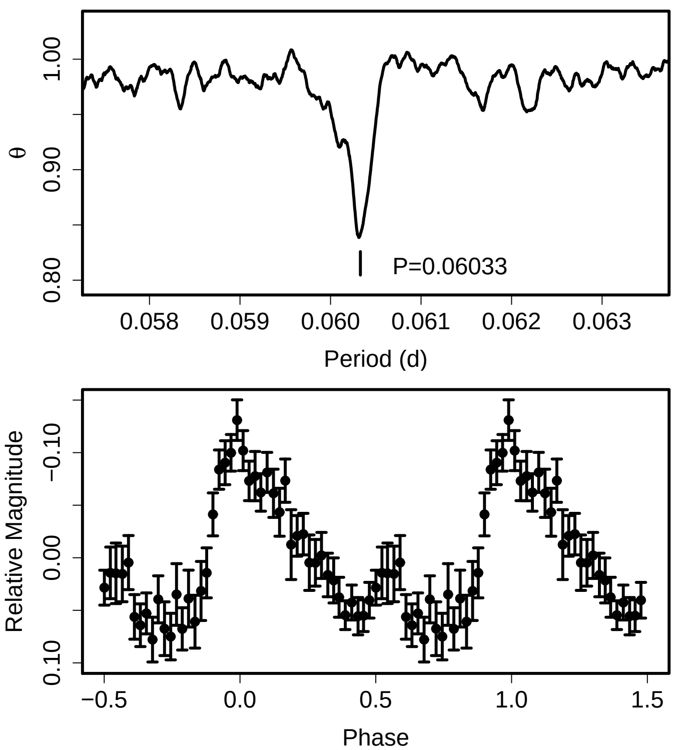

Fig. 48. Superhumps in SDSS J0903 (2010) outside the eclipses. (Upper): PDM analysis. (Lower): Phase-averaged profile.

3.47. *SDSS J090350.73+330036.1*

This object (hereafter SDSS J0903) is a CV selected during the course of the SDSS (Szkody et al. 2005), who suspected its eclipsing nature. Littlefair et al. (2008) confirmed that this object is a deeply eclipsing CV with a short orbital period of 0.059073543(9) d. The 2010 outburst, the first-ever outburst reported in real-time, was detected by CRTS (= CSS100522:090351+330036; cf. vsnet-alert 11994). Subsequent observations have confirmed the eclipsing SU UMa-type nature of this object (vsnet-alert 12006; figure 48).

The times of mid-eclipses were determined with the KW method (table 49). We obtained an updated orbital ephemeris (equation 2) using our data and times of eclipses in Littlefair et al. (2008).

$$\mathrm{Min(BJD)} = 2453800.394708(2) + 0.059073525(4)E. \quad (2)$$

In the following analysis, we removed observations within 0.08 $P_{\rm orb}$ of eclipses.

The times of superhump maxima are listed in table 50. There was a clear stage B–C transition around $E = 116$. The $P_{\rm dot}$ for stage B was $+12.3(3.7) \times 10^{-5}$. This clearly positive $P_{\rm dot}$ in deeply eclipsing short-period SU UMa-type dwarf novae confirmed the finding in XZ Eri (Uemura et al. 2004; Kato et al. 2009a). The fractional superhump excesses for stages B and C were 2.1 % and 1.7 %, respectively. Other parameters are listed in table 2.

Table 49. Eclipse Minima of SDSS J0903.

E	Minimum*	error	$O-C$†	Source‡
0	53800.394700	0.000006	-0.00001	1
2	53800.512854	0.000006	-0.00000	1
34	53802.403198	0.000006	-0.00001	1
35	53802.462279	0.000006	-0.00000	1
36	53802.521361	0.000006	0.00001	1
37	53802.580442	0.000006	0.00001	1
38	53802.639501	0.000006	-0.00000	1
50	53803.348386	0.000006	0.00000	1
51	53803.407462	0.000006	0.00000	1
52	53803.466529	0.000006	-0.00000	1
53	53803.525601	0.000006	-0.00000	1
26086	55341.38690	0.00030	0.00022	2
26087	55341.44648	0.00036	0.00073	2
26102	55342.33163	0.00038	-0.00022	2
26104	55342.44915	0.00038	-0.00085	2
26119	55343.33624	0.00039	0.00013	2
26136	55344.34126	0.00034	0.00091	2
26137	55344.39964	0.00039	0.00020	2
26152	55345.28500	0.00030	-0.00053	2
26154	55345.40339	0.00046	-0.00029	2
26169	55346.29034	0.00029	0.00056	2
26170	55346.34966	0.00032	0.00080	2
26171	55346.40821	0.00045	0.00028	2
26188	55347.41127	0.00056	-0.00091	2
26193	55347.70712	0.00027	-0.00043	2
26204	55348.35745	0.00037	0.00009	2
26205	55348.41652	0.00035	0.00009	2
26209	55348.65271	0.00030	-0.00001	2
26210	55348.71183	0.00036	0.00003	2
26221	55349.36176	0.00037	0.00015	2
26222	55349.42067	0.00040	-0.00001	2
26243	55350.66096	0.00034	-0.00026	2
26244	55350.71996	0.00044	-0.00034	2
26255	55351.36974	0.00028	-0.00037	2
26256	55351.42824	0.00041	-0.00095	2
26272	55352.37433	0.00072	-0.00003	2

*BJD−2400000.

†Against equation 2.

‡1: Littlefair et al. (2008), 2: this work.

Table 50. Superhump maxma of SDSS J0903 (2010).

E	max*	error	$O-C^{\dagger}$	$N^{\ddagger}$
0	55340.4222	0.0009	0.0072	51
31	55342.2882	0.0009	0.0033	26
32	55342.3424	0.0007	−0.0028	57
33	55342.4003	0.0019	−0.0052	31
48	55343.3142	0.0013	0.0039	19
49	55343.3624	0.0016	−0.0083	55
50	55343.4267	0.0017	−0.0043	54
65	55344.3326	0.0008	−0.0032	57
81	55345.2974	0.0008	−0.0035	57
82	55345.3554	0.0047	−0.0058	48
83	55345.4122	0.0040	−0.0093	51
98	55346.3301	0.0017	0.0038	83
99	55346.3923	0.0017	0.0056	47
114	55347.3027	0.0090	0.0112	74
116	55347.4195	0.0024	0.0075	51
121	55347.7186	0.0012	0.0050	52
132	55348.3800	0.0009	0.0028	54
133	55348.4419	0.0017	0.0044	29
137	55348.6809	0.0007	0.0021	62
149	55349.4016	0.0010	−0.0010	50
170	55350.6692	0.0019	−0.0002	49
182	55351.3798	0.0022	−0.0133	29

*BJD−2400000.

†Against $max = 2455340.4150 + 0.060320E$.

‡Number of points used to determine the maximum.

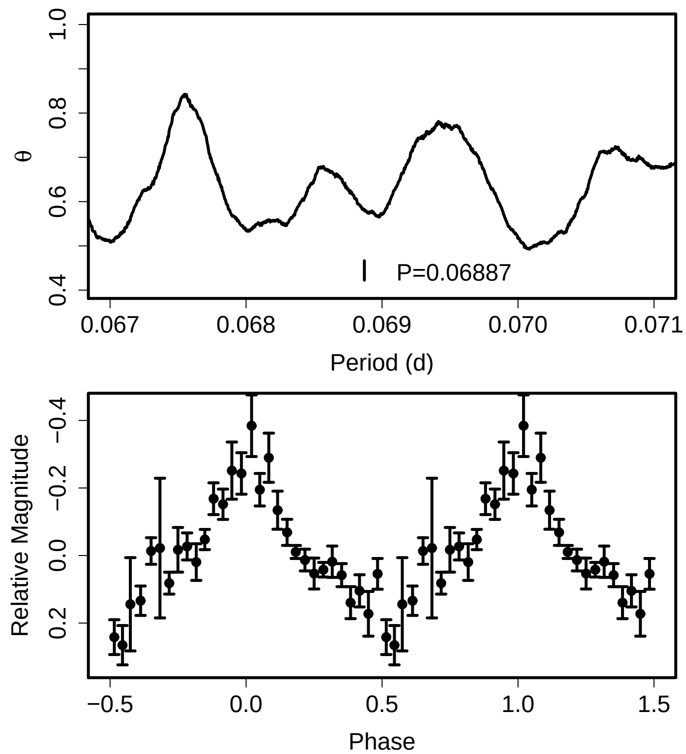

Fig. 49. Superhumps in SDSS J1152 (2009). (Upper): PDM analysis. The alias selection was based on $P_{\rm orb}$. The best period was determined by Bayesian modeling. (Lower): Phase-averaged profile.

3.48. SDSS J115207.00+404947.8

This object (hereafter SDSS J1152) is a CV selected during the course of the SDSS (Szkody et al. 2007), who suspected its eclipsing nature. Southworth et al. (2008) established that this CV is deeply eclipsing and determined its period to be 0.06770(28) d.

The 2009 June outburst was detected by E. Muyllaert at a CCD magnitude of 16.4 on June 9 (cvnet-outburst 3158). Superhumps and eclipses were soon detected (vsnet-alert 11288), establishing the SU UMa-type nature of this object. The times of superhump maxima determined observations outside the eclipses are listed in table 51. The intervening clouds made the epoch of $E = 39$ rather uncertain. A period analysis with the PDM method has yielded a $P_{\rm SH}$ of 0.0689(1) d (figure 49). Since the signal is broad due to the poor phase coverage, we used a Bayesian modeling of the light curve using the template superhump light curve (see Appendix). The best period by this method is 0.06887(4) d, corresponding to ϵ of 1.7 %. We adopted this period in the figure and table. Although the basic nature of the object is well-established, both orbital and superhump periods need to be refined by further observations.

Table 51. Superhump maxima of SDSS J1152 (2009).

E	max*	error	$O-C^{\dagger}$	$N^{\ddagger}$
0	54994.0621	0.0005	0.0056	125
39	54996.7376	0.0068	−0.0135	9
67	54998.6919	0.0021	0.0062	18
68	54998.7564	0.0021	0.0016	28

*BJD−2400000.

†Against $max = 2454994.0565 + 0.069092E$.

‡Number of points used to determine the maximum.

3.49. SDSS J125023.85+665525.5

This object (hereafter J1250) is a CV selected during the course of the SDSS (Szkody et al. 2003), who suggested a high inclination CV. Dillon et al. (2008) confirmed that

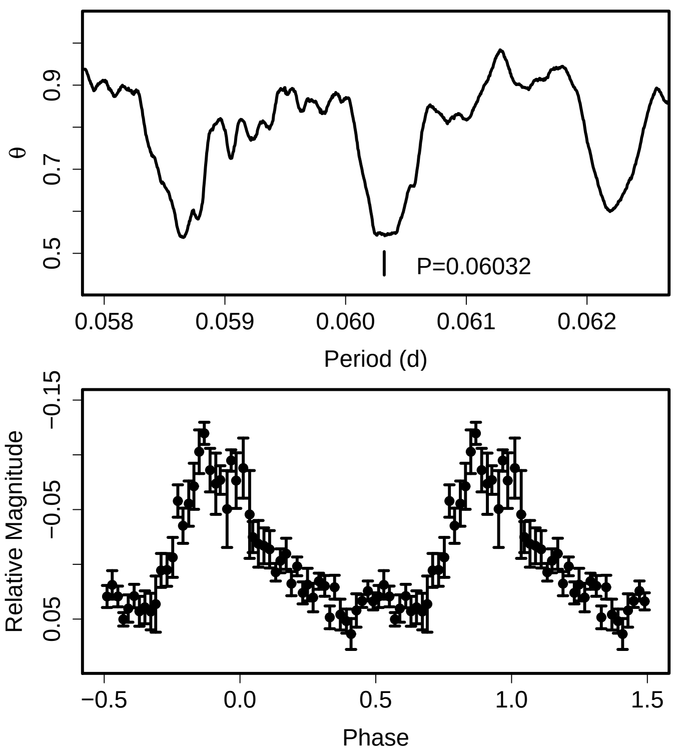

Fig. 50. Superhumps in SDSS J1250 (2008). (Upper): PDM analysis. The selection of the alias is based on the orbital period. (Lower): Phase-averaged profile.

Table 52. Superhump maxima of SDSS J1250 (2008).

E	max*	error	$O-C$†	N‡
0	54491.9263	0.0010	0.0039	6
44	54494.5762	0.0018	−0.0002	18
45	54494.6331	0.0012	−0.0037	41
46	54494.6926	0.0014	−0.0044	39
47	54494.7553	0.0008	−0.0020	42
48	54494.8165	0.0007	−0.0011	41
77	54496.5690	0.0022	0.0021	17
78	54496.6287	0.0011	0.0015	24
79	54496.6906	0.0015	0.0031	24
80	54496.7482	0.0011	0.0003	22
81	54496.8082	0.0009	−0.0000	24
82	54496.8696	0.0013	0.0011	24
83	54496.9293	0.0010	0.0005	20
146	54500.7289	0.0033	0.0000	22
147	54500.7882	0.0029	−0.0010	19

*BJD−2400000.
†Against $max = 2454491.9224 + 0.060319E$.
‡Number of points used to determine the maximum.

Table 53. Superhump maxima of SDSS J1250 (2009).

E	max*	error	N†
0	55144.2715	0.0015	77
1	55144.3338	0.0004	54

*BJD−2400000.
†Number of points used to determine the maximum.

this is indeed a deeply eclipsing CV with a very short orbital period of 0.058735687(4) d.

Shortly before Dillon et al. (2008) becomes available, the object was found to be in outburst in 2008 January (S. Brady, cvnet-discussion 1104), who successfully detected eclipses and reported a period of 0.059 d. Based on these and 2009 observations, we have determined eclipse times and updated the ephemeris.

Both the 2008 and 2009 outbursts were superoutbursts, and the times of superhump maxima are listed in tables 52 and 53 determined from observations outside the eclipses.

A PDM analysis of the 2008 observations has yielded a mean $P_{\rm SH}$ of 0.06032(5) d (figure 50). The $P_{\rm dot}$ for $E \le 83$, apparently stage B, was $+9.4(2.1) \times 10^{-5}$. The period apparently decreased after this, suggesting a transition to stage C. The ϵ of 2.7 % for the mean $P_{\rm SH}$ is relatively large for this $P_{\rm orb}$. Using the ϵ–q relation in Kato et al. (2009a), this ϵ corresponds to $q = 0.14$. Assuming a moderate white-dwarf mass, this q would place the object around the upper (massive secondary) boundary defined by SDSS J0903 and SDSS J1507 in figure 2 of Littlefair et al. (2008) rather than around the period bounce. This identification appears to be favored by the relatively large $P_{\rm dot}$ and rather frequent outbursts (the interval of two superoutburst was $\sim$ 650 d). Further determination of system parameters of this object will improve our knowledge of CV evolution near the period minimum.

3.50. SDSS J150240.98+333423.9

This object (hereafter SDSS J1502) is an eclipsing CV selected during the course of the SDSS (Szkody et al. 2006). Littlefair et al. (2008) performed high-speed photometry in quiescence and obtained orbital parameters [$P_{\rm dot}$ = 0.05890961(5) d and estimated q = 0.109(3)]. Littlefair et al. (2008) attributed this CV to a CV before the "period bounce".

The 2009 July superoutburst of this object was detected by J. Shears (baavss-alert 1997). Subsequent observations detected superhumps (cf. vsnet-alert 11332; figure 51). Shears et al. (2010a) also reported an analysis of the same superoutburst using the slightly different data set from ours.

The times of mid-eclipses were determined with the KW method (table 54). We obtained an updated orbital ephemeris (equation 3) using our data and times of eclipses in Littlefair et al. (2008) and Shears et al. (2010a). We only used times of eclipses in Shears et al. (2010a) which were not covered by our observations. We also disregarded $E = 855$ eclipse due to its large $O-C$.

$$\mathrm{Min(BJD)} = 2453799.64048(6) + 0.058909473(3)E. \quad (3)$$

In the following analysis, we removed observations within 0.08 $P_{\rm orb}$ of eclipses.

The times of superhump maxima are listed in table 55.

Table 54. Eclipse Minima of SDSS J1502.

E	Minimum*	error	$O-C$†	Source‡
0	53799.640618	0.000004	0.00013	1
2	53799.758414	0.000007	0.00011	1
17	53800.642070	0.000006	0.00012	1
18	53800.700966	0.000006	0.00011	1
19	53800.759901	0.000006	0.00014	1
52	53802.703911	0.000002	0.00013	1
68	53803.646461	0.000003	0.00013	1
69	53803.705371	0.000006	0.00013	1
70	53803.764277	0.000003	0.00013	1
854	53849.94908	0.00035	-0.00009	2
866	53850.65615	0.00012	0.00006	2
867	53850.71498	0.00011	-0.00002	2
868	53850.77384	0.00021	-0.00007	2
869	53850.83284	0.00012	0.00002	2
870	53850.89165	0.00014	-0.00008	2
871	53850.95066	0.00013	0.00003	2
883	53851.65760	0.00014	0.00005	2
884	53851.71630	0.00014	-0.00016	2
886	53851.83418	0.00016	-0.00010	2
887	53851.89334	0.00014	0.00015	2
888	53851.95250	0.00014	0.00040	2
900	53852.65899	0.00018	-0.00002	2
901	53852.71800	0.00015	0.00008	2
902	53852.77661	0.00011	-0.00022	2
903	53852.83568	0.00014	-0.00006	2
1308	53876.69411	0.00004	0.00004	2
6454	54179.84201	0.00009	-0.00021	2
6455	54179.90009	0.00009	-0.00104	2
6457	54180.01899	0.00011	0.00004	2
13787	54611.82514	0.00012	-0.00025	2
13788	54611.88411	0.00012	-0.00019	2
13789	54611.94325	0.00017	0.00004	2
13802	54612.70876	0.00019	-0.00027	2
13803	54612.76795	0.00012	0.00001	2
13804	54612.82684	0.00018	-0.00001	2
13805	54612.88550	0.00012	-0.00026	2
13806	54612.94456	0.00027	-0.00011	2
20758	55022.48413	0.00005	0.00081	2
20760	55022.60121	0.00032	0.00007	3
20761	55022.66052	0.00036	0.00047	3
20762	55022.71932	0.00026	0.00036	3
20763	55022.77857	0.00031	0.00070	2
20777	55023.60263	0.00029	0.00003	3
20778	55023.66133	0.00028	-0.00018	2
20779	55023.72066	0.00021	0.00024	3
20780	55023.77951	0.00018	0.00018	3
20781	55023.83814	0.00024	-0.00010	3
20782	55023.89720	0.00040	0.00005	3
20794	55024.60306	0.00050	-0.00101	2
20796	55024.72187	0.00026	-0.00001	3
20797	55024.78077	0.00022	-0.00002	3
20798	55024.83956	0.00028	-0.00014	3
20807	55025.37023	0.00027	0.00034	3

*BJD−2400000.
†Against equation 3.
‡1: Littlefair et al. (2008), 2: Shears et al. (2010a), 3: this work.

Table 54. Eclipse Minima of SDSS J1502 (continued).

E	Minimum*	error	$O-C$†	Source‡
20808	55025.42910	0.00030	0.00030	3
20811	55025.60573	0.00042	0.00020	3
20812	55025.66472	0.00014	0.00028	3
20813	55025.72362	0.00016	0.00027	3
20814	55025.78256	0.00017	0.00030	3
20815	55025.84150	0.00023	0.00034	3
20824	55026.37130	0.00026	-0.00005	3
20825	55026.43013	0.00033	-0.00013	3
20828	55026.60726	0.00011	0.00027	2
20829	55026.66588	0.00029	-0.00002	3
20830	55026.72440	0.00022	-0.00041	3
20831	55026.78290	0.00033	-0.00082	3
20832	55026.84210	0.00100	-0.00053	3
20835	55027.01943	0.00032	0.00008	3
20836	55027.07836	0.00028	0.00010	3
20837	55027.13703	0.00053	-0.00014	3
20841	55027.37299	0.00026	0.00018	3
20845	55027.60852	0.00038	0.00007	3
20846	55027.66772	0.00040	0.00036	3
20847	55027.72659	0.00021	0.00032	3
20848	55027.78561	0.00022	0.00043	2
20849	55027.84470	0.00051	0.00061	3
20858	55028.37421	0.00027	-0.00006	3
20859	55028.43318	0.00019	-0.00000	3
20860	55028.49206	0.00023	-0.00003	3
20861	55028.55083	0.00026	-0.00017	3
20864	55028.72779	0.00037	0.00006	3
20881	55029.72935	0.00035	0.00016	3
20882	55029.78814	0.00036	0.00004	3
20883	55029.84720	0.00033	0.00019	3
20894	55030.49541	0.00105	0.00040	2
20895	55030.55404	0.00024	0.00012	2
20898	55030.73046	0.00014	-0.00019	2
20898	55030.73050	0.00033	-0.00015	3
20899	55030.78951	0.00034	-0.00005	3
20900	55030.84853	0.00035	0.00006	3
20915	55031.73159	0.00076	-0.00052	3
20916	55031.79037	0.00043	-0.00065	2
20917	55031.84916	0.00138	-0.00077	3
20928	55032.49776	0.00068	-0.00017	3
20929	55032.55681	0.00079	-0.00003	3
20932	55032.73351	0.00064	-0.00006	3
20934	55032.85137	0.00065	-0.00002	3
20949	55033.73470	0.00075	-0.00033	3
20950	55033.79383	0.00077	-0.00011	3
20966	55034.73608	0.00118	-0.00041	2
20968	55034.85449	0.00133	0.00018	3
21031	55038.56538	0.00065	-0.00023	3
21758	55081.39289	0.00168	0.00009	2

*BJD−2400000.
†Against equation 3.
‡1: Littlefair et al. (2008), 2: Shears et al. (2010a), 3: this work.

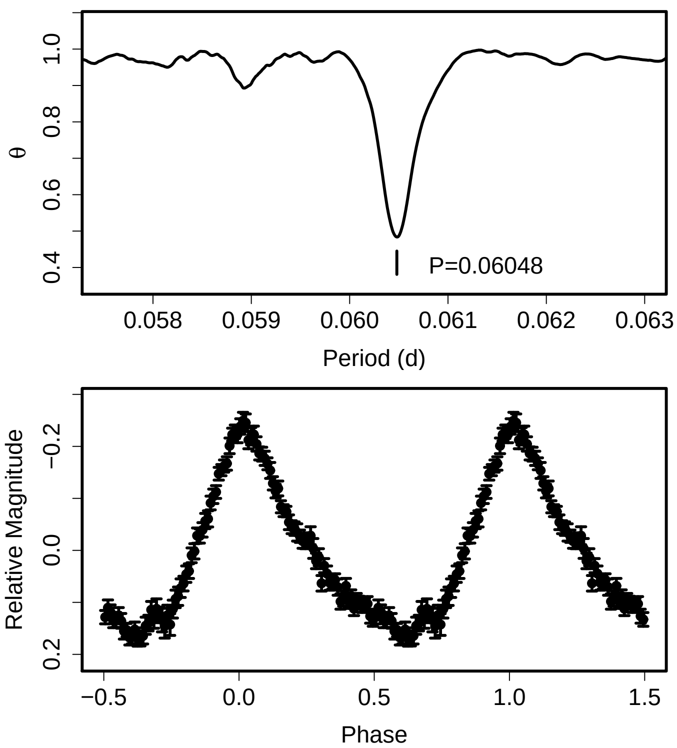

Fig. 51. Superhumps in SDSS J1502 (2009). (Upper): PDM analysis. (Lower): Phase-averaged profile.

There was a likely stage B–C transition around $E = 100$. The values given in table 2 were estimated following this interpretation. The P_{dot} for stage B was $+3.7(1.5) \times 10^{-5}$, which may have been underestimated because the earliest part of the outburst was not sufficiently observed. Although Shears et al. (2010a) detected a pattern of $O-C$ variation basically to ours, we used our values based on larger set of data.[9] The maxima for $E \geq 152$ may not be superhumps, probably strongly affected by orbital modulations, and are excluded from this period analysis.

3.51. SDSS J161027.61+090738.4

This object (hereafter SDSS J1610) was initially selected as a dwarf nova by Wils et al. (2010). The 2009 July outburst was detected by the CRTS (= CSS090727:161028+090739). Double-peaked strong emission lines, characteristic to a relatively high inclination dwarf nova, in SDSS spectrum was announced (vsnet-alert 11350). A remarkable growth of superhumps was observed four days after the outburst detection (vsnet-alert 11366), suggesting a substantial delay in the growth of superhumps. Further observations clarified the potential WZ Sge-type characters (vsnet-alert 11367, 11368, 11381; figure 52.

The times of ordinary superhumps are listed in table 56. There was a clear stage A–B transition around $E = 33$.

[9] Although their dP/dt was reported to be $+2.8(1.0) \times 10^{-4}$, our analysis of their timing data for $E \leq 89$ yielded a P_{dot} of $+12.1(1.3) \times 10^{-5}$ by our definition.

Table 55. Superhump maxima of SDSS J1502 (2009).

E	max*	error	$O-C$†	N‡
0	55022.6300	0.0004	0.0039	92
1	55022.6895	0.0003	0.0029	78
16	55023.5921	0.0004	−0.0009	69
17	55023.6541	0.0008	0.0007	9
18	55023.7122	0.0004	−0.0016	145
19	55023.7736	0.0003	−0.0007	179
20	55023.8343	0.0004	−0.0004	147
21	55023.8946	0.0012	−0.0005	74
34	55024.6790	0.0005	−0.0017	73
35	55024.7401	0.0002	−0.0011	95
36	55024.8015	0.0003	−0.0002	95
46	55025.4060	0.0003	0.0000	91
47	55025.4652	0.0003	−0.0012	91
49	55025.5904	0.0004	0.0031	29
50	55025.6449	0.0002	−0.0028	154
51	55025.7061	0.0001	−0.0020	279
52	55025.7648	0.0001	−0.0038	230
53	55025.8260	0.0003	−0.0029	187
61	55026.3178	0.0011	0.0054	70
62	55026.3694	0.0005	−0.0035	110
63	55026.4387	0.0005	0.0054	108
66	55026.6156	0.0014	0.0010	24
67	55026.6726	0.0004	−0.0024	127
68	55026.7367	0.0005	0.0012	115
69	55026.7966	0.0006	0.0007	111
73	55027.0410	0.0006	0.0033	91
74	55027.1001	0.0003	0.0020	109
79	55027.4019	0.0003	0.0017	94
82	55027.5840	0.0005	0.0025	52
83	55027.6446	0.0005	0.0027	71
84	55027.7070	0.0005	0.0046	75
86	55027.8266	0.0003	0.0033	75
89	55028.0090	0.0006	0.0045	54
90	55028.0678	0.0003	0.0028	131
91	55028.1284	0.0007	0.0030	85
95	55028.3691	0.0003	0.0020	105
96	55028.4293	0.0003	0.0017	135
97	55028.4904	0.0004	0.0024	157
98	55028.5513	0.0003	0.0029	101
101	55028.7293	0.0006	−0.0005	59
118	55029.7516	0.0007	−0.0055	88
119	55029.8127	0.0006	−0.0048	92
120	55029.8733	0.0006	−0.0046	81
134	55030.7147	0.0005	−0.0093	76
135	55030.7763	0.0005	−0.0081	87
136	55030.8392	0.0007	−0.0057	88
152	55031.7872	0.0023	−0.0246	34
153	55031.8347	0.0023	−0.0375	34
163	55032.4860	0.0016	0.0095	47
164	55032.5491	0.0017	0.0121	46
167	55032.7254	0.0010	0.0072	48
168	55032.7880	0.0008	0.0093	46
169	55032.8425	0.0011	0.0034	49
183	55033.6874	0.0037	0.0023	31
184	55033.7398	0.0070	−0.0058	48
185	55033.7996	0.0020	−0.0065	49
186	55033.8721	0.0038	0.0056	27
200	55034.7195	0.0013	0.0070	47
201	55034.7818	0.0016	0.0088	49
202	55034.8427	0.0026	0.0093	49

*BJD−2400000.

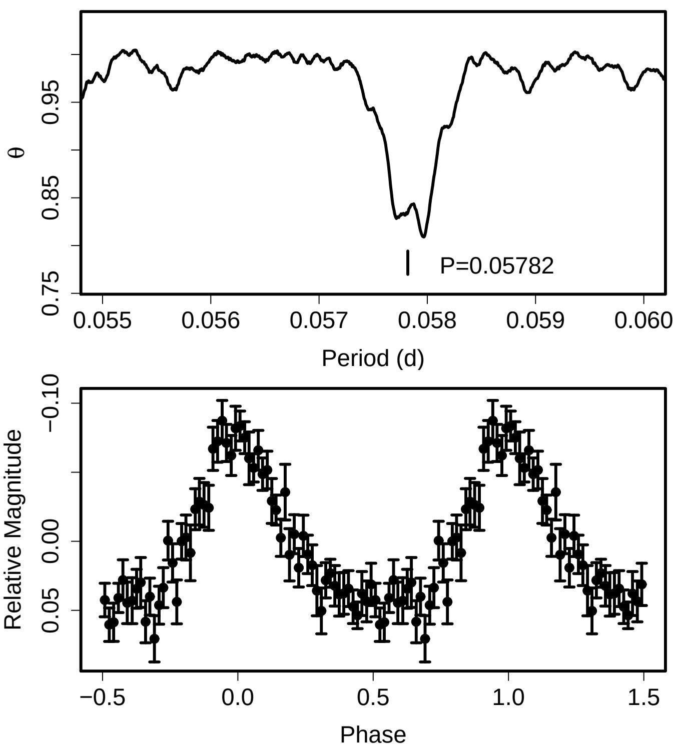

Fig. 52. Superhumps in SDSS J1610 (2009). (Upper): PDM analysis. (Lower): Phase-averaged profile.

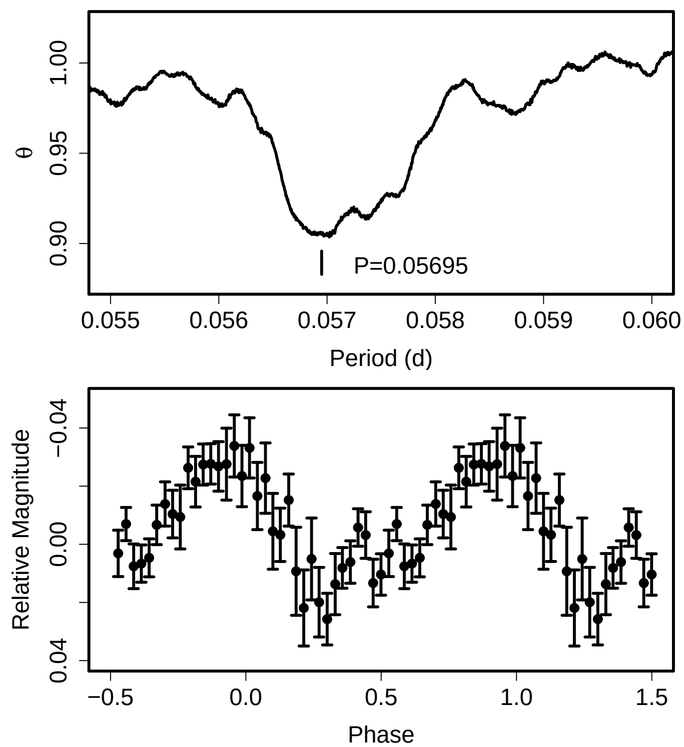

Fig. 53. Early superhumps in SDSS J1610 (2009). (Upper): PDM analysis. (Lower): Phase-averaged profile.

The $P_{\rm dot}$ for the well-observed segment of stage B was $+6.4(1.2) \times 10^{-5}$ ($33 \le E \le 137$). Although an extrapolation to $E = 269$ has yielded a $P_{\rm dot}$ of $+3.2(0.3) \times 10^{-5}$, the identification of superhumps was slightly ambiguous due to the faintness. We thus adopted the former value for the $P_{\rm dot}$ of this object.

An analysis of the light curve before the growth of ordinary superhumps detected early superhumps (figure 53) with a period of 0.05687(1) d (PDM and Bayesian methods), confirming both the WZ Sge-type nature and a relatively high inclination. The resultant ϵ of 1.6 % is relatively large among WZ Sge-type dwarf novae (cf. Kato et al. 2009a), consistent with a relatively large $P_{\rm dot}$.

3.52. SDSS J162520.29+120308.7

This object was selected as a CV candidate by Wils et al. (2010). Although the object was not recognized as a CV during the course of the SDSS, we employed the SDSS designation in this paper (hereafter SDSS J1625).

The 2010 outburst of this object was detected by the CRTS (= CSS100705:162520+120309), a discussion on the SDSS spectrum and the earlier discovery of the object by Wils et al. (2010) can be found in vsnet-alert 12052, 12053. Short-term variations were detected soon after this outburst detection (vsnet-alert 12054, 12059), which later turned out to be developing superhumps (vsnet-alert 12061, 12062). Fully developed superhumps and the course of period evolution were subsequently observed (vsnet-alert 12064, 12065, 12066, 12068, 12071; figure 54). The object entered the rapid decline phase 4–5 d after the development of superhumps, which was unexpectedly early (vsnet-alert 12079). The object was also unusual in its rebrightening phenomenon soon after the rapid decline (vsnet-alert 12087).

The times of superhump maxima are listed in table 57. The epochs for $E \le 21$ correspond to the growing stage of superhumps (stage A). The epochs for $E \ge 130$ were maxima after the rebrightening and these humps may not be true superhumps. We also excluded $E = 114$ (just prior to the rebrightening) in determining period variation due to its low signal. The $P_{\rm dot}$ for $30 \ge E \ge 104$ was $+14.9(3.7) \times 10^{-5}$, which is unusually large for this long $P_{\rm SH}$ = 0.09605(5) d (mean period based on timing analysis). There was also little indication of a stage B–C transition during the superoutburst plateau. These unusual evolution may be related to the unexpectedly early fading during the superoutburst plateau (see figure 55). This object appears to add another variety of superhump evolution in long-$P_{\rm SH}$ systems (cf. Kato et al. 2009a, subsection 4.10).

3.53. SDSS J163722.21−001957.1

This object (hereafter SDSS J1637) is a CV selected during the course of the SDSS (Szkody et al. 2002a). Szkody et al. (2002a) reported the presence of high and low states and suggested the dwarf nova-type classification.

The 2004 outburst of this object was detected by R.

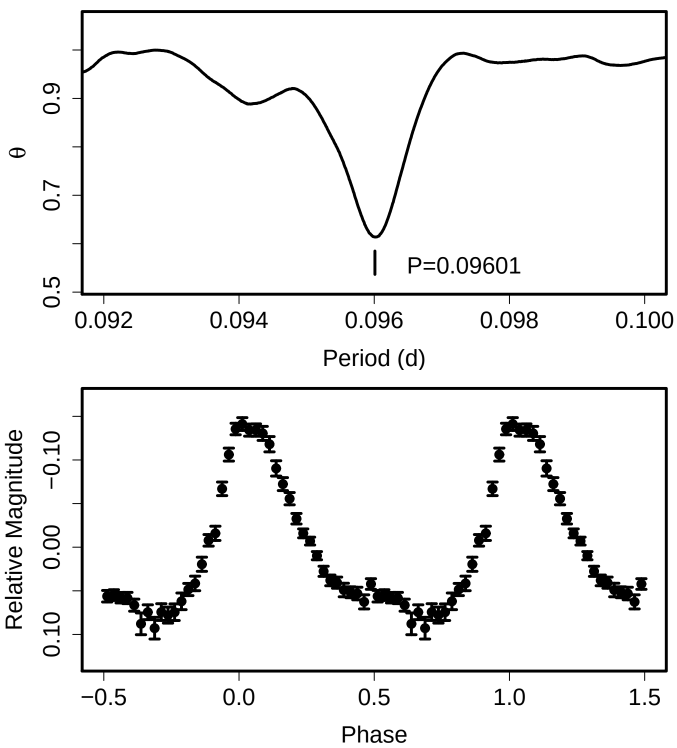

Fig. 54. Superhumps in SDSS J1625 (2010) during stage B. (Upper): PDM analysis. (Lower): Phase-averaged profile.

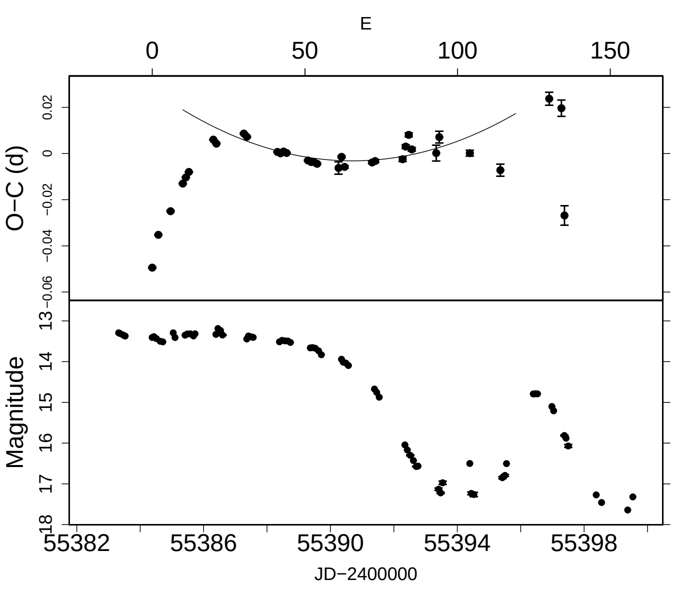

Fig. 55. $O-C$ of superhumps in SDSS J1625 (2010). (Upper): $O-C$ diagram. The $O-C$ values were against the mean period for the stage B ($30 \le E \le 104$, thin curve) (Lower): Light curve. The outburst entered the rapid decline phase during stage B, and was followed by a rebrightening.

Table 56. Superhump maxima of SDSS J1610 (2009).

E	max*	error	$O-C$†	N‡
0	55042.4471	0.0006	−0.0220	120
10	55043.0435	0.0016	−0.0053	99
11	55043.1014	0.0011	−0.0053	184
16	55043.3959	0.0012	−0.0007	29
17	55043.4515	0.0016	−0.0031	28
26	55043.9811	0.0003	0.0048	61
27	55044.0393	0.0002	0.0049	60
28	55044.0986	0.0004	0.0063	60
33	55044.3907	0.0003	0.0085	23
34	55044.4468	0.0006	0.0066	26
35	55044.5061	0.0013	0.0080	17
43	55044.9678	0.0004	0.0059	58
44	55045.0245	0.0006	0.0045	56
45	55045.0839	0.0004	0.0060	46
51	55045.4319	0.0005	0.0061	114
52	55045.4864	0.0005	0.0026	76
61	55046.0067	0.0006	0.0012	49
62	55046.0641	0.0011	0.0006	23
68	55046.4086	0.0009	−0.0028	29
68	55046.4086	0.0010	−0.0027	30
78	55046.9894	0.0012	−0.0017	181
79	55047.0467	0.0012	−0.0023	167
80	55047.1042	0.0008	−0.0029	60
85	55047.3919	0.0008	−0.0050	31
86	55047.4519	0.0009	−0.0029	27
102	55048.3792	0.0009	−0.0033	22
103	55048.4370	0.0010	−0.0034	28
137	55050.4060	0.0028	−0.0055	28
268	55058.0072	0.0025	0.0009	121
269	55058.0659	0.0035	0.0017	123

*BJD−2400000.
†Against $max = 2455042.4690 + 0.057975E$.
‡Number of points used to determine the maximum.

Stubbings at a visual magnitude of 15.0 on 2004 March 27 (vsnet-outburst 6212). The presence of superhumps was soon confirmed (vsnet-alert 8084, 8086, 8088). The mean superhump period determined from the observation was 0.06910(4) d (PDM method, figure 56), and the times of superhump maxima are listed in table 58. Since the outburst entered its rapid decline stage $\sim$ 4 d after the initial detection, these superhumps were very likely stage C superhumps. Using the orbital period of 0.06739(1) d determined by Southworth et al. (2008), we obtained an ϵ of 2.5 %.

3.54. SDSS J165359.06+201010.4

This object (hereafter SDSS J1653) is a CV selected during the course of the SDSS (Szkody et al. 2006), who detected superhumps with a period of 1.58 hr during one of its superoutburst.

The 2010 superoutburst was detected by the CRTS (cf. vsnet-alert 11936). The times of superhump maxima are listed in table 59. It is evident from these data that these

Table 57. Superhump maxima of SDSS J1625 (2010).

E	max*	error	$O-C$†	N‡
0	55384.4489	0.0003	−0.0363	363
2	55384.6553	0.0002	−0.0224	176
6	55385.0497	0.0003	−0.0128	161
10	55385.4459	0.0002	−0.0015	587
11	55385.5446	0.0002	0.0010	365
12	55385.6431	0.0001	0.0032	179
20	55386.4255	0.0001	0.0159	732
21	55386.5198	0.0001	0.0140	662
30	55387.3886	0.0003	0.0169	265
31	55387.4833	0.0003	0.0153	289
41	55388.4373	0.0002	0.0071	328
42	55388.5327	0.0002	0.0064	291
43	55388.6296	0.0002	0.0070	194
44	55388.7250	0.0002	0.0062	158
51	55389.3941	0.0003	0.0018	382
52	55389.4895	0.0003	0.0010	430
53	55389.5855	0.0002	0.0007	189
54	55389.6808	0.0003	−0.0001	200
61	55390.3514	0.0027	−0.0031	135
62	55390.4523	0.0004	0.0016	338
63	55390.5440	0.0006	−0.0029	144
72	55391.4104	0.0005	−0.0025	193
73	55391.5071	0.0007	−0.0021	170
82	55392.3723	0.0010	−0.0027	102
83	55392.4739	0.0008	0.0026	130
84	55392.5750	0.0009	0.0075	144
85	55392.6648	0.0008	0.0010	190
93	55393.4316	0.0034	−0.0019	153
94	55393.5346	0.0025	0.0049	52
104	55394.4882	0.0013	−0.0037	43
114	55395.4413	0.0026	−0.0127	49
130	55397.0091	0.0028	0.0156	200
134	55397.3893	0.0035	0.0108	94
135	55397.4389	0.0042	−0.0358	149

*BJD−2400000.
†Against $max = 2455384.4852 + 0.096218E$.
‡Number of points used to determine the maximum.

Table 58. Superhump maxima of SDSS J1637 (2004).

E	max*	error	$O-C$†	N‡
0	53093.2412	0.0016	−0.0023	145
1	53093.3132	0.0012	0.0004	76
2	53093.3832	0.0012	0.0014	37
4	53093.5206	0.0015	0.0004	18
5	53093.5896	0.0008	0.0002	155
29	53095.2464	0.0027	−0.0030	36
30	53095.3206	0.0025	0.0020	38
31	53095.3890	0.0022	0.0013	30
43	53096.2189	0.0034	0.0012	87
44	53096.2853	0.0028	−0.0016	147

*BJD−2400000.
†Against $max = 2453093.2435 + 0.069167E$.
‡Number of points used to determine the maximum.

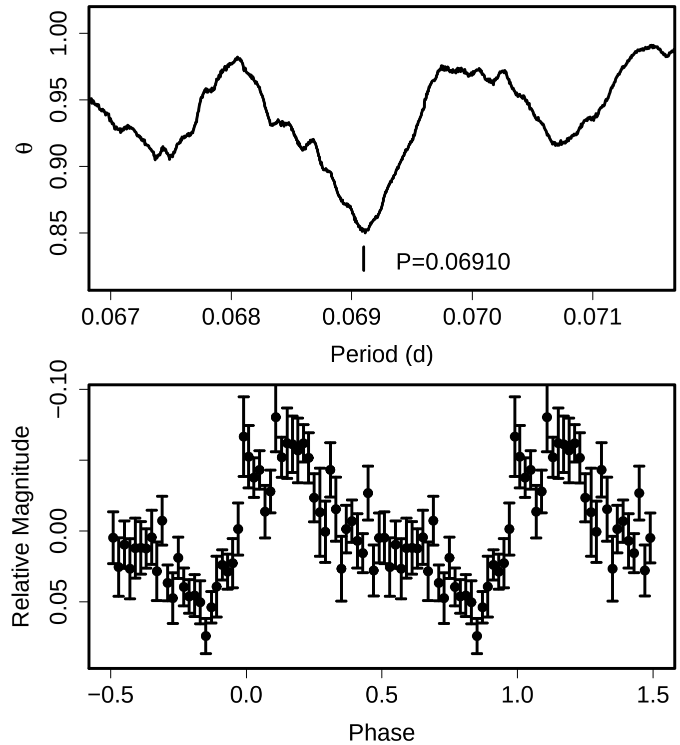

Fig. 56. Superhumps in SDSS J1637 (2004). (Upper): PDM analysis. (Lower): Phase-averaged profile.

Table 59. Superhump maxima of SDSS J1653 (2010).

E	max*	error	$O-C$†	N‡
0	55304.1037	0.0009	−0.0007	67
1	55304.1673	0.0007	−0.0022	59
2	55304.2313	0.0004	−0.0032	66
3	55304.2970	0.0005	−0.0025	66
5	55304.4272	0.0003	−0.0024	73
6	55304.4913	0.0004	−0.0033	67
7	55304.5579	0.0004	−0.0018	72
50	55307.3670	0.0017	0.0110	55
51	55307.4263	0.0014	0.0052	65
52	55307.4906	0.0010	0.0046	69
93	55310.1499	0.0009	−0.0025	45
94	55310.2197	0.0015	0.0023	40
215	55318.0817	0.0041	−0.0045	22

*BJD−2400000.
†Against $max = 2455304.1044 + 0.065032E$.
‡Number of points used to determine the maximum.

observations recorded a stage B–C transition. The derived periods for each stage are listed in table 2. Although the observation only covered the late part of the superoutburst, the evolution of superhump period appears to be typical. As judged from these periods, Szkody et al. (2006) appears to have recorded stage B superhumps.

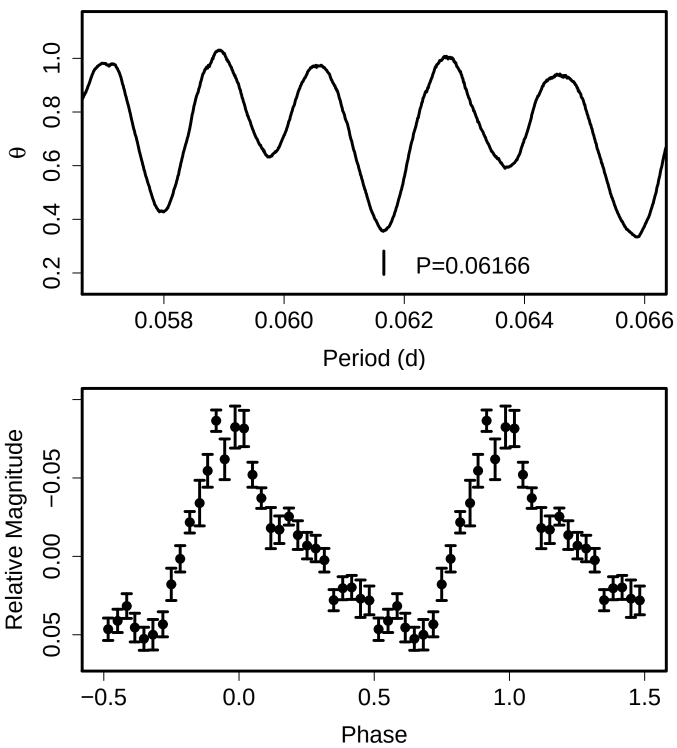

Fig. 57. Superhumps in SDSS J2048 (2009). (Upper): PDM analysis. The selection of the alias was based on the known $P_{\rm orb}$. (Lower): Phase-averaged profile.

Table 60. Superhump maxima of SDSS J2048 (2009).

E	max*	error	$O-C$†	N‡
0	55119.4241	0.0008	−0.0013	45
16	55120.4152	0.0012	0.0029	32
31	55121.3347	0.0007	−0.0029	63
32	55121.4006	0.0011	0.0014	56

*BJD−2400000.
†Against $max = 2455119.4254 + 0.061683E$.
‡Number of points used to determine the maximum.

3.55. SDSS J204817.85−061044.8

This object (hereafter SDSS J2048) is a CV selected during the course of the SDSS (Szkody et al. 2003), who reported the detection of a white dwarf in the spectrum, suggesting a dwarf nova with a low mass-transfer rate.

The outburst in 2009 October was detected by E. Muyllaert (cvnet-outburst 3367). Subsequent observations by I. Miller detected superhumps (cvnet-outburst 3383). Woudt, Warner (2010) observed the object in quiescence and obtained an orbital period of 0.060597(2) d. We identified the superhump period of 0.06166(2) d based om this $P_{\rm orb}$ (figure 57. The times of superhump maxima are listed in table 60. The ϵ was 1.8 %.

Table 61. Superhump maxima of J0406 (2010).

E	max*	error	$O-C$†	N‡
0	55246.9899	0.0009	−0.0011	126
12	55247.9497	0.0010	−0.0000	132
25	55248.9899	0.0011	0.0015	205
49	55250.9069	0.0030	0.0010	156
62	55251.9432	0.0027	−0.0014	207

*BJD−2400000.
†Against $max = 2455246.9909 + 0.079898E$.
‡Number of points used to determine the maximum.

3.56. OT J040659.8+005244

This object (hereafter OT J0406) was discovered by K. Itagaki in 2008 (Yamaoka et al. 2008). The 2010 outburst, detected by the CRTS, is the second known superoutburst of this object. The outburst was apparently detected in its late stage. The times of superhump maxima are listed in table 61. We attribute these superhumps to stage C superhumps. The mean period with the PDM method was 0.07996(3) d, close to that (0.07992 d) recorded during the 2008 superoutburst (Kato et al. 2009a). We adopted this period in table 2.

3.57. OT J050617.4+354738

This object (=USNO−B1.0 1257−0089884, hereafter OT J0506) is a dwarf nova discovered by Kryachko et al. (2010) (see also vsnet-alert 11686 for the initial announcement). The object was rising at the time of the discovery and superhumps were subsequently detected (vsnet-alert 11688; Kryachko et al. 2010). Since the discovery announcement was made sufficiently early, the early stages of the outburst was well observed. The times of superhump maxima are listed in table 62. The mean superhump period excluding the initial night was 0.06928(2) d (PDM method, figure 58).

3.58. OT J102637.0+475426

This object (hereafter OT J1026) is a dwarf nova discovered by K. Itagaki (Yamaoka, Itagaki 2009). Although Kato et al. (2009a) reported on late-stage observations of the 2009 superoutburst, the observational coverage was short. We observed the 2010 superoutburst, detected by I. Miller (baavss-alert 2245). We first time succeeded in recording both stages B and C (table 63). The resultant period is in disagreement with the 2009 result. Since the present coverage is much better than the 2009 observation, the present values are more reliable. A reanalysis of the 2009 data could not yield a continuous $O-C$ diagram, suggesting a discontinuous phase jump (or appearance of stronger secondary superhump peaks) in the final stage of the 2009 superoutburst.

3.59. OT J104411.4+211307

This object (= CSS100217:104411+211307, hereafter OT J1044) was discovered by the CRTS on 2010 February 17. The large outburst amplitude was already sugges-

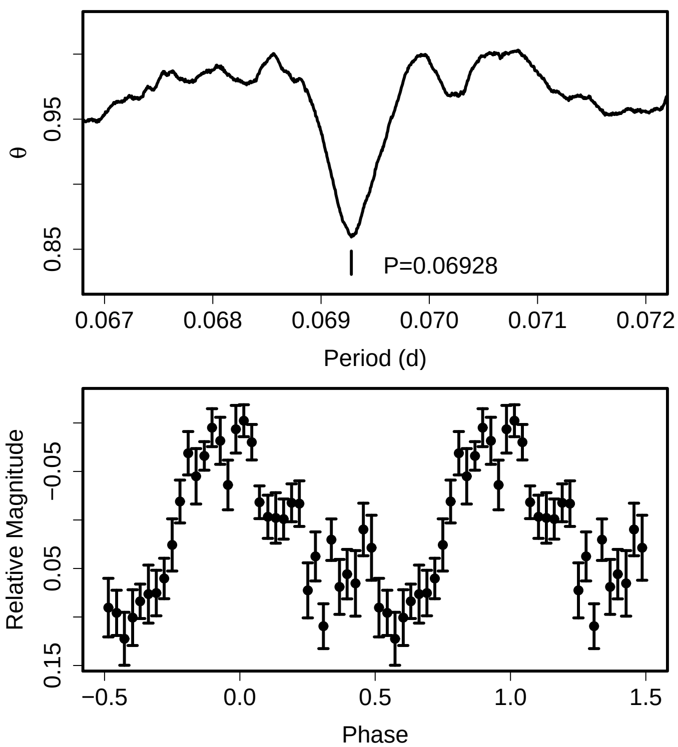

Fig. 58. Superhumps in OT J0506 (2009). (Upper): PDM analysis. (Lower): Phase-averaged profile.

Table 62. Superhump maxima of OT J0506 (2009).

E	max*	error	$O-C$†	N‡
0	55160.5113	0.0034	−0.0010	24
1	55160.5777	0.0008	−0.0039	48
2	55160.6485	0.0007	−0.0024	48
23	55162.1113	0.0006	0.0045	130
24	55162.1810	0.0007	0.0049	149
52	55164.1160	0.0010	−0.0012	102
53	55164.1854	0.0011	−0.0011	140
56	55164.3920	0.0009	−0.0025	12
81	55166.1293	0.0023	0.0016	146
82	55166.2028	0.0099	0.0058	92
85	55166.4085	0.0029	0.0035	7
88	55166.6129	0.0018	−0.0001	13
96	55167.1688	0.0020	0.0013	157
97	55167.2387	0.0020	0.0018	14
98	55167.3056	0.0017	−0.0006	12
99	55167.3755	0.0011	−0.0000	14
100	55167.4428	0.0015	−0.0021	12
101	55167.5116	0.0016	−0.0026	13
102	55167.5774	0.0022	−0.0061	12

*BJD−2400000.
†Against $max = 2455160.5123 + 0.069326E$.
‡Number of points used to determine the maximum.

Table 63. Superhump maxima of OT J1026 (2010).

E	max*	error	$O-C$†	N‡
0	55270.5082	0.0002	−0.0012	67
1	55270.5783	0.0003	0.0002	75
2	55270.6456	0.0003	−0.0011	75
26	55272.2894	0.0009	−0.0048	30
27	55272.3616	0.0005	−0.0013	76
28	55272.4296	0.0005	−0.0020	58
29	55272.5006	0.0006	0.0004	68
43	55273.4636	0.0004	0.0024	60
44	55273.5311	0.0008	0.0012	36
57	55274.4268	0.0039	0.0045	47
58	55274.4972	0.0021	0.0063	67
59	55274.5603	0.0012	0.0007	72
113	55278.2660	0.0013	−0.0004	53
114	55278.3322	0.0012	−0.0029	76
115	55278.4048	0.0011	0.0010	69
116	55278.4718	0.0008	−0.0006	76
117	55278.5393	0.0008	−0.0018	61
118	55278.6091	0.0007	−0.0006	72

*BJD−2400000.
†Against $max = 2455270.5094 + 0.068646E$.
‡Number of points used to determine the maximum.

tive of a WZ Sge-type like outburst (vsnet-alert 11817). Subsequent observation soon established the presence of early superhumps (vsnet-alert 11820, 11828, 11829; figure 60). The object later developed ordinary superhumps (vsnet-alert 11836, 11837). There was a single post-superoutburst rebrightening (vsnet-alert 11885).

The times of ordinary superhumps are listed in table 64. It was most likely that we only sufficiently observed stage A ($E \leq 41$) and stage C ($E \geq 195$). Although the $O-C$ analysis suggests a mean period of ~0.0605 d during stage B, we did not adopt this value in table 2. The superhump period during stage C was, however, reliably determined (figure 60). The period [0.06024(4) d] suggests an ϵ of 1.9 % against the period [0.05909 (1) d] of early superhumps. The waveform of superhumps became double-humped during the rapid fading stage ($E \geq 246$), we only listed maxima having the same phases as in $E < 246$. The last two points ($E = 376$, $E = 377$) were obtained during the fading stage of a rebrightening. Although these humps may have been different from earlier superhumps, we included them because WZ Sge-type dwarf novae are known to exhibit long-enduring superhumps even during the rebrightening phase.

All the observed features, including the outburst amplitude of ~6 mag, the existence of early superhumps, relatively large ϵ, the likely existence of stage C and the single post-superoutburst rebrightening resemble those of large-amplitude borderline WZ Sge-type dwarf novae such as BC UMa and RZ Leo (objects showing "type-C" WZ Sge-type outbursts in Kato et al. 2009a).

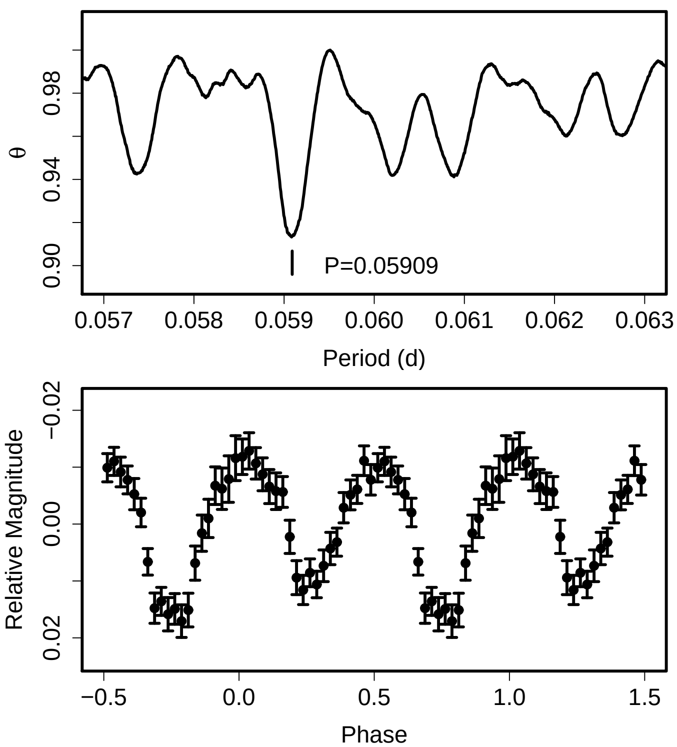

Fig. 59. Early superhumps in OT J1044 (2010). (Upper): PDM analysis. (Lower): Phase-averaged profile.

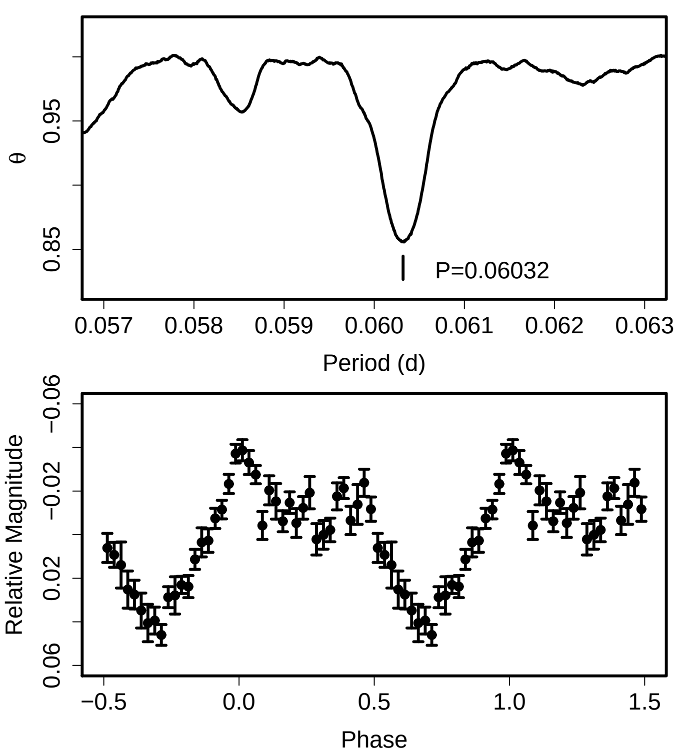

Fig. 60. Ordinary superhumps in OT J1044 during stage C (2010). (Upper): PDM analysis. (Lower): Phase-averaged profile.

Table 64. Superhump maxima of OT J1044 (2019).

E	max*	error	$O-C$†	N‡
0	55250.5223	0.0010	−0.0081	65
1	55250.5847	0.0008	−0.0062	49
2	55250.6440	0.0013	−0.0074	25
8	55251.0082	0.0030	−0.0065	60
9	55251.0696	0.0004	−0.0056	95
10	55251.1309	0.0003	−0.0049	228
11	55251.1920	0.0002	−0.0044	229
24	55251.9822	0.0004	−0.0011	101
25	55252.0459	0.0009	0.0019	100
26	55252.1050	0.0003	0.0005	312
27	55252.1643	0.0002	−0.0008	302
28	55252.2251	0.0004	−0.0004	218
41	55253.0074	0.0019	−0.0052	61
92	55256.1063	0.0017	0.0060	105
113	55257.3823	0.0041	0.0106	32
114	55257.4322	0.0019	−0.0000	61
115	55257.4891	0.0011	−0.0037	67
116	55257.5505	0.0013	−0.0028	65
195	55262.3421	0.0014	0.0059	21
196	55262.4117	0.0011	0.0149	87
197	55262.4689	0.0009	0.0116	85
198	55262.5285	0.0008	0.0106	89
199	55262.5863	0.0010	0.0079	96
200	55262.6474	0.0011	0.0084	76
212	55263.3763	0.0028	0.0109	30
213	55263.4288	0.0010	0.0028	92
214	55263.4911	0.0010	0.0046	93
215	55263.5524	0.0017	0.0053	94
216	55263.6158	0.0012	0.0082	97
217	55263.6732	0.0017	0.0051	49
227	55264.2828	0.0014	0.0093	62
228	55264.3384	0.0012	0.0043	76
229	55264.3995	0.0016	0.0048	86
230	55264.4557	0.0015	0.0005	96
231	55264.5205	0.0016	0.0047	82
232	55264.5774	0.0011	0.0011	93
233	55264.6271	0.0026	−0.0097	86
244	55265.2995	0.0022	−0.0033	78
245	55265.3571	0.0012	−0.0062	91
246	55265.4192	0.0027	−0.0047	97
247	55265.4772	0.0013	−0.0072	92
248	55265.5405	0.0026	−0.0045	100
249	55265.6008	0.0043	−0.0047	85
376	55273.2741	0.0018	−0.0204	63
377	55273.3328	0.0023	−0.0222	63

*BJD−2400000.
†Against $max = 2455250.5304 + 0.060543E$.
‡Number of points used to determine the maximum.

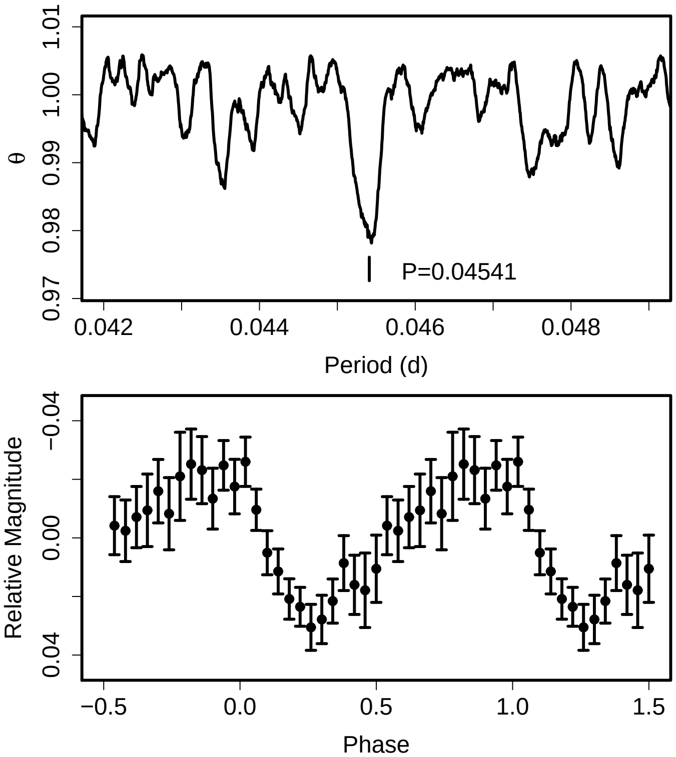

Fig. 61. Superhumps in OT J1122 (2010). (Upper): PDM analysis. (Lower): Phase-averaged profile.

3.60. *OT J112253.3−111037*

This object (= CSS100603:112253−111037, hereafter OT J1122) is a transient discovered by the CRTS. The object was soon suspected to be a large-amplitude dwarf nova (vsnet-alert 12020). H. Maehara detected short-period superhumps (vsnet-alert 12025; figure 61) indicating that the object is an unusual short-$P_{\rm orb}$ CV with an evolved secondary. J. Greaves pointed out that this object is included in the public SDSS DR7 archive. The spectrum indicates that the object is hydrogen-rich, rather than an AM CVn-type helium CV (vsnet-alert 12025), although the strength of helium emission lines suggests an helium enrichment (vsnet-alert 12026).

The times of superhump maxima are listed in table 65. There is an indication of a systematic period decrease after $E=96$. We attributed this to a stage B–C transition and give the derived parameters based in this interpretation in table 2.

More detailed analysis and discussion will be presented in Maehara et al., in preparation.

3.61. *OT J144011.0+494734*

We reported on the detection of superhumps and period variation in this object (= CSS090530:144011+494734, hereafter OT J1440) in Kato et al. (2009a). We present here a re-analysis after incorporating the data in Boyd et al. (2010). The times of superhump maxima are listed in table 66.

Table 65. Superhump maxima of OT J1122 (2010).

E	max*	error	$O-C$†	N‡
0	55350.9981	0.0034	−0.0001	95
1	55351.0405	0.0033	−0.0032	89
36	55352.6341	0.0007	0.0019	54
37	55352.6784	0.0007	0.0007	83
44	55352.9942	0.0015	−0.0012	96
45	55353.0346	0.0033	−0.0061	95
49	55353.2263	0.0004	0.0040	148
52	55353.3564	0.0022	−0.0021	45
72	55354.2685	0.0006	0.0022	189
73	55354.3118	0.0012	0.0001	189
93	55355.2223	0.0007	0.0029	188
94	55355.2656	0.0007	0.0007	219
95	55355.3096	0.0012	−0.0006	211
96	55355.3646	0.0048	0.0089	48
132	55356.9831	0.0030	−0.0066	95
137	55357.2187	0.0012	0.0020	83
138	55357.2635	0.0012	0.0014	94
139	55357.3070	0.0011	−0.0005	101
154	55357.9839	0.0046	−0.0044	42

*BJD−2400000.
†Against $max = 2455350.9982 + 0.045390E$.
‡Number of points used to determine the maximum.

It has now become evident that $E<10$ corresponds to stage A, when the superhumps were indeed still in development and the object once started to fade temporarily (figure 62). The period break reported in Kato et al. (2009a) and Boyd et al. (2010) after $E=54$ this is most likely a stage B–C transition. It is unusual for such a short-$P_{\rm SH}$ system to show a stage B–C transition at such an early stage. The apparent lack of distinct positive $P_{\rm dot}$ during the stage B is also unusual. The development of the superhump period the presence of a likely precursor (or a stagnation) in the light curve are similar to those of BZ UMa, which has been proposed to critically exhibit the SU UMa-type phenomenon Kato et al. (2009a). Since BZ UMa is known to show many normal outbursts in addition to a very rare superoutburst (Jurcevic et al. 1994; Ringwald, Thorstensen 1990), a further systematic observation of OT J1440 is encouraged to explore the similarity between these objects and potential cause of the unusual period behavior.

3.62. *OT J163120.9+103134*

This object (= CSS080505:163121+103134, hereafter OT J1631) underwent another superoutburst in 2010 (I. Miller, baavss-alert 2268). The times of superhump maxima are listed in table 67. Although there seems to have a change in the period between $E=0$ and $E=14$, the change was apparently too large to be attributed to a stage A–B or B–C transition. It is likely that observation at $E=0$ was insufficient to derive a reliable maximum. Disregarding observations before BJD 2455307, we obtained a period of 0.06395(2) d with the PDM method.

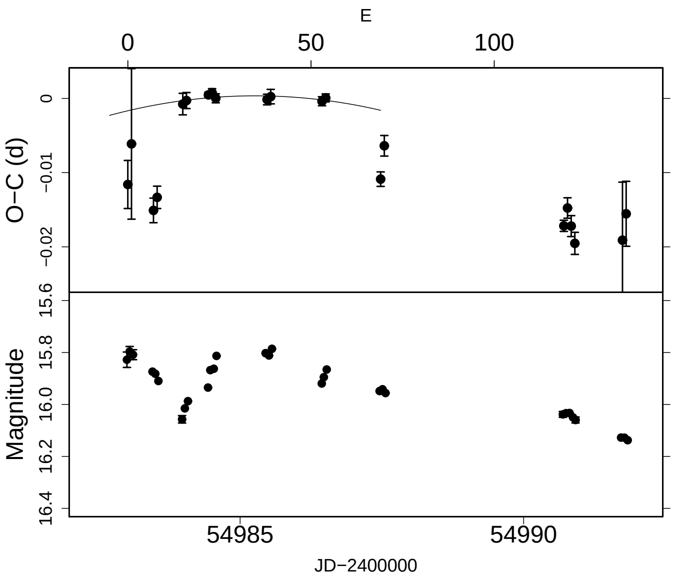

Fig. 62. $O-C$ of superhumps OT J1440 (2009). (Upper): $O-C$ diagram. The $O-C$ values were against the mean period for the stage B ($15 \le E \le 54$, thin curve) (Lower): Light curve. There was a temporary fading before the superhumps fully grew.

Table 66. Superhump maxima of OT J1440 (2009).

E	max*	error	$O-C$†	N‡
0	54983.0245	0.0032	−0.0095	69
1	54983.0946	0.0101	−0.0039	64
7	54983.4733	0.0017	−0.0123	68
8	54983.5397	0.0015	−0.0104	68
15	54984.0046	0.0014	0.0029	191
16	54984.0697	0.0011	0.0034	223
22	54984.4581	0.0004	0.0048	164
23	54984.5231	0.0005	0.0052	168
24	54984.5869	0.0006	0.0046	74
38	54985.4914	0.0007	0.0059	106
39	54985.5564	0.0010	0.0063	105
53	54986.4604	0.0006	0.0072	71
54	54986.5254	0.0005	0.0077	64
69	54987.4837	0.0010	−0.0017	110
70	54987.5528	0.0014	0.0029	125
119	54990.7082	0.0008	−0.0028	47
120	54990.7752	0.0014	−0.0003	102
121	54990.8374	0.0014	−0.0026	169
122	54990.8997	0.0015	−0.0049	143
135	54991.7401	0.0078	−0.0031	98
136	54991.8083	0.0044	0.0006	119

*BJD−2400000.
†Against $max = 2454983.0341 + 0.064512E$.
‡Number of points used to determine the maximum.

Table 67. Superhump maxima of OT J1631 (2010).

E	max*	error	$O-C$†	N‡
0	55306.6220	0.0008	−0.0103	42
14	55307.5341	0.0009	0.0047	68
15	55307.6010	0.0010	0.0074	69
55	55310.1595	0.0018	0.0026	133
71	55311.1836	0.0020	0.0014	138
72	55311.2404	0.0012	−0.0059	108

*BJD−2400000.
†Against $max = 2455306.6323 + 0.064082E$.
‡Number of points used to determine the maximum.

Table 68. OT J1703 (2009).

E	max*	error	$O-C$†	N‡
0	55009.4145	0.0021	0.0011	94
1	55009.4716	0.0012	−0.0026	100
2	55009.5366	0.0014	0.0016	103
51	55012.5157	0.0004	−0.0000	58

*BJD−2400000.
†Against $max = 2455009.4134 + 0.060830E$.
‡Number of points used to determine the maximum.

3.63. OT J170343.6+090835

This object (= CSS090622:170344+090835, hereafter OT J1703) was discovered by the CRTS on 2009 June 22. The detection of superhumps (vsnet-alert 11297, 11298) led to a classification as an SU UMa-type dwarf nova. Although there still remain possibilities of aliases, we have adopted $P_{\rm SH}$ = 0.06085(2) d (figure 63) based on the best period determined from the single-night observation (vsnet-alert 11298). The times of superhump maxima are listed in table 68. The outburst appears to have been caught when the amplitude of superhumps decayed (the initial observation was performed $\sim$ 5 d after the CRTS detection). According to CRTS observations, this object were further detected in outburst on 2009 July 22 and 29. Since there were no previous CRTS detections before 2009 June, there may have been an enhanced outburst activity (either normal outbursts or post-superoutburst rebrightenings) in 2009 July.

3.64. OT J182142.8+212154

This object (hereafter OT J1821) was discovered by K. Itagaki (vsnet-alert 11952). The SDSS color suggested that the object is a dwarf nova in outburst. Superhumps were subsequently detected (vsnet-alert 11956; figure 64). The times of superhump maxima are listed in table 69. These observations covered the final part of the superoutburst, and the recorded superhumps were likely stage C superhumps. The lack of variation in the period is compatible with this interpretation.

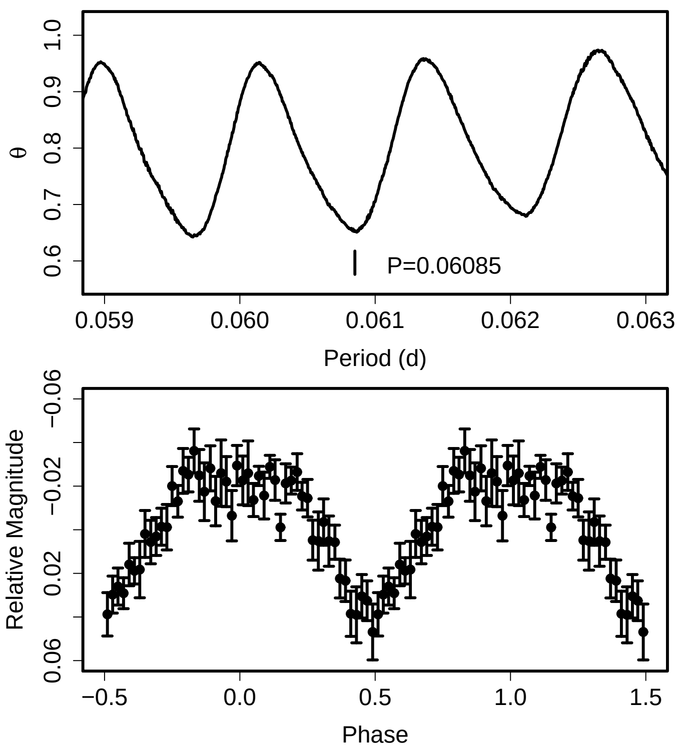

Fig. 63. Superhumps in OT J1703 (2009). (Upper): PDM analysis. (Lower): Phase-averaged profile.

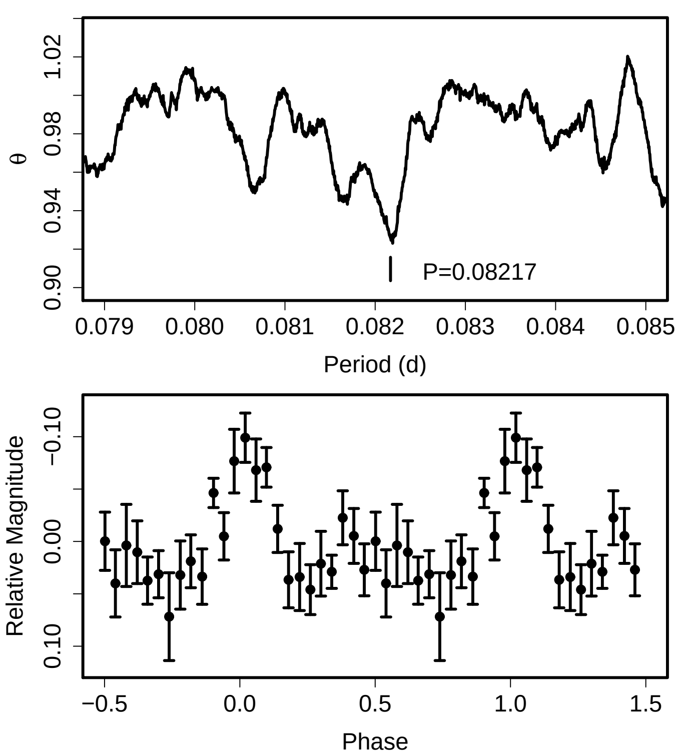

Fig. 64. Superhumps in OT J1821 (2010). (Upper): PDM analysis. (Lower): Phase-averaged profile.

Table 69. Superhump maxima of OT J1821 (2010).

E	max*	error	$O-C$†	N‡
0	55312.1638	0.0008	−0.0034	80
1	55312.2544	0.0039	0.0052	50
18	55313.6433	0.0018	−0.0016	53
48	55316.1072	0.0011	−0.0005	46
49	55316.1883	0.0021	−0.0014	59
74	55318.2444	0.0055	0.0023	118
85	55319.1458	0.0119	0.0007	19
86	55319.2259	0.0284	−0.0013	31

*BJD−2400000.
†Against $max = 2455312.1671 + 0.082094E$.
‡Number of points used to determine the maximum.

3.65. OT J213806.6+261957

This transient (hereafter OT J2138) was independently discovered by D.-A. Yi (Yamaoka 2010) and S. Kaneko (Nakano 2010). Arai (2010) spectroscopically confirmed that this is an outbursting dwarf nova (see also vsnet-alert 11971). The spectrum by Graham et al. (2010) indicated the presence of highly excited emission lines, suggesting that this is a WZ Sge-type outburst [cf. vsnet-alert 11974, see also vsnet-alert 11987 (K. Kinugasa, Gunma Astronomical Observatory) and follow-up spectroscopy by Tovmassian et al. 2010].

The earliest indication of short-period modulations (likely early superhumps) was detected by G. Masi (vsnet-alert 11977, see also 11978, 11985; figure 65). Ordinary superhumps subsequently appeared (vsnet-alert 11990; figure 66), strengthening the identification as a WZ Sge-type dwarf nova. Hudec (2010) reported a detection of another outburst in 1942, which is the only known outburst other than the present one.

The times of maxima for ordinary superhumps are listed in table 70. Although there was an indication of double maxima during the late plateau phase, we did not attempt to distinguish the different peaks, and listed most prominent ones. The overall $O-C$ diagram (figure 67) bears a high degree of similarity to that of ASAS J0025 in 2004 Kato et al. (2009a).[10] The main difference is that OT J2138 did not fade from the plateau before entering stage C. Combined with the apparent presence of multiple hump peaks, this stage in OT J2138 appears to phenomenologically correspond to the phase between the rapid fading from the plateau and rebrightening in ASAS J0025. The apparent absence of a rebrightening in OT J2138 may be explained if this object somehow succeeded in maintaining the plateau phase (or avoiding the quenching of the outbursting state) when ASAS J0025 once returned to quiescence before the rebrightening. The

[10] OT J2138 is a companion to a close visual double (Yamaoka 2010), which dominates when the variable becomes fainter. Since all the observers measured combined magnitudes, the contribution from the visual companion is responsible for the apparently low outburst amplitude as in figure 67 and the low amplitudes of post-superoutburst superhumps.

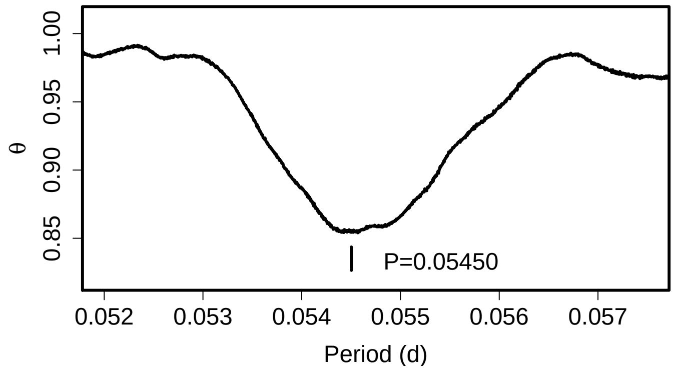

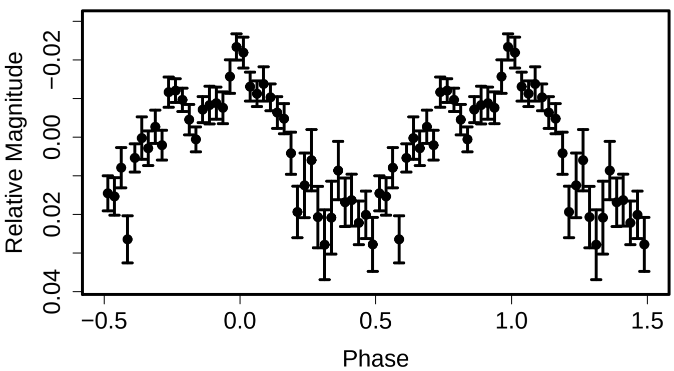

Fig. 65. Early superhumps in OT J2138 (2010) before BJD 2455327.5. (Upper): PDM analysis. (Lower): Phase-averaged profile.

predominance of type-D superoutbursts (superoutbursts without a rebrightening, see Kato et al. 2009a) in very short-$P_{\rm orb}$ systems may be understood as this kind of variety. In table 2, we listed intervals exhibiting best-defined maxima and omitted a phase with multiple peaks. The post-superoutburst stage with $E > 521$ showed a slightly shorter superhump period and the signal was persistent even during the very late post-superoutburst stage (P = 0.05487(1) d, figure 68). There was no indication of a longer late-stage superhumps as observed in GW Lib, V455 And, EG Cnc, WZ Sge and several newly discovered WZ Sge-type dwarf novae (Kato et al. 2008; Kato et al. 2009a).

More detailed analysis and discussion will be presented in Maehara et al., in preparation.

3.66. *OT J215815.3+094709*

This object (= CSS100615:215815+094709, hereafter OT J2158) was discovered by the CRTS in 2010 June. Astrokolkhoz team immediately detected superhumps (vsnet-outburst 11306). The times of superhump maxima are listed in table 71. The mean period determined with the PDM method was 0.07755(9) d. The large amplitudes (0.35 mag, figure 69) and waveform suggest that these superhumps are stage B superhumps at their early evolution.

Table 70. Superhump maxima of OT J2138 (2010).

E	max*	error	$O-C$†	N‡
0	55330.8319	0.0006	0.0019	89
6	55331.1881	0.0013	0.0274	309
36	55332.8555	0.0002	0.0412	76
37	55332.9109	0.0002	0.0414	83
38	55332.9650	0.0002	0.0404	116
41	55333.1300	0.0005	0.0401	125
42	55333.1838	0.0002	0.0388	662
43	55333.2391	0.0002	0.0390	832
44	55333.2940	0.0002	0.0387	503
54	55333.8428	0.0002	0.0363	128
55	55333.8963	0.0002	0.0347	149
56	55333.9519	0.0002	0.0351	106
60	55334.1724	0.0004	0.0352	145
61	55334.2265	0.0003	0.0342	477
62	55334.2810	0.0004	0.0335	427
66	55334.5003	0.0009	0.0324	35
67	55334.5554	0.0004	0.0324	53
68	55334.6094	0.0003	0.0313	53
73	55334.8845	0.0002	0.0307	152
80	55335.2689	0.0002	0.0293	110
86	55335.5978	0.0005	0.0275	151
87	55335.6535	0.0005	0.0281	117
90	55335.8173	0.0003	0.0265	102
91	55335.8749	0.0004	0.0290	130
103	55336.5340	0.0014	0.0267	52
104	55336.5871	0.0008	0.0246	134
105	55336.6417	0.0009	0.0241	171
108	55336.8067	0.0003	0.0238	153
109	55336.8625	0.0002	0.0244	244
110	55336.9171	0.0002	0.0239	145
114	55337.1408	0.0024	0.0271	56
115	55337.1938	0.0005	0.0250	97
116	55337.2511	0.0002	0.0272	387
122	55337.5806	0.0007	0.0260	179
123	55337.6346	0.0007	0.0249	182
127	55337.8545	0.0002	0.0242	104
128	55337.9101	0.0002	0.0247	106
129	55337.9647	0.0004	0.0242	146
132	55338.1396	0.0018	0.0338	131
133	55338.1893	0.0005	0.0284	500
134	55338.2408	0.0004	0.0248	578
137	55338.4063	0.0006	0.0248	92
138	55338.4633	0.0003	0.0267	113
139	55338.5180	0.0005	0.0263	163
140	55338.5746	0.0008	0.0278	141
141	55338.6259	0.0008	0.0239	159
145	55338.8472	0.0004	0.0248	89
146	55338.9023	0.0003	0.0247	74
156	55339.4574	0.0005	0.0287	175
157	55339.5065	0.0005	0.0227	208
158	55339.5705	0.0017	0.0315	85
159	55339.6238	0.0017	0.0297	76
162	55339.7897	0.0029	0.0302	51
163	55339.8426	0.0006	0.0280	82
164	55339.8972	0.0007	0.0275	82
187	55341.1909	0.0016	0.0535	82

*BJD−2400000.

†Against $max = 2455330.8300 + 0.055120E$.

‡Number of points used to determine the maximum.

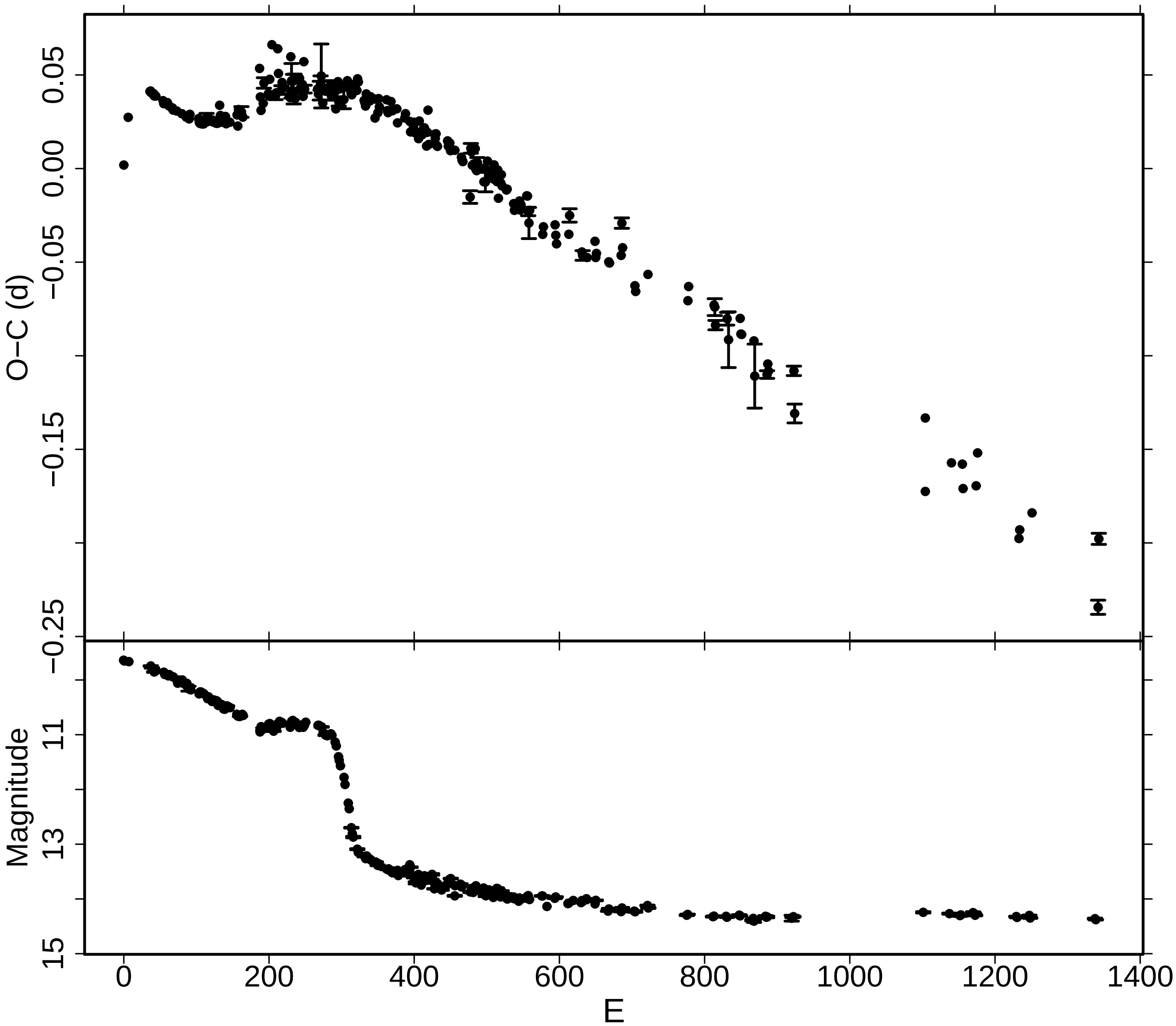

Fig. 67. $O-C$ variation in OT J2138 (2010). (Upper) $O-C$. (Lower) Light curve. The earliest stage of the superoutburst is not shown in this figure.

3.67. OT J223003.0−145835

This object (= CSS090727:223003−145835, hereafter OT J2230) was discovered by the CRTS in 2009 July. The large outburst amplitude exceeding 6 mag was immediately noted (vsnet-alert 11351). Superhump-like modulations were soon reported (vsnet-alert 11353). It became evident by later observations that these modulations were early superhumps of a WZ Sge-type dwarf nova rather than ordinary superhumps (vsnet-alert 11365, 11388). We obtained a mean period of 0.05841(1) d with the PDM method (figure 70). Doubly humped modulations characteristic to early superhumps (cf. Kato 2002) are clearly seen. Due to the faintness of the object, the appearance of ordinary superhumps was not recorded. The outburst lasted for at least 18 d.

3.68. OT J234440.5−001206

This object (= MLS100904:234441−001206, hereafter OT J2344) was discovered by the CRTS in 2010 September during the course of the Mount Lemmon survey. P. Wils notified this event (cvnet-outburst 3828). Immediately following this announcement, superhumps were clearly detected (vsnet-alert 12143, 12144; figure 71).

The times of superhump maxima are listed in table 72. These superhumps were likely stage C superhumps since there was little evidence of period variation and the object started a rapid fading 4 d after the start of the observation.

4. Discussion and summary

4.1. Period Derivatives during Stage B

The new data for SU UMa-type dwarf novae have improved the statistics presented in Kato et al. (2009a). Although the presentations in Kato et al. (2009a) covered a wide range of relations, we restrict only to key figures after combining the samples with Kato et al. (2009a) in this paper.

Figure 72 represents the relation between P_{SH} and P_{dot} during stage B. The enlarged figure (corresponding to fig-

Table 70. Superhump maxima of OT J2138 (2010) (continued).

E	max*	error	$O-C$†	N‡
188	55341.2308	0.0011	0.0383	264
189	55341.2788	0.0010	0.0311	292
192	55341.4479	0.0015	0.0348	78
193	55341.5139	0.0028	0.0457	75
199	55341.8388	0.0019	0.0400	118
200	55341.8928	0.0009	0.0388	119
201	55341.9568	0.0011	0.0477	158
204	55342.1406	0.0011	0.0662	44
209	55342.3890	0.0021	0.0390	46
210	55342.4457	0.0012	0.0405	113
212	55342.5794	0.0020	0.0640	101
213	55342.6214	0.0016	0.0508	84
217	55342.8330	0.0023	0.0419	169
218	55342.8921	0.0011	0.0460	174
228	55343.4363	0.0005	0.0389	116
229	55343.4904	0.0008	0.0379	115
230	55343.5673	0.0012	0.0597	89
231	55343.6096	0.0092	0.0469	99
233	55343.7196	0.0036	0.0466	51
234	55343.7661	0.0036	0.0381	62
235	55343.8313	0.0023	0.0481	95
236	55343.8757	0.0011	0.0374	116
241	55344.1558	0.0013	0.0419	90
242	55344.2173	0.0009	0.0483	103
246	55344.4345	0.0012	0.0449	107
247	55344.4832	0.0011	0.0386	107
248	55344.5569	0.0009	0.0571	88
249	55344.5973	0.0021	0.0424	57
267	55345.5896	0.0014	0.0425	81
268	55345.6420	0.0013	0.0399	83
270	55345.7540	0.0050	0.0416	60
271	55345.8132	0.0038	0.0457	59
272	55345.8721	0.0171	0.0495	44
274	55345.9678	0.0007	0.0350	83
278	55346.1947	0.0004	0.0413	398
279	55346.2512	0.0004	0.0427	508
284	55346.5280	0.0011	0.0439	46
285	55346.5840	0.0022	0.0448	130
286	55346.6330	0.0022	0.0387	116
290	55346.8566	0.0019	0.0418	104
291	55346.9111	0.0011	0.0411	104
292	55346.9569	0.0019	0.0319	165
295	55347.1368	0.0010	0.0464	177
296	55347.1814	0.0025	0.0359	198
297	55347.2432	0.0016	0.0425	80
302	55347.5203	0.0019	0.0440	47
303	55347.5682	0.0049	0.0368	84
304	55347.6304	0.0009	0.0440	113
308	55347.8539	0.0005	0.0469	103
309	55347.9080	0.0006	0.0459	104
310	55347.9612	0.0008	0.0440	67
313	55348.1229	0.0014	0.0403	98
314	55348.1771	0.0002	0.0394	2499
315	55348.2376	0.0018	0.0448	76
321	55348.5653	0.0005	0.0418	76

*BJD−2400000.
†Against $max = 2455330.8300 + 0.055120E$.
‡Number of points used to determine the maximum.

Table 70. Superhump maxima of OT J2138 (2010) (continued).

E	max*	error	$O-C$†	N‡
322	55348.6266	0.0011	0.0480	101
323	55348.6800	0.0008	0.0462	45
331	55349.1111	0.0008	0.0364	119
332	55349.1650	0.0007	0.0352	264
333	55349.2184	0.0008	0.0334	358
334	55349.2800	0.0004	0.0399	396
339	55349.5518	0.0004	0.0362	72
340	55349.6091	0.0017	0.0383	82
341	55349.6629	0.0007	0.0370	50
346	55349.9285	0.0013	0.0270	49
347	55349.9937	0.0006	0.0371	53
349	55350.1040	0.0011	0.0371	142
350	55350.1519	0.0008	0.0299	262
351	55350.2145	0.0012	0.0374	363
352	55350.2652	0.0005	0.0329	325
362	55350.8202	0.0011	0.0367	53
363	55350.8695	0.0005	0.0309	73
364	55350.9235	0.0007	0.0299	73
368	55351.1500	0.0012	0.0358	291
369	55351.2004	0.0004	0.0311	374
370	55351.2553	0.0004	0.0309	383
376	55351.5870	0.0013	0.0319	57
377	55351.6347	0.0004	0.0244	57
387	55352.1884	0.0006	0.0270	47
388	55352.2459	0.0008	0.0293	236
394	55352.5725	0.0009	0.0252	58
395	55352.6220	0.0009	0.0196	59
399	55352.8451	0.0006	0.0223	61
400	55352.9027	0.0005	0.0247	73
401	55352.9523	0.0006	0.0191	151
406	55353.2247	0.0008	0.0160	240
407	55353.2892	0.0011	0.0254	175
410	55353.4490	0.0002	0.0198	184
411	55353.5024	0.0006	0.0181	172
412	55353.5589	0.0006	0.0195	104
413	55353.6161	0.0015	0.0216	58
414	55353.6714	0.0007	0.0218	41
417	55353.8271	0.0016	0.0120	59
418	55353.8895	0.0013	0.0194	73
419	55353.9565	0.0010	0.0312	121
420	55353.9933	0.0008	0.0129	56
428	55354.4397	0.0005	0.0183	120
429	55354.4925	0.0004	0.0160	123
430	55354.5502	0.0008	0.0186	80
431	55354.5990	0.0003	0.0123	58
432	55354.6537	0.0018	0.0119	58
446	55355.4283	0.0004	0.0148	123
447	55355.4806	0.0006	0.0119	122
448	55355.5368	0.0010	0.0130	72
449	55355.5925	0.0008	0.0136	56
450	55355.6435	0.0004	0.0095	56
456	55355.9745	0.0008	0.0098	52
465	55356.4668	0.0003	0.0060	155
466	55356.5203	0.0004	0.0044	169
467	55356.5748	0.0010	0.0037	25
477	55357.1070	0.0034	−0.0152	54

*BJD−2400000.
†Against $max = 2455330.8300 + 0.055120E$.
‡Number of points used to determine the maximum.

Table 70. Superhump maxima of OT J2138 (2010) (continued).

E	max*	error	$O-C$†	N‡
478	55357.1882	0.0026	0.0108	256
479	55357.2414	0.0009	0.0089	272
480	55357.2894	0.0009	0.0018	119
482	55357.4003	0.0016	0.0024	61
483	55357.4555	0.0010	0.0025	62
484	55357.5187	0.0014	0.0107	63
485	55357.5628	0.0011	−0.0004	52
486	55357.6172	0.0004	−0.0011	54
487	55357.6766	0.0027	0.0032	29
496	55358.1624	0.0008	−0.0071	259
497	55358.2249	0.0011	0.0003	301
498	55358.2725	0.0052	−0.0072	269
501	55358.4491	0.0007	0.0040	59
502	55358.4989	0.0006	−0.0013	61
503	55358.5534	0.0006	−0.0020	46
504	55358.6081	0.0017	−0.0024	54
505	55358.6608	0.0010	−0.0048	45
508	55358.8288	0.0004	−0.0022	59
509	55358.8805	0.0006	−0.0055	73
510	55358.9432	0.0006	0.0020	73
514	55359.1547	0.0013	−0.0070	177
515	55359.2161	0.0009	−0.0007	222
516	55359.2561	0.0006	−0.0159	224
519	55359.4297	0.0011	−0.0075	60
520	55359.4892	0.0004	−0.0033	61
521	55359.5382	0.0007	−0.0093	35
527	55359.8668	0.0004	−0.0115	73
528	55359.9224	0.0019	−0.0110	73
537	55360.4107	0.0006	−0.0187	61
538	55360.4622	0.0019	−0.0223	61
545	55360.8531	0.0004	−0.0173	73
546	55360.9034	0.0005	−0.0221	73
547	55360.9613	0.0011	−0.0193	49
555	55361.4070	0.0009	−0.0146	53
556	55361.4620	0.0008	−0.0147	62
557	55361.5089	0.0022	−0.0229	54
558	55361.5579	0.0083	−0.0291	60
559	55361.6198	0.0009	−0.0223	56
577	55362.5991	0.0005	−0.0352	56
578	55362.6583	0.0006	−0.0311	42
594	55363.5412	0.0005	−0.0301	39
595	55363.5908	0.0020	−0.0356	56
596	55363.6413	0.0010	−0.0402	54
613	55364.5834	0.0011	−0.0351	55
614	55364.6486	0.0036	−0.0251	52
631	55365.5662	0.0010	−0.0446	56
632	55365.6194	0.0026	−0.0464	54
638	55365.9491	0.0005	−0.0475	85
649	55366.5640	0.0007	−0.0389	42
650	55366.6105	0.0009	−0.0475	55
651	55366.6678	0.0011	−0.0453	29
668	55367.6003	0.0006	−0.0498	52
669	55367.6548	0.0011	−0.0505	46
685	55368.5408	0.0009	−0.0464	36
686	55368.6132	0.0028	−0.0291	53
687	55368.6551	0.0008	−0.0423	47

*BJD−2400000.
†Against $max = 2455330.8300 + 0.055120E$.
‡Number of points used to determine the maximum.

Table 70. Superhump maxima of OT J2138 (2010) (continued).

E	max*	error	$O-C$†	N‡
704	55369.5719	0.0015	−0.0626	55
705	55369.6239	0.0012	−0.0657	52
722	55370.5701	0.0011	−0.0566	50
777	55373.5876	0.0012	−0.0706	47
778	55373.6503	0.0012	−0.0630	50
813	55375.5696	0.0014	−0.0729	55
814	55375.6237	0.0045	−0.0740	56
815	55375.6692	0.0025	−0.0836	35
831	55376.5545	0.0034	−0.0802	49
833	55376.6535	0.0149	−0.0914	53
849	55377.5468	0.0006	−0.0800	37
850	55377.5936	0.0013	−0.0884	56
851	55377.6485	0.0013	−0.0886	54
868	55378.5821	0.0014	−0.0921	57
869	55378.6184	0.0171	−0.1109	56
886	55379.5563	0.0020	−0.1100	45
887	55379.6170	0.0012	−0.1044	46
888	55379.6683	0.0015	−0.1082	39
923	55381.5977	0.0025	−0.1081	55
924	55381.6300	0.0050	−0.1309	54
1104	55391.5100	0.0004	−0.1725	49
1104	55391.5492	0.0018	−0.1333	58
1140	55393.5096	0.0004	−0.1572	92
1155	55394.3357	0.0019	−0.1579	53
1156	55394.3778	0.0007	−0.1710	71
1174	55395.3714	0.0011	−0.1695	82
1176	55395.4992	0.0019	−0.1519	54
1233	55398.5953	0.0007	−0.1977	54
1234	55398.6551	0.0006	−0.1930	43
1251	55399.6012	0.0011	−0.1839	53
1342	55404.5667	0.0038	−0.2344	42
1343	55404.6583	0.0030	−0.1978	42

*BJD−2400000.
†Against $max = 2455330.8300 + 0.055120E$.
‡Number of points used to determine the maximum.

Table 71. Superhump maxima of OT J2158 (2010).

E	max*	error	$O-C$†	N‡
0	55366.5092	0.0008	0.0001	25
1	55366.5868	0.0003	0.0000	50
2	55366.6644	0.0005	−0.0000	56
4	55366.8190	0.0003	−0.0007	108
5	55366.8979	0.0005	0.0005	74

*BJD−2400000.
†Against $max = 2455366.5091 + 0.077655E$.
‡Number of points used to determine the maximum.

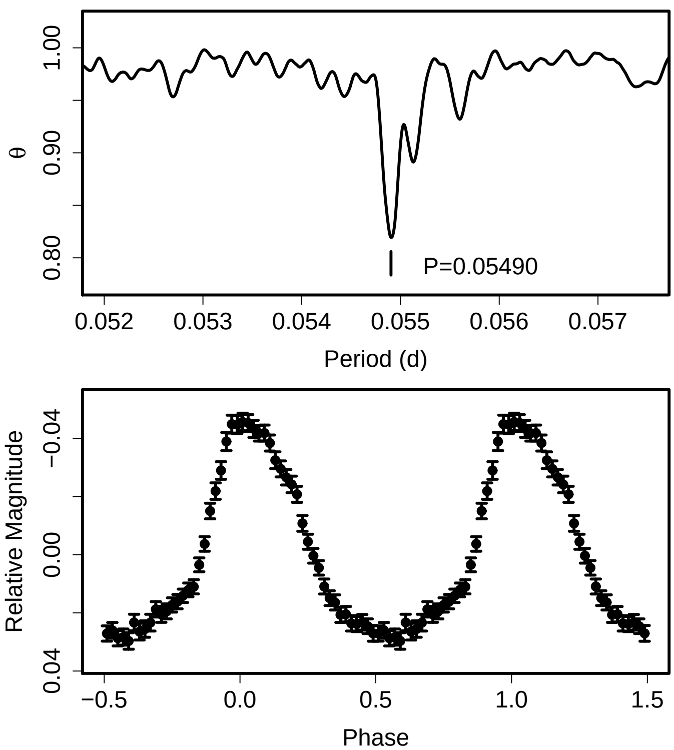

Fig. 66. Superhumps in OT J2138 (2010) during the plateau phase. (Upper): PDM analysis. (Lower): Phase-averaged profile.

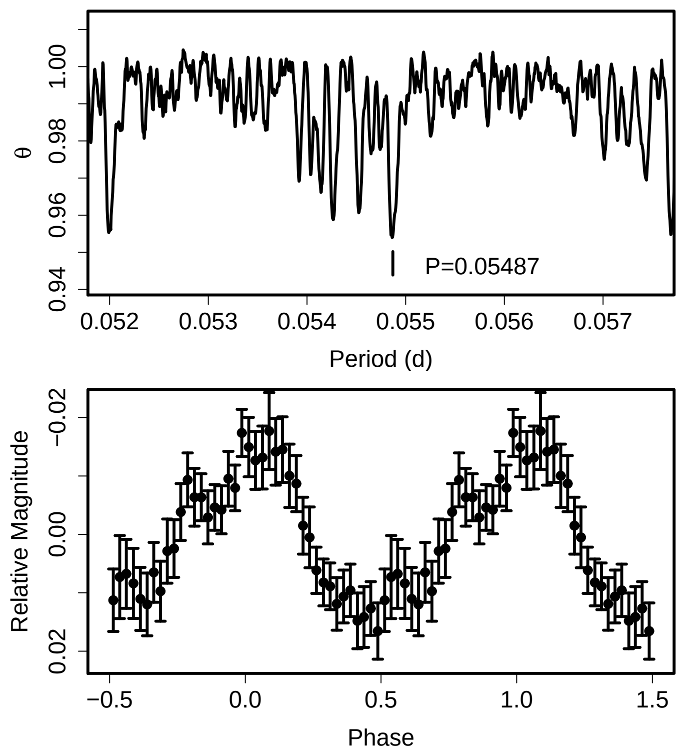

Fig. 68. Superhumps in OT J2138 (2010) during the late post-superoutburst stage. (Upper): PDM analysis. (Lower): Phase-averaged profile.

Table 72. Superhump maxima of OT J2344 (2010).

E	max*	error	$O-C$†	N‡
0	55444.4661	0.0009	0.0024	38
1	55444.5425	0.0005	0.0020	77
2	55444.6163	0.0005	−0.0008	104
9	55445.1507	0.0066	−0.0035	76
12	55445.3861	0.0010	0.0019	38
13	55445.4615	0.0012	0.0005	39
14	55445.5387	0.0005	0.0010	39
15	55445.6111	0.0011	−0.0033	39
26	55446.4576	0.0005	−0.0006	170
27	55446.5316	0.0007	−0.0034	195
28	55446.6107	0.0011	−0.0009	149
38	55447.3778	0.0009	−0.0009	172
39	55447.4547	0.0009	−0.0008	173
40	55447.5373	0.0020	0.0052	112
48	55448.1513	0.0081	0.0054	111
51	55448.3756	0.0011	−0.0005	172
52	55448.4519	0.0014	−0.0009	172
53	55448.5283	0.0018	−0.0011	173
60	55449.0629	0.0026	−0.0035	40
61	55449.1448	0.0042	0.0017	21

*BJD−2400000.
†Against $max = 2455444.4637 + 0.076711E$.
‡Number of points used to determine the maximum.

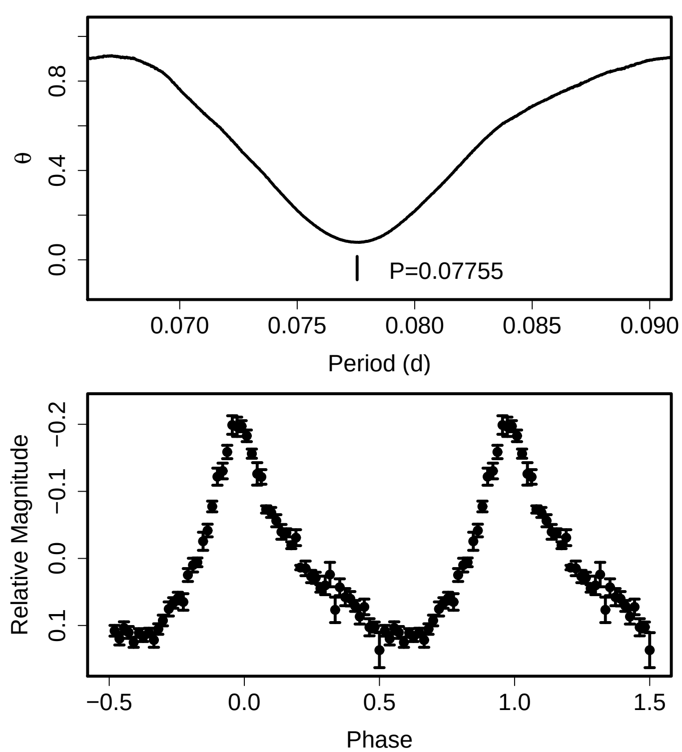

Fig. 69. Superhumps in OT J2158 (2010). (Upper): PDM analysis. (Lower): Phase-averaged profile.

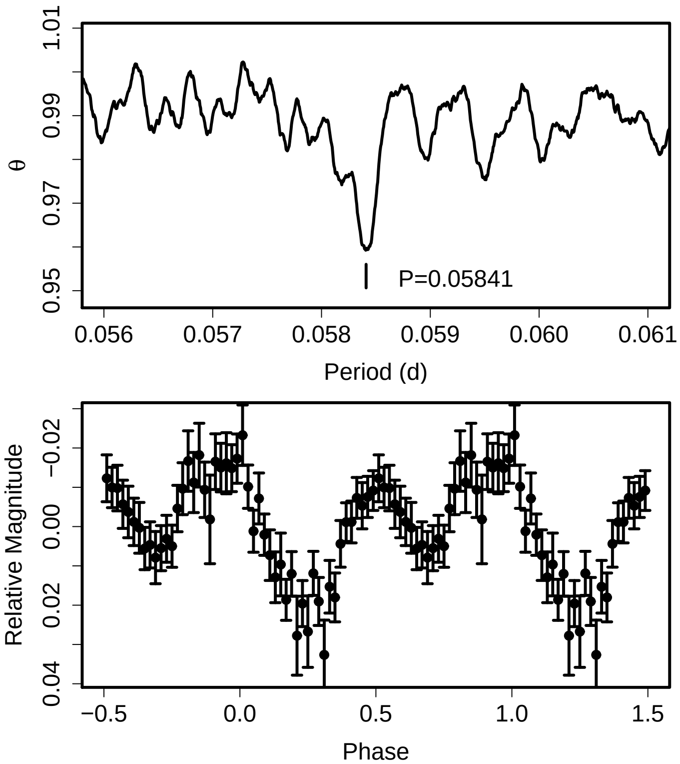

Fig. 70. Early superhumps in OT J2230 (2009). (Upper): PDM analysis. (Lower): Phase-averaged profile.

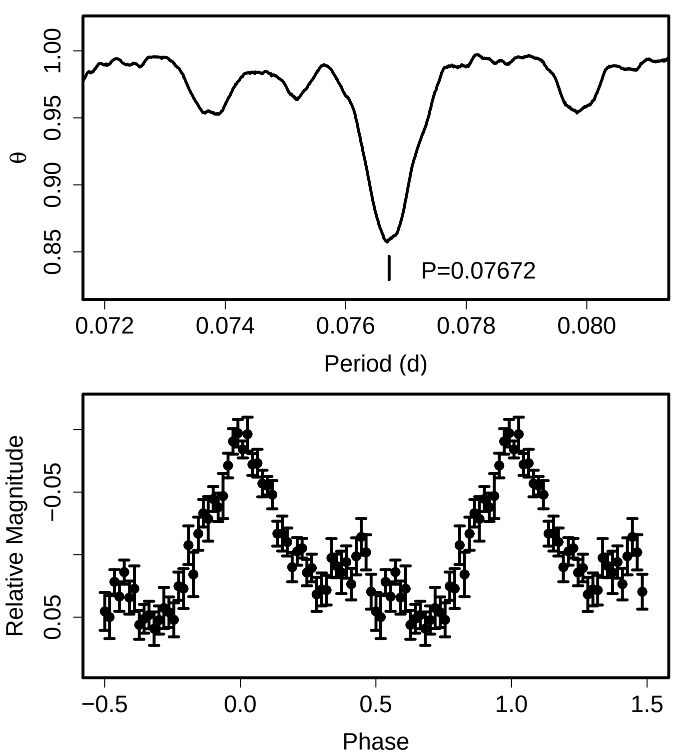

Fig. 71. Superhumps in OT J2344 (2010). (Upper): PDM analysis. (Lower): Phase-averaged profile.

ure 10 in Kato et al. 2009a) is only shown here. The estimated density map is overlaid for a better visualization. The new data generally confirmed the predominance of positive period derivatives during stage B in systems with superhump periods shorter than 0.07 d, in agreement with the tendency reported in Kato et al. (2009a).

4.2. Period Derivatives in Long-$P_{\rm SH}$ Systems

In figure 72, there appears to be a systematic difference in $P_{\rm dot}$ for systems with $P_{\rm SH}$ longer than 0.075 d. We have selected samples for $0.075 < P_{\rm SH}({\rm d}) < 0.085$ from Kato et al. (2009a) and this paper. After using the same criterion for samples described in Kato et al. (2009a) and rejecting poorly determined (nominal error of $P_{\rm dot}$ exceeding 7×10^{-5}) superoutbursts, we applied Student's t-test. The test indicated that these samples are different at a significance level of 0.09. This test suggests that the properties of samples are different between these two data sets. It is already apparent all well-determined $P_{\rm dot}$'s in this paper for this $P_{\rm SH}$ region has positive $P_{\rm dot}$'s, while many systems had negative $P_{\rm dot}$'s in Kato et al. (2009a).

This might have been caused by a small number of long-$P_{\rm SH}$ samples in this paper, since most of newly discovered SU UMa-type dwarf novae have short $P_{\rm SH}$. There would also be a possibility, however, that most of long-$P_{\rm SH}$ with frequent superoutbursts were already discovered at the time of Kato et al. (2009a) and that long-$P_{\rm SH}$ systems in this papers were heavily biased toward systems with infrequent superoutbursts. This possibility would be supported considering that all systems with supercycles longer than 1000 d (V1251 Cyg, RZ Leo, QY Per) have large positive $P_{\rm dot}$ (see also a discussion in Kato et al. 2009a subsection 4.10) while systems with $P_{\rm dot} < -4 \times 10^{-5}$ are restricted to systems with supercycles shorter than 400 d (DH Aql, V1316 Cyg, CU Vel). Although a direct correlation coefficient (0.20) between log supercycle and $P_{\rm dot}$ is not significant, these results seem to strengthen the idea in Kato et al. (2009a) that the degree of period variation is more diverse in long-$P_{\rm SH}$ systems. There is, however, a case of IY UMa, with frequent superoutbursts, which showed a positive $P_{\rm dot}$ in this new sample. It is not yet clear whether some of long-$P_{\rm SH}$ have different $P_{\rm dot}$'s between different superoutbursts or whether this was a mere consequence of poor sampling in the past. Future studies in these viewpoints would be fruitful.

4.3. Difference Between Different Superoutbursts

The apparent lack of systematic difference between different superoutbursts of the same system is one of the main conclusions in Kato et al. (2009a). We further examined this issue using new materials. The new data strengthen this conclusions, including well-observed superoutbursts preceded by precursor outbursts (e.g. PU CMa and 1RXS J0532. It would be noteworthy 1RXS J0532 almost completely reproduced the behavior in 2005, which has been reported to be rather unusual Imada et al. (2009). This suggests that peculiarities found in certain systems are specific to these systems, rather than a chance

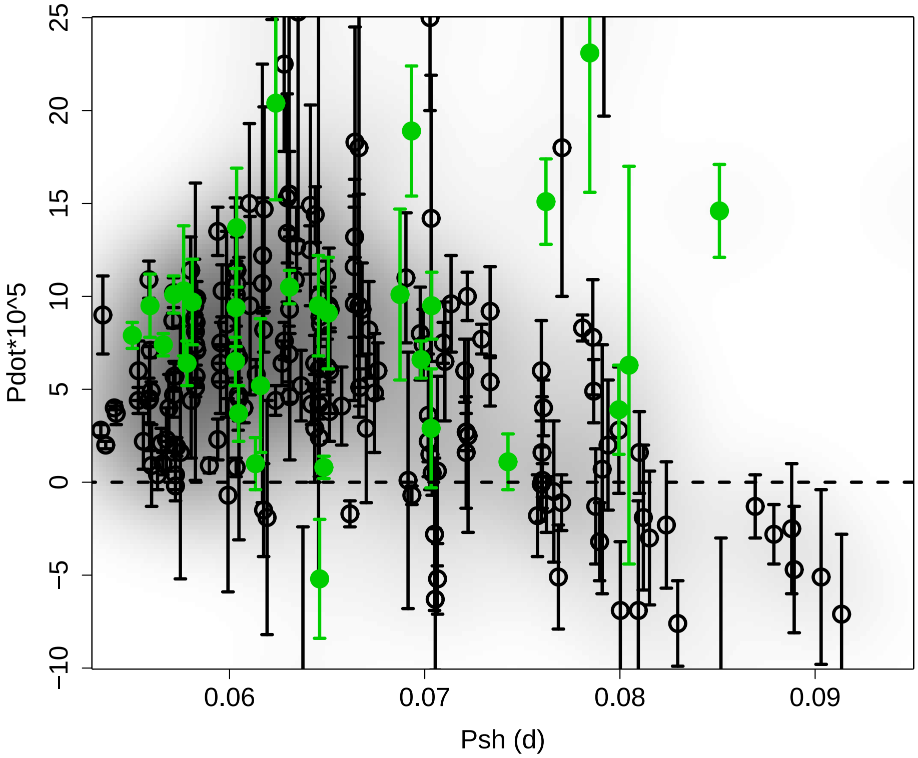

Fig. 72. $P_{\rm dot}$ for stage B versus $P_{\rm SH}$. Open and filled circles represent samples in Kato et al. (2009a) and this paper, respectively. An estimated density map is overlaid in gray scale.

occurrence. This might suggest the existence of parameters specific to systems in addition to general parameters such as q or $P_{\rm orb}$.

In V844 Her, our observations give additional support to the hypothesis that the delay time in development of superhumps is shorter in significantly smaller superoutbursts.

4.4. Beat phenomenon and period variation

In the 2009 superoutburst of IY UMa, we recorded a strong beat phenomenon (in the total luminosity) between superhumps and orbital variation. The beat period largely varied between stage B and C, and were in very good agreement with the beat periods expected from superhump periods during the corresponding stages. The close correlation between the beat period and the superhump period suggests that the change in the angular velocity of the global apsidal motion is more responsible for the stage B–C transition rather than the appearance of a more localized new component with a different period (or angular velocity), such as a bright spot on the disk. Future research focusing on this relation between the beat period and superhump period will be an important key in clarifying the nature of period variations of superhumps.

4.5. Behavior in WZ Sge-Type Systems

The new sample includes three new WZ Sge-type objects with established early superhumps, SDSS J1610, OT J1044 and OT J2230, and one WZ Sge-type object with likely early superhumps (OT J2138). All objects have $P_{\rm SH}$ shorter than 0.061 d. We also suggest that two systems, VX For and EL UMa, are WZ Sge-type dwarf novae with multiple rebrightenings. Although the stage with early superhumps was not observed in VX For, the observed $P_{\rm dot}$ for the first time predicted for its multiple rebrightening in real-time. This success strengthens the relationship between $P_{\rm dot}$ and type of rebrightenings in WZ Sge-type dwarf novae proposed in Kato et al. (2009a). Although EL UMa was only observed for its supposed rebrightening phase, all the known properties are strongly suggestive of a WZ Sge-type system with multiple rebrightenings. The $O-C$ analysis of OT J2138 and its comparison to ASAS J0025 suggest an interpretation that the frequent absence of rebrightenings in very short-$P_{\rm orb}$ objects can be a result of sustained superoutburst plateau when usual SU UMa-type dwarf novae return to quiescence preceding a rebrightening. Although this phenomenon may be somehow related to a small binary separation resulting stronger tidal torque and thereby stronger tidal dissipation to maintain the outbursting state, the exact mechanism should await further clarification.

The authors are grateful to observers of VSNET Collaboration and VSOLJ observers who supplied vital data. We acknowledge with thanks the variable star observations from the AAVSO International Database contributed by observers worldwide and used in this research. This work is deeply indebted to outburst detections and announcement by a number of variable star observers worldwide, including participants of CVNET,

BAA VSS alert and AVSON networks. We are grateful to D. Boyd and his collaborators for making the data for OT J1440 available. The CCD operation of the Bronberg Observatory is partly sponsored by the Center for Backyard Astrophysics. The CCD operation by Peter Nelson is on loan from the AAVSO, funded by the Curry Foundation. We are grateful to the Catalina Real-time Transient Survey team for making their real-time detection of transient objects available to the public. We are also grateful to H. Takahashi and K. Kinugasa for making unpublished spectra of EL UMa available to us. We are grateful to the anonymous referee for pointing out the apparent difference of distribution of $P_{\rm dot}$ between this paper and Kato et al. (2009a).

Appendix 1. Bayesian Applications to Period Analysis

We explored three applications of Bayesian statistics in period analysis employed in this paper. Bayesian statistics (see e.g. Trotta 2008) provide a framework in estimating a posterior probability density function (PDF) of model parameters from a combination of the observed data, a likelihood function defined by the model, and a prior PDF of the model parameters. According to the Bayes' theorem, the posterior PDF of the model parameters θ is

$$Pr(\theta|D) = \frac{Pr(D|\theta)\pi(\theta)}{Pr(D)} \propto Pr(D|\theta)\pi(\theta), \tag{A1}$$

where θ is the model parameter, D is the data, $Pr(\theta|D)$ is the posterior probability of the model, $Pr(D|\theta) \equiv \mathcal{L}(\theta)$ is the likelihood, $\pi(\theta)$ is the prior probability and

$$Pr(D) = \int Pr(D|\theta)d\theta \tag{A2}$$

is a normalization factor, also known as Bayesian evidence.

We usually employ Markov-Chain Monte Carlo (MCMC) method in order to obtain the PDF. The Metropolis-Hastings algorithm (Metropolis et al. 1953; Hastings 1970), one of the best known of MCMC implementation, is as follows: starting with $\theta^{(1)}$, and at the n-th step of MCMC, we obtain $p(\theta^{(n)}) = Pr(D|\theta^{(n)})\pi(\theta^{(n)})$. We then move to a new point $\theta^{(n+1)}$ following a proposal density distribution $q(\theta^{(n)},\theta^{(n+1)})$. The new point is accepted with a probability

$$\alpha(\theta^{(n)},\theta^{(n+1)}) = \min\left\{1, \frac{p(\theta^{(n+1)})q(\theta^{(n+1)},\theta^{(n)})}{p(\theta^{(n)})q(\theta^{(n)},\theta^{(n+1)})}\right\}. \tag{A3}$$

Multivariate Gaussian movements are frequently used to cancel out $q(\theta^{(n+1)},\theta^{(n)})$ and $q(\theta^{(n)},\theta^{(n+1)})$. If the proposal is rejected, $\theta^{(n+1)} = \theta^{(n)}$.[11] After discarding initial 'burn-in' steps, we sample the remaining steps of the Markov chain to obtain the PDF.[12] Typical numbers of steps are 10^4–10^7 for the entire chain and 10^2–10^5 for the 'burn-in' steps.

A.1.1. $O-C$ Analysis of SU UMa-Type Dwarf Novae

As reviewed in Kato et al. (2009a), the $O-C$ diagrams of superhump maxima in SU UMa-type dwarf novae generally follow discrete stages: most frequently a segment with a positive $P_{\rm dot}$ and a later segment with a discontinuously shorter constant period (stages B and C in Kato et al. (2009a)). Determining the parameters for periods and $P_{\rm dot}$ and the time of transition is not a trivial task for the classical statistics. Uemura et al. (2010a) dealt with this problem using the Bayesian statistics and the MCMC method. We formulate this problem for a wider usage.

In this problem, $D = \{t_{obs}(E_i)\}$ are the observed $O-C$'s (or directly observed maxima) for the epochs $\{E_i\}$, and the parameter space is $\theta = \{a, b, c, T, p\}$ defined by the model (t_{model})

$$\begin{aligned} t_{early}(E_i) &= aE_i^2 + bE_i + c \quad (0 \le E \le T) \\ t_{late}(E_i) &= \quad pE_i + q \quad (E > T) \\ t_{early}(T) &= \quad t_{late}(T), \end{aligned} \tag{A4}$$

where T is the epoch of the transition (cf. Uemura et al. 2010a).

Assuming that $\epsilon_i = t_{obs}(E_i) - t_{model}(E_i)$ follows a normal distribution $N(0,\sigma_i^2)$, the likelihood function can be written as

$$\mathcal{L}(\theta) = \prod_i \frac{1}{\sqrt{2\pi\sigma_i^2}} \exp\left[-\frac{\{t_{obs}(E_i) - t_{model}(E_i)\}^2}{2\sigma_i^2}\right]. \tag{A5}$$

Using this likelihood, or its combination with priors, we can obtain the PDF with the MCMC method. Figure 73 is a sample application to superhump timings in QZ Vir in 2004 (Ohshima et al. 2010). The initial T was chosen as 85 and other initial parameters were determined by linear least-squares fitting. The σ's of the multivariate Gaussian distribution for the proposal density were 0.04 times 1-σ errors of the initial fitting. The total length of the chain was 10^5 and the first 5000 samples were discarded for obtaining the PDF. The mean parameters and standard errors were $a = 1.52(12) \times 10^{-6}$, $b = -9.6(1.1) \times 10^{-5}$, $c = 2.50(2) \times 10^{-2}$, $T = 89.0(6)$ and $p = -5.05(6) \times 10^{-4}$. The posterior means of two parameters a and T are shown in figure 74.

We can also introduce priors such as a form of

$$\pi(a) = \frac{1}{\sqrt{2\pi\sigma_a^2}} \exp\left\{-\frac{(a-a_0)^2}{2\sigma_a^2}\right\}, \tag{A6}$$

when expected values of some parameters are empirically known. This application of priors would be useful when $P_{\rm dot}$ of a certain object is known from observation of other superoutbursts while a particular observation has a significant gap to determine parameters by itself. Figure

[11] The description in Uemura et al. (2010b), dealing with a similar class of problems, is incorrect in this step.

[12] Sampling with constant (e.g. 3 to 100) spacings is formally used in order to avoid correlations between steps. In our analysis, we took all remaining steps because our main interest is in means and dispersions of parameters of the PDF, which are little affected by correlation between steps.

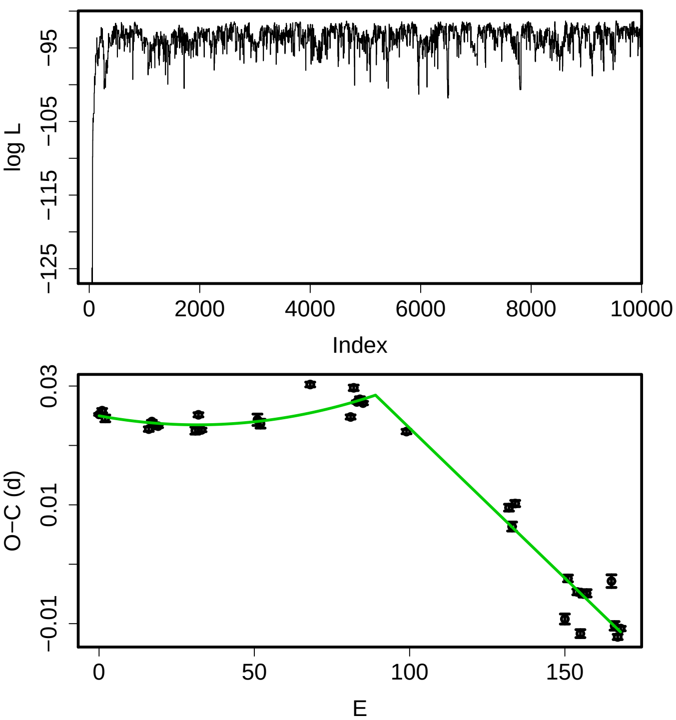

Fig. 73. MCMC analysis of $O-C$ diagram (1). (Upper): Log-likelihood value of the first 10000 chains of a MCMC sampling of $O-C$'s for superhump timings of QZ Vir in 2008. (Lower): Best-fit model using posterior means derived from the PDF.

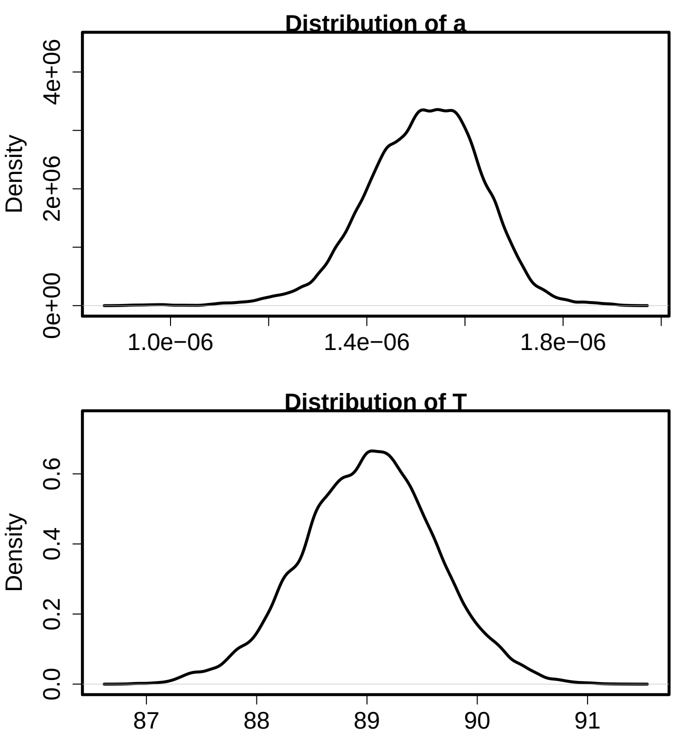

Fig. 74. MCMC analysis of $O-C$ diagram (2). (Upper): Distribution of a. (Lower): Distribution of T.

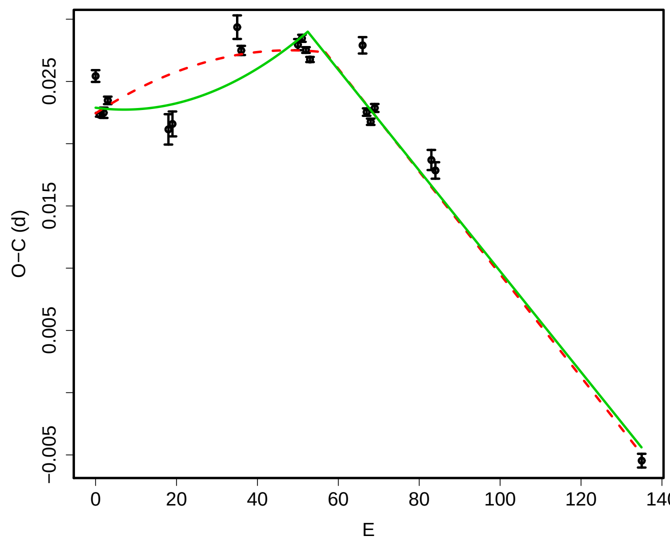

Fig. 75. Effect of priors for observations with a gaps. Dashed and solid curves represent Bayesian estimates for unrestricted model and a model with a prior, respectively. (See text for details).

75 demonstrates the effect of priors for observations with a gaps. The data are times of superhumps of QZ Vir during the 2007 superoutburst. An unconstrained model gives a negative $P_{\rm dot}$ of $a = -2.3(6) \times 10^{-6}$ and a break at $T = 57.0(9)$ (dashed curve). Incorporating prior knowledge that this object has a positive $P_{\rm dot}$, i.e. setting a prior with $a_0 = 4 \times 10^{-6}$ and $\sigma_a = 4 \times 10^{-7}$, we get a reasonable fit (solid curve) with a break at $T = 48(4)$. Since this example is for a demonstration purpose of Bayesian approach, we did not use these values in the main text. Although a proper way of using priors in such a problem need to be further investigated, this formulation would provide a way of analyzing a badly sampled observations when we have firm knowledge in choosing the prior.

A.1.2. Application to Period Analysis

We consider a Bayesian extension of parameter fitting of observed light curves with a cyclic function. In this case, $D = \{y_{obs}(t_i)\}$ is the observations at $\{t_i\}$, and the parameter space is $\theta = \{f, a, b, c\}$ defined by the model

$$y_{model} = aF(2\pi f(t_i - t_0) - b) + c, \tag{A7}$$

where f is frequency and t_0 is an arbitrary constant defining the zero phase. F is an arbitrary cyclic function having a period of 1.

Assuming that $\epsilon_i = y_{obs}(t_i) - y_{model}(t_i)$ follows a normal distribution $N(0, \sigma_i^2)$, the likelihood function can be written as

$$\mathcal{L}(\theta) = \prod_i \frac{1}{\sqrt{2\pi\sigma_i^2}} \exp\left[-\frac{\{y_{obs}(t_i) - y_{model}(t_i)\}^2}{2\sigma_i^2}\right]. \tag{A8}$$

In practice, we can choose a sine function or a template function for F. The parameter σ_i can be either individually set or determined as a constant form $\sigma_i = \sigma$ from the best fit.

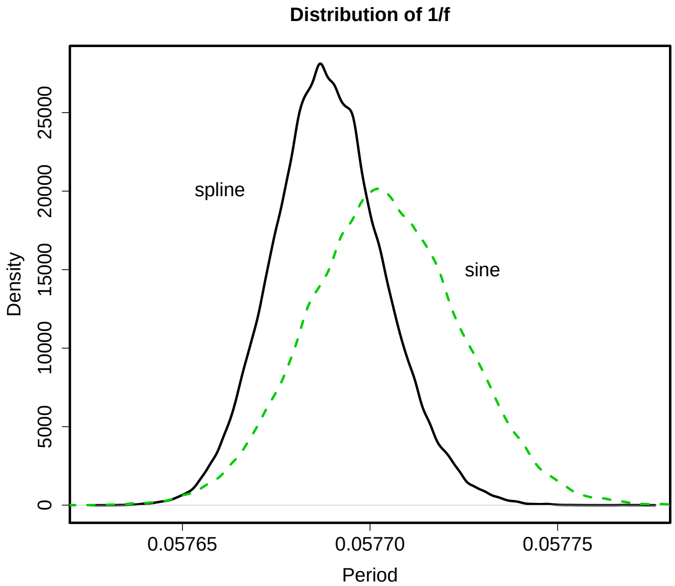

Fig. 76. Application to period analysis. The solid and dashed curves represent results of modeling by spline-interpolated templat profile of superhumps Kato et al. (2009a) sine function, respectively. The used data were for V1454 Cyg (2009), the same as in figure 14.

Although a directed application of the original MCMC to solve the aliasing problem is limited due to the slow mixing between widely separate peaks, it is well suited for sampling the detailed structure of individual peaks. Figure 76 illustrates the dependence on the model functions. Although a spline-interpolated model light curve usually gives a smaller standard error for parameter estimates, the difference is not usually very big. In the present application to V1454 Cyg, spline and sine fits give $1/f = 0.057689(15)$ and $0.057704(20)$, respectively. These analysis has confirmed the results, both period and error estimate, of the PDM analysis. This method would be advantageous when the model description becomes more complex than what the original PDM method describes.

A.1.3. Bayesian Extension to PDM

The PDM method evaluates dispersions of the observed data against phase-binned averages. This prescription sometimes produces spurious scatters in the resultant theta diagram when the number of data (and data in each bin) is small.

Instead of getting phase-averaged light curves (at given trial periods) using a small number of discrete bins, we introduce a Bayesian approach for obtaining continuous phase-averaged light curves. We model light curves by a set of parameters $\theta \equiv \{\theta(j)\} \equiv \{y_{model}(\phi_j)\}$ (at a trial period) for phases $\{\phi_j\}(j=1,\ldots,N)$, where N is the number of phase bins, which are large (~ 100) enough to describe continuous functions.

The likelihood function is

$$\mathcal{L}(\theta) = \prod_i \frac{1}{\sqrt{2\pi\sigma_i^2}} \exp\left[-\frac{\{y_{obs}(\phi_i) - \bar{y}_{obs} - y_{model}(\phi_i)\}^2}{2\sigma_i^2}\right], \quad \text{(A9)}$$

where $y_{model}(\phi_i)$ is linearly interpolated from ϕ_j and ϕ_{j+1} containing ϕ_i in the interval $[\phi_j, \phi_{j+1})$.

Following a standard technique in Bayesian analysis, we then express the condition of smoothness of θ by introducing a prior function assuming that second order differences of $\{\theta(j)\}$ follow a normal distribution $N(0, \sigma_s^2)$ [13]

$$\pi(\theta) = \prod_j \frac{1}{\sqrt{2\pi\sigma_s^2}} \exp\left[-\frac{\{\theta(j-1) - 2\theta(j) + \theta(j+1)\}^2}{2\sigma_s^2}\right], \quad \text{(A10)}$$

where $\theta(0) = \theta(N-1)$ and $\theta(N+1) = \theta(1)$ reflecting the cyclic condition.

In order to obtain maximum a posteriori (MAP) estimates, we solve

$$\frac{\partial \log(\mathcal{L}(\theta)\pi(\theta))}{\partial \theta_j} = 0 \quad \text{(A11)}$$

and

$$\sum_j \theta_j = 0. \quad \text{(A12)}$$

These equations reduce to a set of linear, first-order, equations for θ_j.

Although the smoothing parameter σ_s can be estimated from individual fits by different trial periods, we adopt a constant σ_s for all periods. The value is estimated from the best fit, i.e. from the period the giving smallest dispersion. Using this smooth phase-average light curve, we can then estimate overall variance as prescribed as in Stellingwerf (1978).

This extension of the PDM method is particularly useful when the number of observations is relatively small and the signal of variations is comparable to the noise (figure 77).

References

Anderson, S. F., et al. 2005, AJ, 130, 2230
Arai, A. 2010, Cent. Bur. Electron. Telegrams, 2275, 7
Bakowska, K., Olech, A., Zloczewski, K., & Wisniewski, M. 2010, Acta Astron., in press (arXiv astro-ph/1005.3278)
Bateson, F. M. 1989, Publ. Variable Stars Sect. R. Astron. Soc. New Zealand, 16, 40
Boyd, D., Dunckel, N., Foote, J., & Miller, I. 2010, J. Br. Astron. Assoc., in press (arXiv astro-ph/0911.0272)
Brady, S., Thorstensen, J. R., Koppelman, M. D., Prieto, J. L., Garnavich, P. M., Hirschauer, A., & Florack, M. 2008, PASP, 120, 301
Dillon, M., et al. 2008, MNRAS, 386, 1568
Drake, A. J., et al. 2009, ApJ, 696, 870
Duerbeck, H. W., & Mennickent, R. E. 1998, IBVS, 4637
Garbusov, G. A. 1979, Perem. Zvezdy, Prilozh., 3, 639
Graham, M. L., Broekhoven-Fiene, H., Parker, A. H., Sadavoy, S., Maxwell, A. J., Hsiao, E. Y., & Balam 2010, Cent. Bur. Electron. Telegrams, 2275, 6
Green, R. F., Schmidt, M., & Liebert, J. 1986, ApJS, 61, 305

[13] This distribution can be confirmed by differentiating well-sampled mean profiles of superhumps.

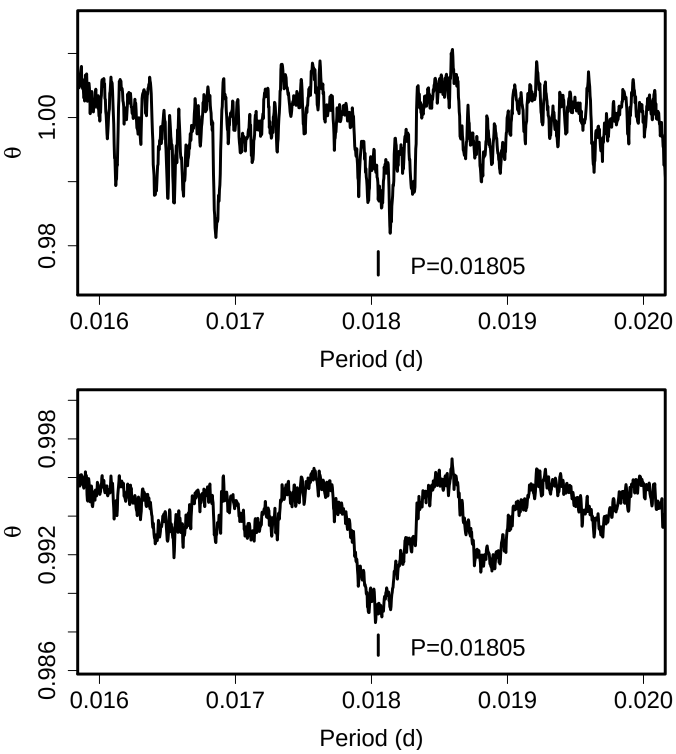

Fig. 77. Comparison of PDM and Bayesian-extended PDM. The used data were SDSS J0129 (subsection 3.42). (Upper) PDM. (Lower) Bayesian-extended PDM.

Hastings, W. K. 1970, Biometrika, 57, 97
Hudec, R. 2010, Astron. Telegram, 2619
Huruhata, M. 1940, Harvard Coll. Obs. Bull., 913, 14
Imada, A., et al. 2009, PASJ, 61, L17
Imada, A., et al. 2005, PASJ, 57, 193
Ishioka, R., et al. 2003, PASJ, 55, 683
Jurcevic, J. S., Honeycutt, R. K., Schlegel, E. M., & Webbink, R. F. 1994, PASP, 106, 481
Kato, T. 1997, PASJ, 49, 583
Kato, T. 2002, PASJ, 54, L11
Kato, T., et al. 2002a, A&A, 396, 929
Kato, T., et al. 2009a, PASJ, 61, S395
Kato, T., Maehara, H., & Monard, B. 2008, PASJ, 60, L23
Kato, T., et al. 2009b, PASJ, 61, 601
Kato, T., Sekine, Y., & Hirata, R. 2001a, PASJ, 53, 1191
Kato, T., Stubbings, R., Monard, B., Butterworth, N. D., Bolt, G., & Richards, T. 2004a, PASJ, 56, S89
Kato, T., & Uemura, M. 2000, IBVS, 4902
Kato, T., Uemura, M., Buczynski, D., & Schmeer, P. 2001b, IBVS, 5123
Kato, T., Uemura, M., Ishioka, R., Nogami, D., Kunjaya, C., Baba, H., & Yamaoka, H. 2004b, PASJ, 56, S1
Kato, T., Uemura, M., Matsumoto, K., Kinnunen, T., Garradd, G., Masi, G., & Yamaoka, H. 2002b, PASJ, 54, 999
Kinman, T. D., Wirtanen, C. A., & Janes, K. A. 1965, ApJS, 11, 223
Kryachko, T., Samokhvalov, A., Satovskiy, B., & Prokopovich, A. 2010, Perem. Zvezdy, 30, 1
Kwee, K. K., & van Woerden, H. 1956, Bull. Astron. Inst. Netherlands, 12, 327
Lanning, H. H., & Meakes, M. 2000, PASP, 112, 251
Liller, W., Frasca, A., & Messina, S. 1999, IAU Circ., 7327
Liller, W., Phillips, M., Hamuy, M., Lamontagne, R., Baganoff, F., Maza, J., & Wischnjewsky, M. 1990, IAU Circ., 5127
Littlefair, S. P., Dhillon, V. S., Marsh, T. R., Gänsicke, B. T., Southworth, J., Baraffe, I., Watson, C. A., & Copperwheat, C. 2008, MNRAS, 388, 1582
Mayall, M. W. 1968, JRASC, 62, 141
Mayall, M. W. 1973, JRASC, 67, 157
Mennickent, R. E., Tappert, C., Gallardo, R., Duerbeck, H. W., & Augusteijn, T. 2002, A&A, 395, 557
Metropolis, N., Rosenbluth, A. W., Rosenbluth, M. N., Teller, A. H., & Teller, E. 1953, J. Chem. Phys., 21, 1087
Nakano, S. 2010, Cent. Bur. Electron. Telegrams, 2275, 2
Nogami, D., et al. 2004, PASJ, 56, S99
Ohshima, T., et al. 2010, PASJ, in preparation
Oizumi, S., et al. 2007, PASJ, 59, 643
Pesch, P., & Sanduleak, N. 1987, IBVS, 2989
Pretorius, M. L., Knigge, C., O'Donoghue, D., Henry, J. P., Gioia, I. M., & Mullis, C. R. 2007, MNRAS, 382, 1279
Richter, G. A. 1968, IBVS, 293
Richter, G. A. 1991, IBVS, 3619
Ringwald, F. A., & Thorstensen, J. R. 1990, BAAS, 22, 1291
Schmidtobreick, L., Galli, L., Whiting, A., Tappert, C., & Carver, A. J. 2005, PASP, 117, 944
Shears, J., et al. 2010a, J. Br. Astron. Assoc., in press (arXiv astro-ph/1005.3219)
Shears, J., et al. 2010b, J. Br. Astron. Assoc., in press (arXiv astro-ph/1009.1725)
Shears, J., Koff, R., Sabo, R., Staels, B., Stein, W., & Wils, P. 2010c, J. Br. Astron. Assoc., in press (arXiv astro-ph/1005.5378)
Shears, J., Miller, I., & Sabo, R. 2010d, J. Br. Astron. Assoc., in press (arXiv astro-ph/0912.4056)
Shears, J., Wils, P., Bolt, G., Hambsch, F.-J., Krajci, T., Miller, I., Sabo, R., & Staels, B. 2010e, J. Br. Astron. Assoc., in press (arXiv astro-ph/1005.3222)
Skillman, D. R., et al. 2002, PASP, 114, 630
Smak, J. 2000, New Astron. Rev., 44, 171
Southworth, J., et al. 2008, MNRAS, 391, 591
Stellingwerf, R. F. 1978, ApJ, 224, 953
Szkody, P., et al. 2002a, AJ, 123, 430
Szkody, P., et al. 2003, AJ, 126, 1499
Szkody, P., Gänsicke, B. T., Sion, E. M., & Howell, S. B. 2002b, ApJ, 574, 950
Szkody, P., et al. 2006, AJ, 131, 973
Szkody, P., et al. 2005, AJ, 129, 2386
Szkody, P., et al. 2007, AJ, 134, 185
Tappert, C., & Bianchini, A. 2003, A&A, 401, 1101
Tappert, C., & Mennickent, R. E. 2001, IBVS, 5101
Thorstensen, J. R., & Fenton, W. H. 2003, PASP, 115, 37
Tovmassian, G., Clark, D., & Zharikov, S. 2010, Cent. Bur. Electron. Telegrams, 2283, 1
Trotta, R. 2008, Contemporary Physics, 49, 71
Uemura, M., et al. 2010a, PASJ, 62, 187
Uemura, M., et al. 2004, PASJ, 56, S141
Uemura, M., et al. 2002, PASJ, 54, L15
Uemura, M., et al. 2010b, PASJ, 62, 69
Uemura, M., et al. 2005, A&A, 432, 261
Walker, A. D., & Olmsted, M. 1958, PASP, 70, 495
Warner, B. 1995, Cataclysmic Variable Stars (Cambridge: Cambridge University Press)

Wils, P., Gänsicke, B. T., Drake, A. J., & Southworth, J. 2010, MNRAS, in press (arXiv astro-ph/0910.3218)
Wils, P., & Henden, A. A. 2009, IBVS, 5914
Woudt, P. A., & Warner, B. 2010, MNRAS, in press (arXiv astro-ph/0912.4656)
Yamaoka, H. 2010, Cent. Bur. Electron. Telegrams, 2273
Yamaoka, H., & Itagaki, K. 2009, Cent. Bur. Electron. Telegrams, 1644
Yamaoka, H., Itagaki, K., Kaneda, H., Jacques, C., Pimentel, E., Maehara, H., & Bolt, G. 2008, Cent. Bur. Electron. Telegrams, 1463